CDF/ANAL/BOTTOM/CDFR/9204
Revision 1.1

Measurement of $B_c^{\pm}$ Lifetime in $B_c^{\pm} \rightarrow \mathrm{J}/\psi + \mathrm{l}^{\pm} + \mathrm{X}$ with Run II Data

Mark Hartz, Paul Shepard, Karen Gibson, Turgun Nigmanov

University of Pittsburgh

February, 2008

Abstract

This note describes the measurement of the $B_c^{\pm}$ lifetime using the decay mode $B_c^{\pm} \rightarrow \mathrm{J}/\psi + \mathrm{e}^{\pm} + \mathrm{X}$, as well as a combination with the $B_c^{\pm} \rightarrow \mathrm{J}/\psi + \mu^{\pm} + \mathrm{X}$ result from CDF Note 8155 to give an average result for $B_c^{\pm} \rightarrow \mathrm{J}/\psi + \mathrm{l}^{\pm} + \mathrm{X}$. The measurement is carried out with 1 fb^{-1} of data. We collect a sample of 1935 $J/\psi + e$ candidate events and see 343 ± 44 events in excess of background predictions. We measure a lifetime of $121.7^{+18.0}_{-16.3}(stat.) \pm 8.0(syst.)$ μm. Averaged with the $B_c^{\pm} \rightarrow \mathrm{J}/\psi + \mu^{\pm} + \mathrm{X}$ result, we measure a lifetime with $B_c^{\pm} \rightarrow \mathrm{J}/\psi + \mathrm{l}^{\pm} + \mathrm{X}$ decays of $142.5^{+15.8}_{-14.8}(stat.)5.5(syst.)$ μm.

Contents

1 Introduction

In this note we describe the measurement of the $B_c^\pm$ lifetime in the $B_c^\pm \rightarrow$ J/ψ+e$^\pm$+X decay channel where the J/ψ decays to two oppositely charged muons. The procedures followed in this analysis are similar to those used in the previous measurement in the electron channel of $139^{+22}_{-20} \pm 11\ \mu m$ which was carried out by M. Aoki et al using 360 pb^{-1} of data [1]. In many instances the procedure is also similar to that carried out in the $B_c^\pm \rightarrow$ J/$\psi + \mu^\pm +$ X decay channel, which is described in CDF Note 8155 [2]. The general structure of this note will mirror that of CDF Note 8155, referencing said note where the procedures for the two decay channels are the same, and concentrating on those areas where they are different.

See CDF Note 8155 for general discussions of the following topics which are common to the measurements in both decay channels:

- A discussion of the physics motivation for a measurement of the B_c lifetime.
- A discussion of the per event measured ct^* and σ_{ct^*} that are used in the lifetime measurement.
- A general outline of the steps in the analysis.
- A discussion of fitting procedures used in the analysis.

2 Event Selection

We use similar cuts to those used for the muon channel measurement, as outlined in CDF Note 8155, making changes were they are dictated by the presence of an electron instead of a muon. The description of cuts has been broken into three categories: J/ψ selection, electron selection and cuts on the three track system.

2.1 J/ψ Selection

As with the muon analysis we use events from the J/ψ di-muon trigger in the xpmm0d-0i datasets with run<212133, consisting of $\sim 1\ fb^{-1}$ of integrated luminosity. Our selection requirements are similar to those used for the muon analysis. The cuts applied for the J/ψ selection are listed in Table 1. The resulting di-muon mass distribution with J/ψ mass peak can be seen in Figure 1. In the electron channel we do not require trigger confirmation for the J/ψ legs (as we did in the muon channel) because there is no related bias on the electron in the event. We do, however, require that the event come from the CMUCMU1.5 or CMU1.5_CMX2 trigger paths to avoid uncertainties in later data where higher p_T triggers are enhanced to reduce the trigger cross section at higher luminosities.

Selection Requirement	Value
Two Muons	CMU+CMU or CMU+CMX
Trigger Path Selection	CMUCMU1.5 or CMU1.5_CMX2 Trigger Paths
Muon Likelihood (Bottom Taggers)	> 0.06
CMU Muon p_T	$> 1.5\ GeV/c$
CMX Muon p_T	$> 2.0\ GeV/c$
COT Hits	2 Stereo + 2 Axial Superlayers (5 hits each SL)
Silicon Hits	>= 3 hits in ϕ layers (SVX+ISL)
J/ψ 2D Vertex χ^2	<15
J/ψ Mass	$\lvert M_{J/\psi} - 3.09687\ GeV/c^2 \rvert < 0.05\ GeV/c^2$

Table 1: Cuts applied to J/ψ legs or the two particle J/ψ system.

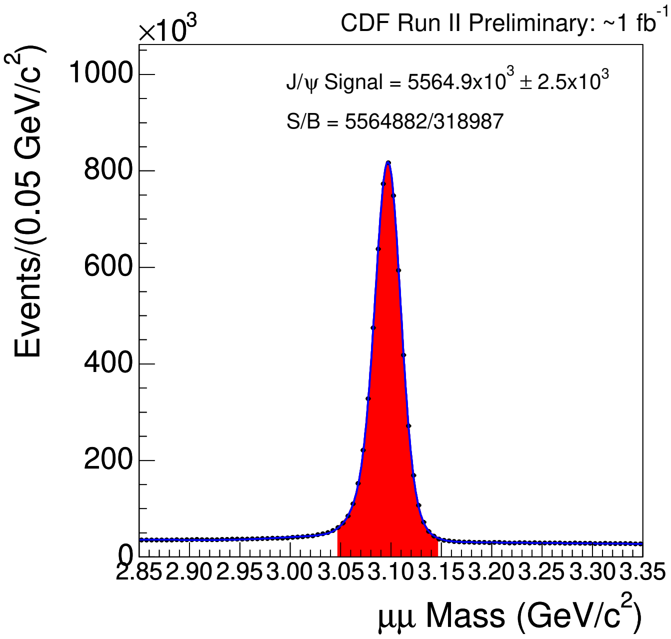

Figure 1: Di-muon mass distribution. Red region is J/ψ mass window used for this analysis.

2.2 Electron Selection

In addition to the J/ψ we require that the event have a third track that passes typical track cuts and is identified as an electron. The cuts are listed in Table 2. The electron identification is done using dE/dx information and an electron likelihood function originally developed for B tagging. The details of both will be outlined in the following sections. We also attempt to veto electrons that come from photon conversion, which will be discussed as well.

Selection Requirement	Value
Fiducial Requirement	In CES Fiducial Region
p_T Cut	$> 2.0 GeV/c$
COT Hits	2 Stereo + 2 Axial Superlayers (5 hits each SL)
dE/dx Hits	>= 43 Hits
Silicon Hits	>= 3 hits in ϕ layers (SVX+ISL)
dE/dx Cut	Z_e/σ_Z >-1.3
Electron Likelihood	$> p_T$ Dependent Cut
Conversion Veto	$\|\Delta(cot(\theta))\| > 0.05 \,\|\|\, \Delta_{xy} < -0.03$ cm $\|\|\, \Delta_{xy} > 0.05$ cm

Table 2: Cuts applied to the third track that is identified as an electron.

2.2.1 Electron dE/dx Z_e Pull Cut

The Z_e of a track is defined as:

$$Z_e = log(dE/dx_{meas.}) - log(dE/dx_{pred.}) = log(\frac{dE/dx_{meas.}}{dE/dx_{pred.}})$$

Here the predicted dE/dx is calculated using an electron hypothesis. We can make this a pull distribution by dividing by the error in Z_e, σ_Z. As is discussed in Appendix B we use pure samples of pions, kaons, protons and muons to estimate the efficiency for a cut of $Z_e/\sigma_Z > -1.3$ on those particle types. Figure 2 summarizes the cut efficiencies as a function of particle momentum, and one can see that it is possible to exlude a large fraction of hadrons and muons at the cost of about 10% of signal events.

2.2.2 Electron Likelihood

In addition to dE/dx information, we can use information from other parts of the detector, specifically the calorimeters, to identify particles as electrons. To this end we use the electron likelihood function from the BottomTaggers software package, which is described in detail in CDF Note 7121 [3]. The only modification we have made to the likelihood function is to remove the dE/dx component as we are cutting on that separately.

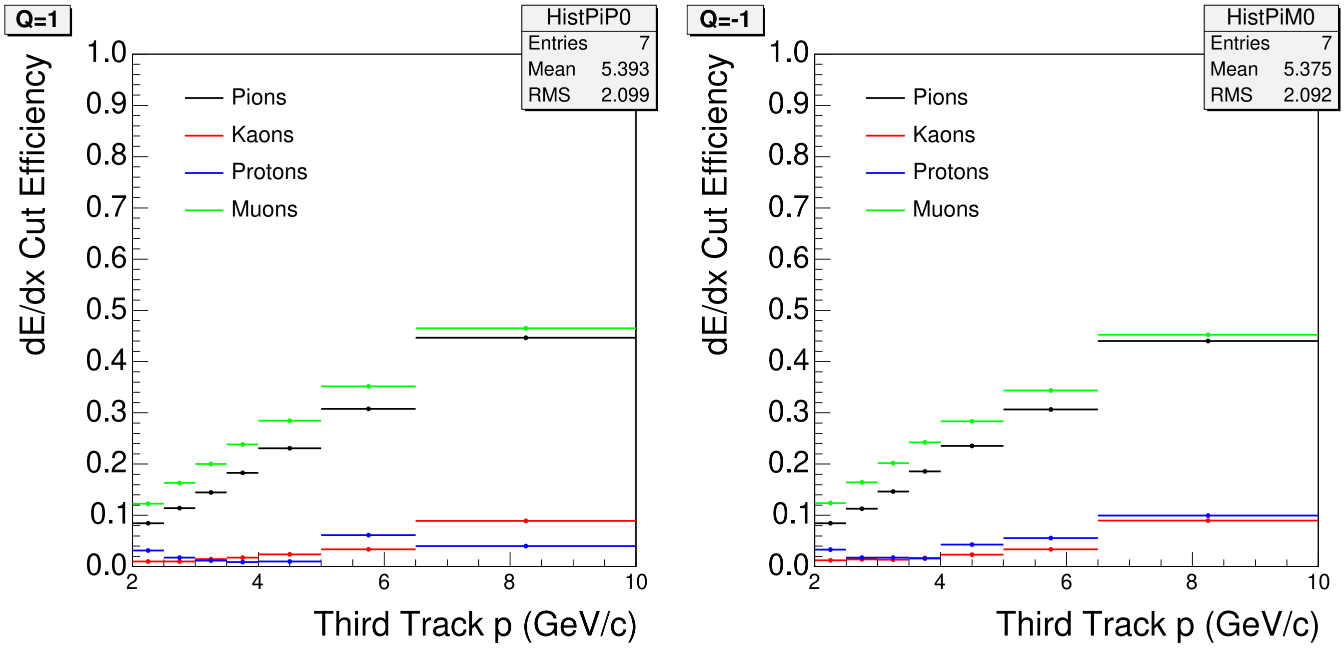

Figure 2: Efficiency of Z_e pull cut for different particle types.

To test the likelihood function we use the blpc0d dataset, selecting events from the "ELECTRON_CENTRAL_8" trigger path. We identify a track with $p_T > 8\ GeV/c$ and electromagnetic $E_T > 8\ GeV/c^2$ as the trigger track and look for a conversion partner track, which will be unbiased. Figure 3 shows the $\Delta(cot(\theta))$ distribution for trigger tracks and conversion partner candidates. We select events in the ± 0.01 window and subtract the background component using sidebands centered at ± 0.04, leaving a sample of conversion partner candidates that are a pure electron sample.

With our sample of pure unbiased electrons we can study the distribution of electron likelihoods for electrons, which can be seen in Figure 4. We then use models of our backgrounds to estimate the optimal value for an electron likelihood cut. We find that the optimal case is a transverse momentum dependent cut that is shown in Figure 5 along with the transverse momentum dependent efficiency. The overall effect is an average efficiency of about 80% for electrons.

2.2.3 Conversion Electron Veto

One source of electrons that we attempt to remove are electrons from photon conversions. Idealy these types of electrons with have a partner track of opposite charge that originates at the same point and has a small opening angle with the electron of interest. To remove these electrons we cut on two variables: Δ_{xy}, which is the distance of closest approach in the xy plane for the two tracks, and $\Delta(cot(\theta))$. The events are removed if $|\Delta(cot(\theta)| < 0.05$ and $-0.3 < \Delta_{xy} < 0.5$ cm.

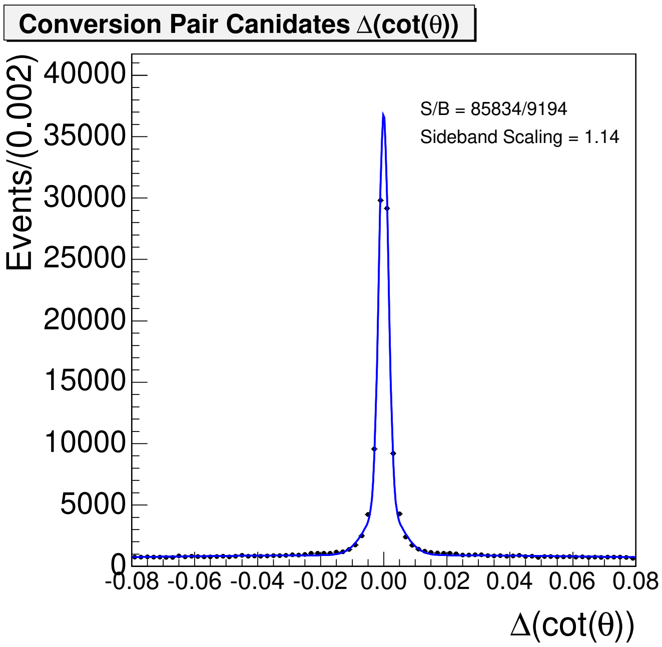

Figure 3: $\Delta(cot(\theta))$ for conversion partner candidates where one of the tracks is a trigger track. Peak at 0 is the conversion signal

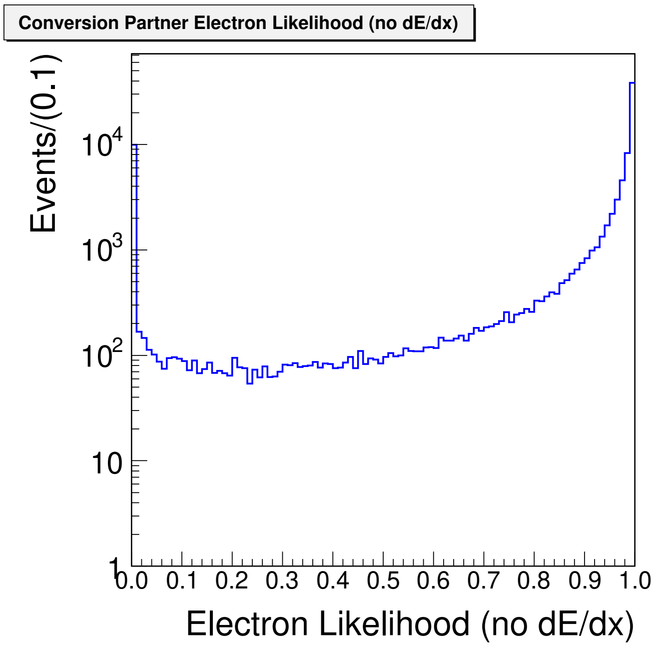

Figure 4: Electron likelihood for unbiased conversion partners.

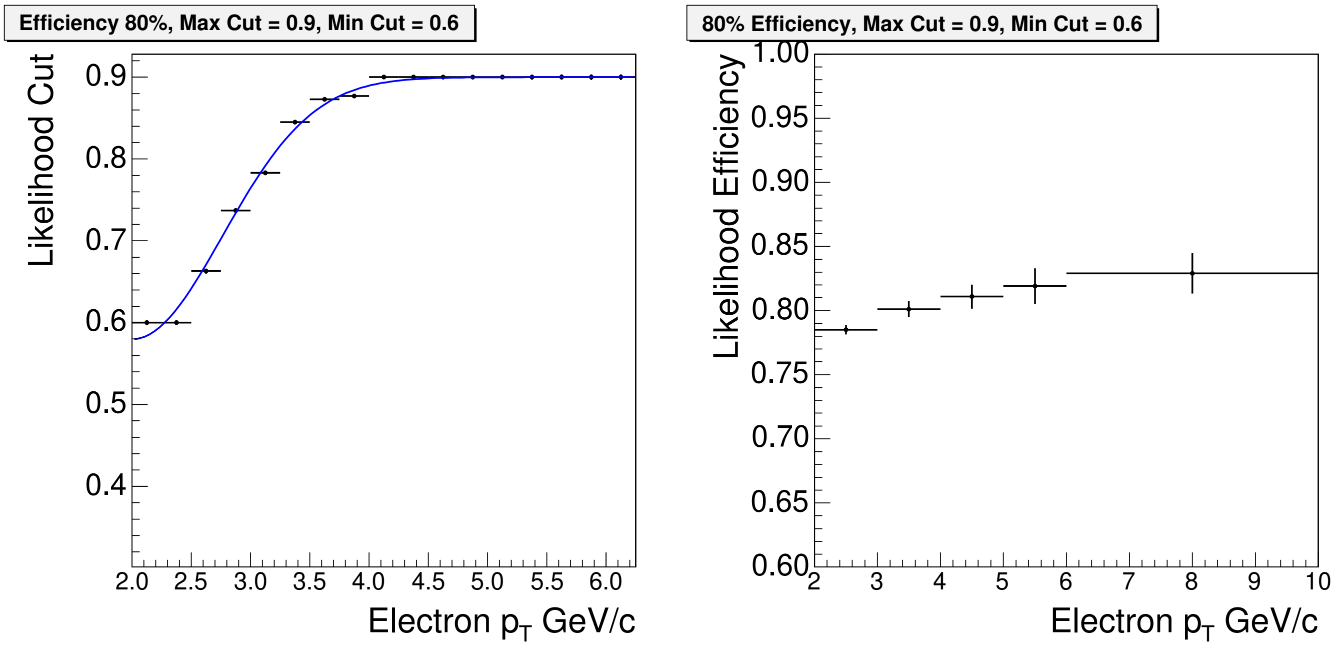

Figure 5: Right: electron likelihood cut value as a functions of transverse momentum. Left: corresponding transverse momentum dependent efficiency.

2.3 Three Track System

We apply a number of cuts to the three track system to select the kinematic regions populated by B_c decays and and reduce the contributions from backgrounds. The cuts are listed in Table 3. Here we discuss a couple of those cuts.

Selection Requirement	Value
Vertex Probability	> 0.001
$\Delta\phi$	$< \pi/2$
$\sigma_{L_{xy}}$	$< 90\ \mu m$
p_T	$> 5\ GeV/c$
$J/\psi e$ Mass	$\lvert M_{J/\psi e} - 5.0\ GeV/c^2 \rvert < 1.0\ GeV/c^2$
$J/\psi K^{\pm}$ Mass Veto	$\lvert M_{J/\psi K^{\pm}} - 5.279\ GeV/c^2 \rvert > 0.05\ GeV/c^2$

Table 3: Cuts applied to the three track system.

2.3.1 $J/\psi e$ L_{xy} Error

We remove events with $> 90\ \mu m$ error on the three track L_{xy} measurement ($\sigma_{L_{xy}}$). The purpose of this cut is to remove the sensitivity of the $b\bar{b}$ background, which is modeled with Pythia Monte Carlo and consists of events with a fake vertex, to the tails in the $\sigma_{L_{xy}}$ distribution which may not be perfectly modeled by the simulation.

Figure 6 shows that this has a small effect on signal events modeled using a Bgenerator Monte Carlo, cutting out about 2%. We also check that the lifetime remains unbiased after applying this cut. Figure 7 shows the true B_c lifetime in the Bgenerator sample with an input lifetime of 140 μm after all cuts have been applied. The fitted lifetime 139.0 ± 1.4 μm is consistent with the generated lifetime.

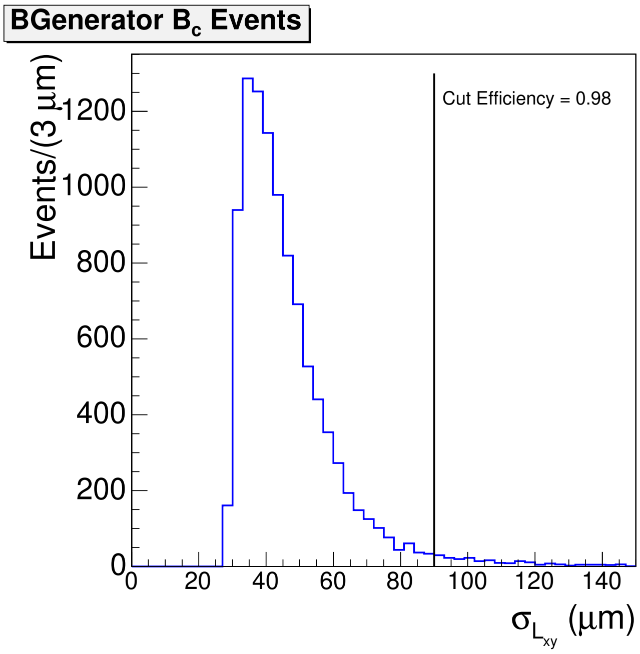

Figure 6: $\sigma_{L_{xy}}$ for simulated signal events generated with Bgenerator. Line shows position of cut.

2.3.2 $J/\psi e$ p_T Cut

We find that this cut removes 28% of the background from events where the J/ψ is not real, while only removing 14% of signal events. The cut was not applied in the muon analysis for two reasons: the $p_T > 3.0$ GeV/c cut for the third track in the muon analysis already puts a strong constraint on the p_T of the three track system, and the muon channel has fewer signal events to start with due to smaller acceptance in p_T and η of the third track.

3 Backgrounds

Four of the backgrounds in the electron channel are similar to those present in the muon channel, with one additional background due to photons converting to electrons. The backgrounds are:

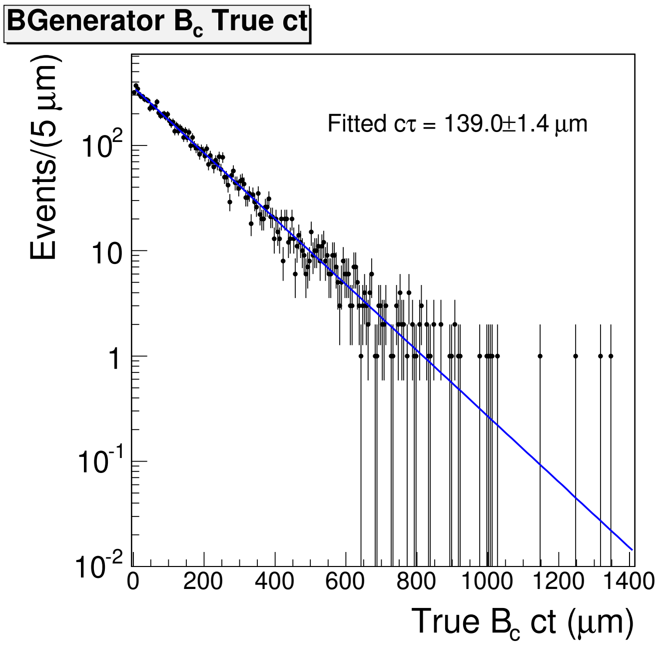

Figure 7: Fitted ct of B_c events in the Bgenerator sample after all cuts, including $\sigma_{L_{xy}} < 90\ \mu m$ have been applied.

- Fake Electron - A J/ψ particle is matched with a third track that is typically from a long lived hadron (π, K or P). This third track can fake an electron if it passes the Z_e/σ_Z cut and has a signature in the calorimeters that is sufficiently like an electron to pass the electron likelihood cut.

- Fake J/ψ - Background J/ψ events in our J/ψ mass window are matched with a third track that is identified as an electron.

- $b\bar{b}$ - The event contains two b jets, one of which produces a J/ψ, the other an electron. The J/ψ and electron have a small probability of reconstructing to a common vertex.

- Residual Conversion - In events with a J/ψ and a photon, the photon may convert to give an e^+e^- pair, one of which may make a vertex with the J/ψ. We attempt to remove conversion electrons by finding the conversion partner, but a residual background remains.

- Prompt J/ψ - J/ψ from prompt charm production in events that also have an electron.

3.1 Fake J/ψ Background

The fake J/ψ background consists of J/ψ background events that are matched with a track that is identified as a electron. To model this background we look for di-muon pairs in the J/ψ sideband regions with an electron that match all of our cuts except for the J/ψ mass window cut.

3.1.1 Fake J/ψ Normalization

Figure 8 shows the fitted J/ψ mass distribution from $J/\psi + e$ candidate events where the J/ψ mass cut has been opened. The signal component of the fit is constrained by the high statistics J/ψ candidate mass fit shown previously. The sideband regions are used to model the fake J/ψ background. From the fit, we estimate the number of background events under the mass peak to be 325.2 ± 10.0 events.

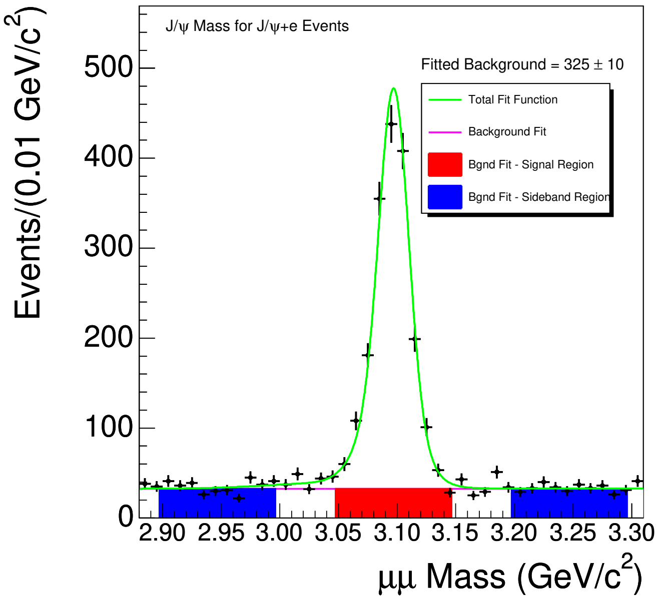

Figure 8: Fitted J/ψ mass for $J/\psi + e$ candidates.

3.1.2 Fake J/ψ ct^*

We model the ct^* of fake J/ψ events by fitting the events in the J/ψ sideband regions. We use a PDF with one prompt, two positive exponential decay and one negative exponential decay components:

$$F_{FJ}(ct^*, \sigma) = [F_{prmt}\delta(ct^*) + \frac{F_+}{c\tau_+}e^{\frac{-ct^*}{c\tau_+}}\theta(ct^*) + \frac{F_{++}}{c\tau_{++}}e^{\frac{-ct^*}{c\tau_{++}}}\theta(ct^*) +$$

$$\frac{F_-}{c\tau_-}e^{\frac{ct^*}{c\tau_-}}\theta(-ct^*)] \otimes \frac{1}{\sqrt{2\pi}s\sigma}e^{-\frac{1}{2}(\frac{ct^*}{s\sigma})^2}$$

The resulting fit can be seen in Figure 9 and the fitted parameters are listed in Table 4.

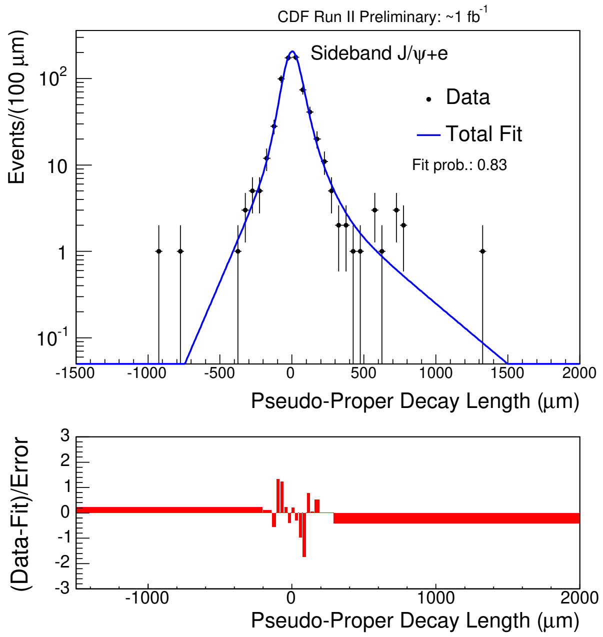

Figure 9: Fitted ct^* distributions for sideband $J/\psi + e$ events.

Parameter	Fit Value	Error
s	1.30	0.02
F_{prmt}	0.664	0.062
F_+	0.056	0.029
$c\tau_+$	310	97
F_{++}	0.111	0.033
$c\tau_{++}$	112	24
F_-	0.168	0.047
$c\tau_-$	82	22

Table 4: Parameters describing the fake J/ψ ct^* fit. $c\tau$ are in μm

3.1.3 Fake J/ψ σ_{ct^*}

The σ_{ct^*} of the sideband events is fitted with the following function:

$$P_{FJ}(\sigma) = \frac{1}{\sqrt{2\pi}P_0}e^{-\frac{1}{2}(\frac{\sigma}{P_0})^2} \otimes \frac{1}{P_1}e^{-\frac{(\sigma-P_2)}{P_1}}$$

The fitted distribution can be seen in Figure 10 and the fitted parameters are listed in Table 5.

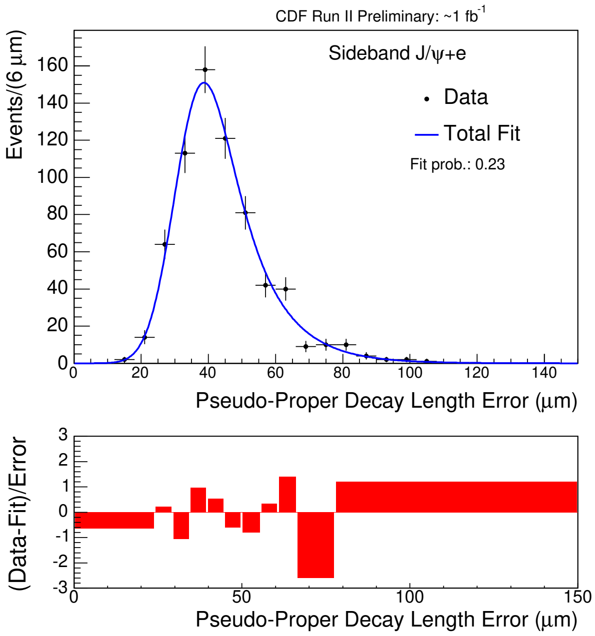

Figure 10: Fit of σ_{ct^*} for events in the J/ψ sideband region.

Parameter	Fit Value	Error
P_0	6.93	0.46
P_1	11.5	0.7
P_2	32.3	0.6

Table 5: Parameters from σ_{ct^*} fit of events in J/ψ sidebands.

3.2 Fake Electron Background

As mentioned previously this background comes from J/ψ+hadron events where the hadron looks sufficiently like an electron to pass our electron likelihood cut. To model this background we begin with the J/ψ+track sample, which is the same as the $J/\psi + e$ sample of signal candidates, but with the electron likelihood cut removed. We use dE/dx and TOF information from the third tracks in the J/ψ+track sample to estimate the percentage of third tracks that are one of the three long lived charged hadrons (pions, kaons and protons). We then use pure samples of pions, kaons and protons to estimate the probability that a given hadron will pass the electron likelihood cut, which we call the fake rate. Applying the fake rates and measured particle fractions to third tracks in the J/ψ+track sample, we can reweight the events in that sample to get an estimate of the fake electron background. We also fit the reweighted ct^* and σ_{ct^*} distributions to give a model for this background to be used in our lifetime fit of $J/\psi + e$ signal candidates.

3.2.1 Fake Electron Rates

To estimate the probability for a hadron to be identified as an electron we look at samples where we can positively identify a hadron as a decay product in a fully reconstructed system of particles with a narrow mass peak. For pions and kaons, we have used the decay chain $D^{*+} \to D^0\pi^+ \to \pi^+K^-\pi^+ + c.c.$ where the charge of the soft pion from D^* decay is used to identify the D^0 children. We are then able to find the probability that one of the D^0 children will pass our muon requirements. For protons, we have looked at $\Lambda \to P^+\pi^- + c.c.$ decays where the proton is identified as the decay product with the higher momentum. The details of the fake probability calculations can be found in Appendix A and are summarized in Figure 11.

3.2.2 J/ψ+track Third Track Particle Fractions

As with the muon channel analysis, we use dE/dx and TOF to measure the sample composition of third tracks in the J/ψ+track sample. We do this in three ct^* regions, since the physics sources of events can vary by region:

1. $ct^* < 0\mu m$ - This region consists mostly of prompt J/ψ from $c\bar{c}$ production, vertexed with a third track.
2. $0 < ct^* < 150\mu m$ - This region contains prompt J/ψ+track, events where the J/ψ and track come from different b jets and events where both come from the same b jet.
3. $ct^* > 150\mu m$ - This region contains mostly J/ψ+track from a single b jet.

. The details of the procedure for estimating the particle fractions can be found in Appendix B, while Figure 12 summarizes the results.

3.2.3 Fake Electron Normalization

Using the fake electron rates and particle composition fractions we can estimate the number of fake electron events by weighting the events in the J/ψ+track sample. We subtract the J/ψ sideband components from the J/ψ+track sample to avoid double counting with the fake J/ψ background. Doing this we estimate 312.0 ± 4.1 events.

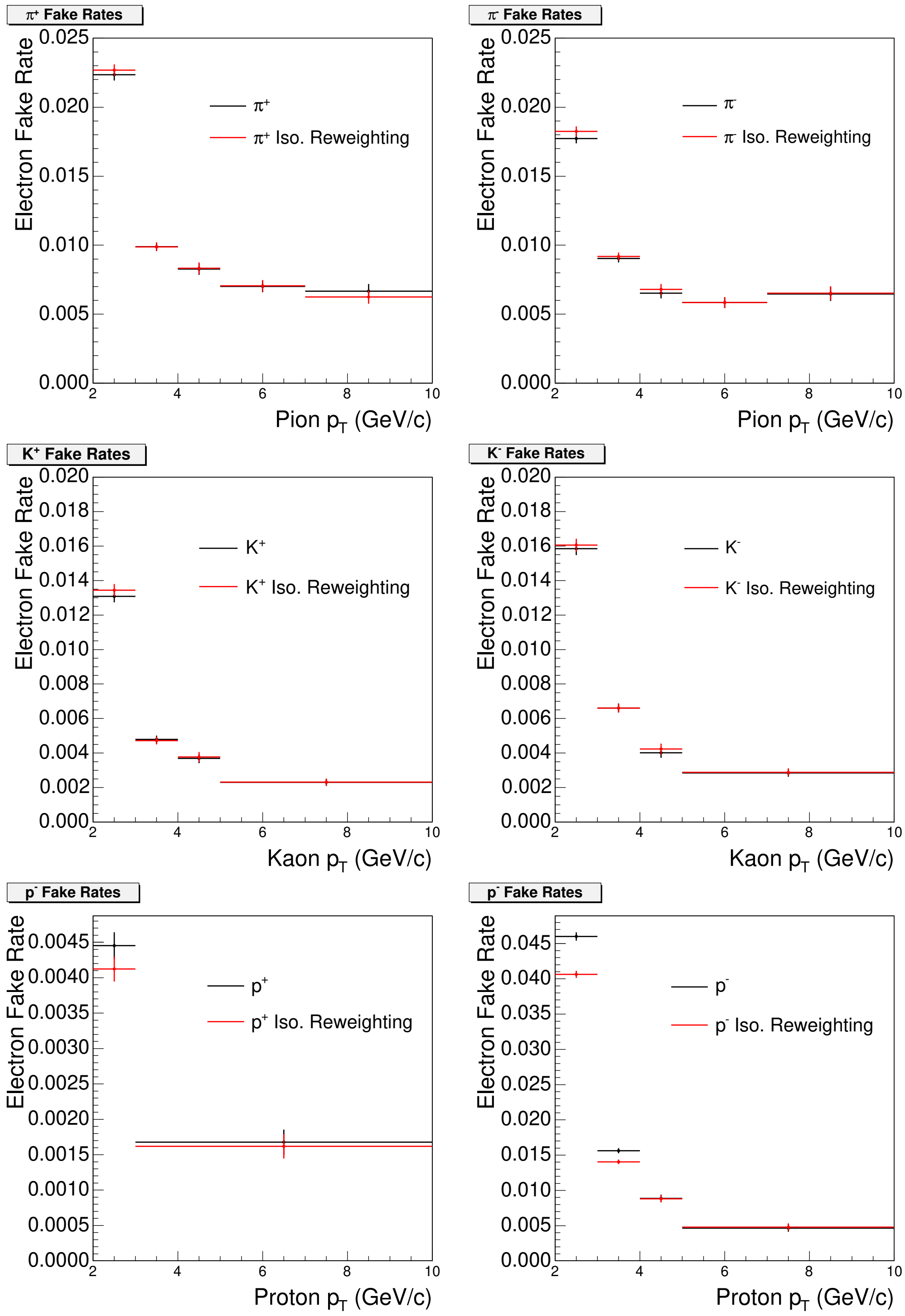

Figure 11: p_T dependent probabilities for a hadron to fake an electron. Top: pions. Middle: kaons. Bottom: protons.

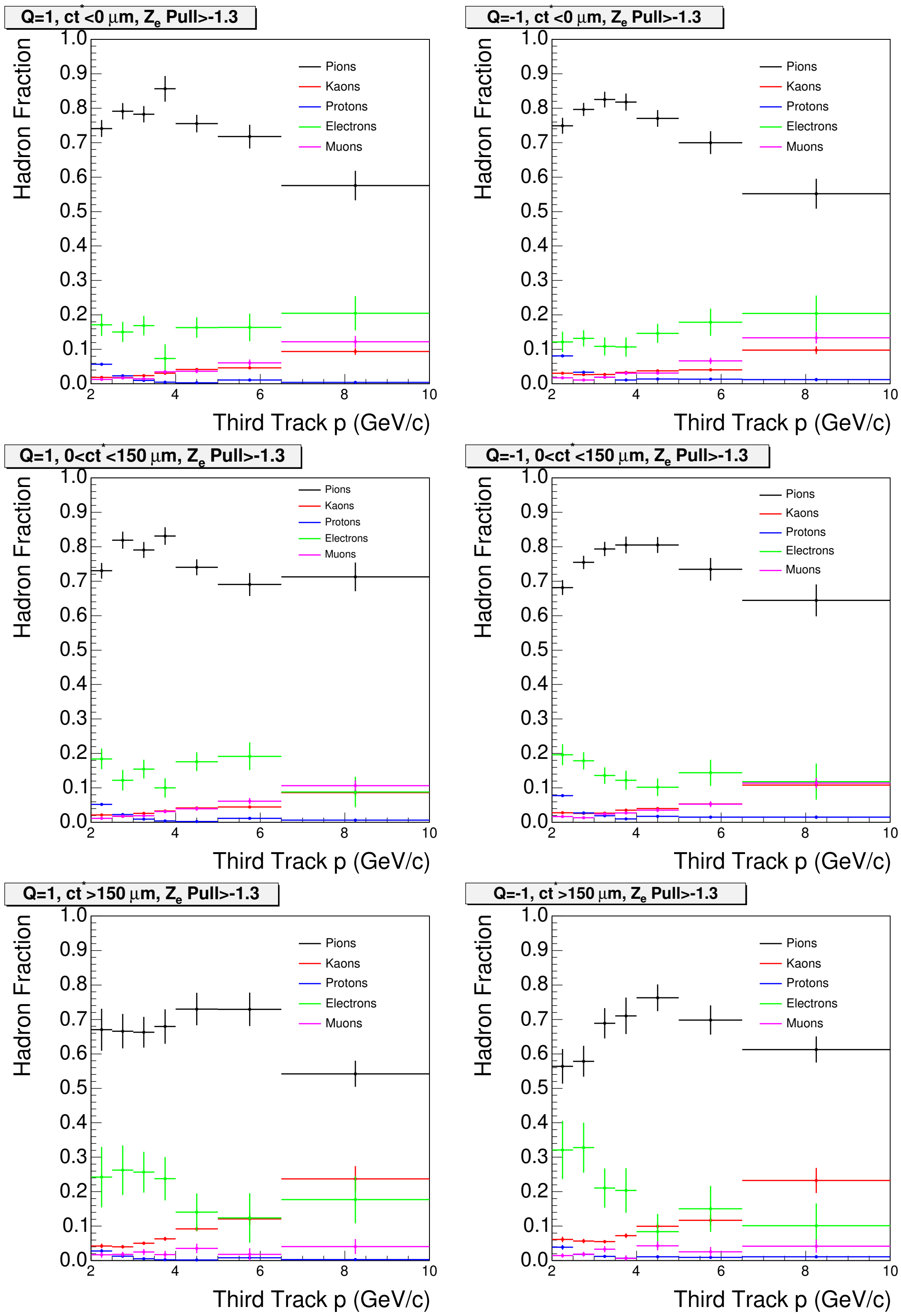

Figure 12: Particle composition fractions for third tracks in the J/ψ+track sample as a function of the third track momentum. Left are positive charge, right are negative charge. Top row is $ct^* < 0\ \mu m$, middle row is $0 < ct^* < 150\ \mu m$ and bottom row is $ct^* > 150\ \mu m$.

3.2.4 Fake Electron ct^*

We fit the weighted J/ψ+track sample to get the ct^* distribution for the fake electron background. As mentioned previously, we do not want to double count fake J/ψ events where the third lepton is a fake electron. For the fits of ct^* and σ_{ct^*} we first fit the sideband J/ψ+track events weighted by the fake electron rates. We then constrain the J/ψ background component while fitting in the J/ψ signal region, using the fit results from the J/ψ sideband regions.

To extract the fake J/ψ+fake electron ct^* PDF from the fake J/ψ+track (J/ψ sideband events matched with a third track) sample, we need to be able to write a likelihood function which describes the fake J/ψ+track sample in terms of the fake J/ψ+fake electron PDF and our previously determined fake electron probabilities. This can be done with a function of the form:

$$L = \prod_i \frac{N_i}{W_{FF}} F_{FF}(ct^*_i, \sigma_i)$$

The index i is over the fake J/ψ+track events, $F_{FF}(ct^*_i, \sigma_i)$ is the fake J/ψ+fake μ PDF for which we wish to extract parameter values, $1/W_{FF}$ is the inverse of the expected fake probability, and N_i is a normalization constant defined such that:

$$\int_{-\infty}^{\infty} \frac{N_i}{W_{FF}} F_{FF}(ct^*, \sigma_i) d(ct^*) = 1$$

$F_{FF}(ct^*, \sigma)$ can be written in terms of the fit parameters as:

$$F_{FF}(ct^*, \sigma) = [F_0\delta(ct^*) + \frac{F_1}{ct_1} e^{-\frac{ct^*}{c\tau_1}}\theta(ct^*) + \frac{F_2}{c\tau_2} e^{\frac{ct^*}{c\tau_2}}\theta(ct^*) + \frac{F_3}{c\tau_3} e^{-\frac{ct^*}{c\tau_3}}\theta(ct^*) + \frac{F_4}{c\tau_4} e^{\frac{ct^*}{c\tau_4}}\theta(-ct^*) + \frac{F_5}{c\tau_5} e^{\frac{ct^*}{c\tau_5}}\theta(-ct^*)] \otimes \frac{1}{\sqrt{2\pi}s\sigma} e^{-\frac{1}{2}(\frac{ct^*}{s\sigma})^2}$$

The functional form of this PDF is motivated by our expectation of prompt and exponential components for the background, although the specific combination of terms is chosen for the best empirical result.

We now fit ct^* for fake J/ψ+track events and resulting $F_{FF}(ct^*_i, \sigma_i)$ can be seen in Figure 13 overlaid on the fake J/ψ+track ct^* sample where the fake probabilities have been applied event by event. The resulting parameter values are listed in Table 6.

Having extracted parameters to constrain the fake J/ψ+fake electron contribution we now look in the J/ψ signal region. Here we can write our likelihood function in terms of a fake J/ψ+fake electron PDF and a real J/ψ+fake electron PDF:

$$L = e^{-\frac{1}{2}V_{FF}C_{FF}^{-1}V_{FF}} \prod_i [F_{sig}\frac{N^i_{FE}}{W_{FE}} F_{FE}(ct^*_i, \sigma_i) + (1 - F_{sig})\frac{N^i_{FF}}{W_{FF}} F_{FF}(ct^*_i, \sigma_i)]$$

F_{FF} and $1/W_{FF}$ are the same as in the previously, and constrained by V_{FF} and C_{FF} from the previous fit. $1/W_{FE}$ is defined in the same manner as $1/W_{FF}$, but using events in the J/ψ signal region. N^i_{FE} and N^i_{FF} normalize the real J/ψ+fake electron

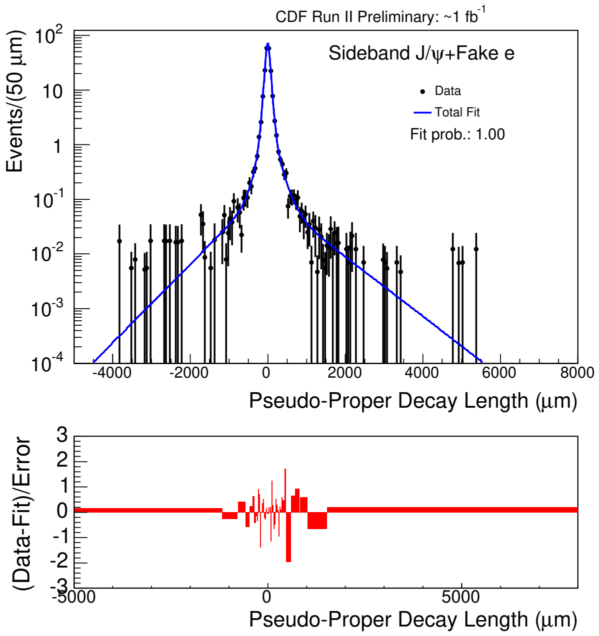

Figure 13: Right: Fit of fake J/ψ+fake electron ct^* distribution using J/ψ+track sideband events.

Parameter	Fit Value	Error
s	1.167	0.024
F_0	0.600	0.357
$c\tau_1$	797	254
F_1	0.0088	0.0044
$c\tau_2$	46.2	12.2
F_2	0.157	0.041
$c\tau_3$	164	75
F_3	0.043	0.003
$c\tau_4$	126	72
F_4	0.039	0.004
$c\tau_5$	51.0	13.2
F_5	0.140	0.029

Table 6: Parameters describing fake J/ψ+fake electron ct^* distributions from fit of J/ψ+track sideband data. $c\tau$ are in μm

and fake J/ψ+fake electron terms respectively, while F_{sig} defines the fraction of real J/ψ events. $F_{FE}(ct_i^*, \sigma_i)$ is the PDF for real J/ψ+fake electron events and can be described in terms of its parameters:

$$F_{FE}(ct^*, \sigma) = [F_0\delta(ct^*) + \frac{F_+}{c\tau_+}e^{\frac{-ct^*}{c\tau_+}}\theta(ct^*) + \frac{F_{++}}{c\tau_{++}}e^{\frac{-ct^*}{c\tau_{++}}}\theta(ct^*) + \frac{F_-}{c\tau_-}e^{\frac{ct^*}{c\tau_-}}\theta(-ct^*)] \otimes \frac{1}{\sqrt{2\pi}s\sigma}e^{-\frac{1}{2}(\frac{ct*}{s\sigma})^2}$$

The functional form of one prompt component and two positive lifetime components is expected as the J/ψs in the sample can be created at the primary interaction point (prompt) or through B decays (long lived). An additional negative lifetime component is added to improve agreement with data.

We fit our PDF to the J/ψ+track sample to extract parameters for $F_{FE}(ct^*, \sigma)$ which can be found in Table 7. Figure 14 shows the resulting $F_{FE}(ct^*, \sigma)$ and $F_{FF}(ct^*, \sigma)$ functions overlaid on the J/ψ+track sample where the fake probabilities have been applied event by event.

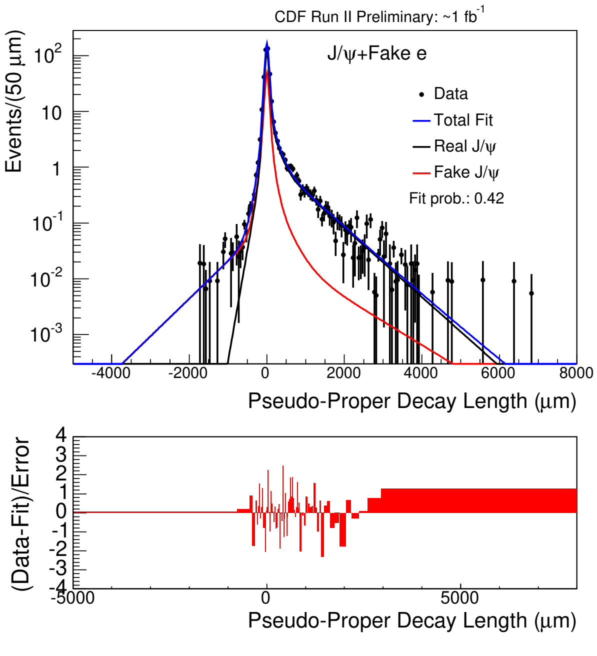

Figure 14: Fit of J/ψ+fake electron ct^* distribution using J/ψ+track events.

3.2.5 Fake Electron σ_{ct^*}

For the fits to extract our real J/ψ+fake PDF for σ_{ct^*} we follow the same procedure as in the previous section, but changing the PDFs. The PDFs for σ_{ct^*} of real J/ψ+fake

Parameter	Fit Value	Error
s	1.274	0.016
F_0	0.831	0.017
$c\tau_{++}$	675	45
F_{++}	0.064	0.007
$c\tau_{+}$	138	25
F_{+}	0.083	0.008
$c\tau_{-}$	114	31
F_{-}	0.019	0.007

Table 7: Parameters for the real J/ψ+fake electron ct^* distributions from fit of J/ψ+track data. $c\tau$ are in μm

electron and fake J/ψ+fake electron are defined as $P_{FE}(\sigma)$ and $P_{FF}(\sigma)$. They have the same functional form:

$$P_{XX}(\sigma) = \frac{1}{\sqrt{2\pi}P_0} e^{-\frac{1}{2}(\frac{\sigma}{P_0})^2} \otimes [\frac{P_5}{P_1} e^{-\frac{(\sigma-P_2)}{P_1}} + \frac{(1-P_5)}{P_3} e^{-\frac{(\sigma-P_4)}{P_3}}]$$

The form is, once again, chosen empirically to allow for good agreement with the distributions in data. The resulting fits of the $\sigma(ct^*)$ distribution for the J/ψ sideband regions and subsequently the signal region can be seen in Figure 15. The extracted parameter values for the PDF, $P_{FE}(\sigma)$, are listed in Table 8.

Parameter	Fit Value	Error
P_0	4.37	0.15
P_1	10.48	1.67
P_2	22.52	0.39
P_3	10.43	0.41
P_4	32.17	0.311
P_5	0.352	0.043

Table 8: Parameters for the real J/ψ+fake electron σ distributions from fit of J/ψ+track data.

3.3 Residual Conversion Background

As discussed previously, one source of electrons are e^+e^- pairs that are created either when a photon converts or a light neutral meson decays with e^+e^- in the final state. We attempt to identify and remove these types of electrons by finding the partner track that satisfies the veto cuts outlined in Section 2.2.3. Since this procedure will not find e^+e^- pairs with an efficiency of 1, there will be a residual background left

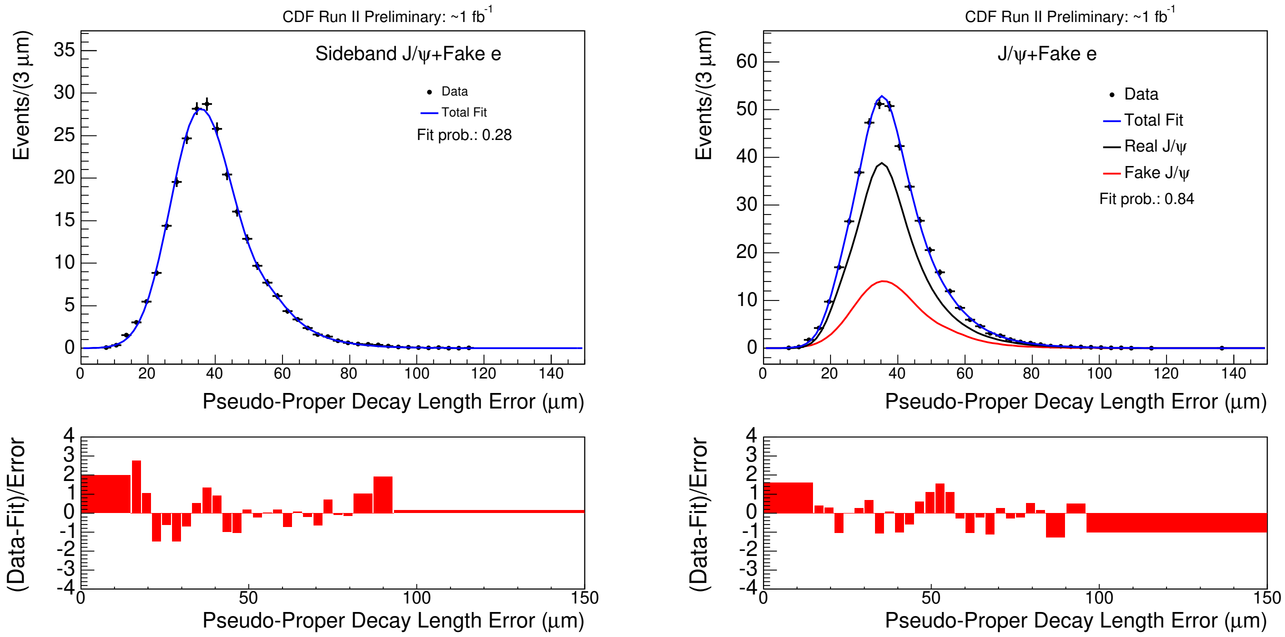

Figure 15: Left: Fit of fake J/ψ+fake electron σ distribution. Right: Fit of J/ψ+fake electron σ distribution using J/ψ+track events.

which we call residual conversions (we will show that about 15% of the e^+e^- are not actually conversion events, but light meson decays).

To estimate the size of this background, we use a Pythia Monte Carlo of $B \to J/\psi + X$ decays where the event can contain a photon or a light neutral meson. We select events where e^+e^- pairs are present and apply the cuts for our $J/\psi + e$ candidates. Using truth information we can identify the source of the e^+e^- and measure the efficiency for said pair to be identified and vetoed. Having measured the efficiency for identifying events where the electron comes from an e^+e^- pair, we can calculate the residual background from the events that are vetoed. We can also use the vetoed events as a model for the residual background ct^* and σ_{ct^*} distributions.

Since the efficiencies for e^+e^- removal are measured using a Pythia Monte Carlo sample, we will be sensitive to differences between data and Monte Carlo in reconstructing the partner track. To identify and correct for any difference, we study the signed impact parameter of electrons in data which can be used to estimate a conversion identification efficiency that can be compared to Monte Carlo.

3.3.1 e^+e^- Identification Efficiency

To measure the efficiency for identifying and vetoing e^+e^- pairs we use a Pythia Monte Carlo sample generated with msel 5 and Tune A for the underlying event, where B decays were forced to final states with a J/ψ. Using truth information, we select events that have either a photon conversion or light neutral meson decay to

e^+e^-. After applying our analysis cuts we split the sample into these two classes and then measure the efficiency to identify e^+e^- pairs using our veto cuts on Δ_{xy} and $\Delta(cot(\theta))$. Figure 16 shows the conversion identification efficiencies as a function of p_T.

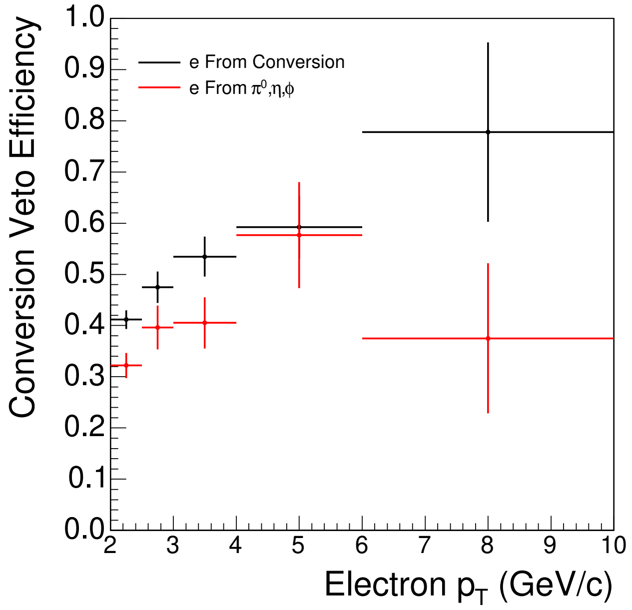

Figure 16: Efficiency for identifying $J/\psi + e$ events where the electron comes from an e^+e^- pair. Efficiencies come from a Pythia Monte Carlo sample.

3.3.2 Sources of e^+e^-

In the study of e^+e^- identification efficiencies in the previous section we saw a significant disparity between the two sources. To accurately estimate the residual background, we will need to know the fraction of each source for e^+e^- identified events in the $J/\psi + e$ sample. To do this we use the measured radius of origin for the e^+e^- pair, R_{ee}. Since conversions happen when a photon interacts with material, ignoring measurement resolution, we should expect to only find pairs that originate beyond the beam pipe at $r = 1.25$ cm. Neutral light mesons, on the other hand, have a lifetime typical of strong interactions and tend to come from the primary or secondary vertices. Therefore, we expect R_{ee} from neutral light meson decays to be near 0 on the scale of centimeters. Figure 17 shows R_{ee} in Pythia for the two sources, and verifies our intuition.

We expect the sample of $J/\psi + e$ events in data, where the e^+e^- pair is identified, to show a distribution of R_{ee} that is a combination of those typical of the two sources. Since the R_{ee} distribution for conversion events is irregular due to the distribution of material in the detector, we do not try to fit the Pythia distributions to data. Instead we count the fraction of events with $r < 1.0\ cm$ and use that to estimate the fractions for the two sources. This can be can be done starting with the following equation:

$$N^R_{data} = F^R_{conv} \times N^D_{conv} + F^R_{\pi^0} \times N^D_{\pi^0}$$

Here N^R_{data} is the number of e^+e^- events in data with $r < 1.0\ cm$, F^R_{conv} and $F^R_{\pi^0}$ are the fractions of conversions and light meson decays in the Pythia sample that have $r < 1.0\ cm$, and N^D_{conv} and $N^D_{\pi^0}$ are the numbers of e^+e^- from the two sources in data. We can divide both sides by the total number of events to get the same equation written in fractions:

$$F^R_{data} = F^R_{conv} \times F^D_{conv} + F^R_{\pi^0} \times F^D_{\pi^0}$$

Since $F^D_{conv} + F^D_{\pi^0} = 1$ we can solve for $F^D_{\pi^0}$ to get:

$$F^D_{\pi^0} = \frac{F^R_{conv} - F^R_{data}}{F^R_{conv} - F^R_{\pi^0}}$$

Figure 18 shows R_{ee} for $J/\psi + e$ events in data where the electron is identified as coming from e^+e^-, and gives us F^R_{data}. Plugging in the numbers we get the fraction of e^+e^- in $J/\psi + e$ events from light neutral meson decays $F^D_{\pi^0} = 0.140 \pm 0.047$, which is consistent with the fraction of 0.1 seen in Pythia.

3.3.3 Checking Monte Carlo with Signed Impact Parameter

We can compare the efficiency for identifying conversion events in Pythia to that in data by looking at the signed impact parameter, d_0^{sign}, of conversion candidates in data as shown in CDF Note 6263 [4]. To summarize the procedure, the signed impact parameter is defined as the impact parameter of a track, d_0, times its charge, q. In a photon conversion, the e^+e^- pair will tend to have a very small angle relative to the photon. In the majority of cases where the photon originates at the primary vertex, the impact parameter of the track will be largely determined by the charge of the track, meaning that electrons and positrons from conversion events will tend to have a positively signed d_0^{sign}. This can be seen in the illustration in Figure 19.

Electrons from other sources, however, have impact parameters that are more strongly determined by the opening angle of the decay at which it originates, leaving very little asymmetry in the d_0^{sign} distribution. Figure 20 shows d_0^{sign} for electrons in various sources of $J/\psi + e$ which are estimated using the methods outlined in this note. The samples shown here are similar to our $J/\psi + e$ signal candidates, but the vertex, opening angle and mass cuts have been removed to increase the sample sizes.

Figure 21 shows the d_0^{sign} for $J/\psi + e$ events in data, which is a combination of the sources shown in the previous figure. The expected asymmetry is present, and

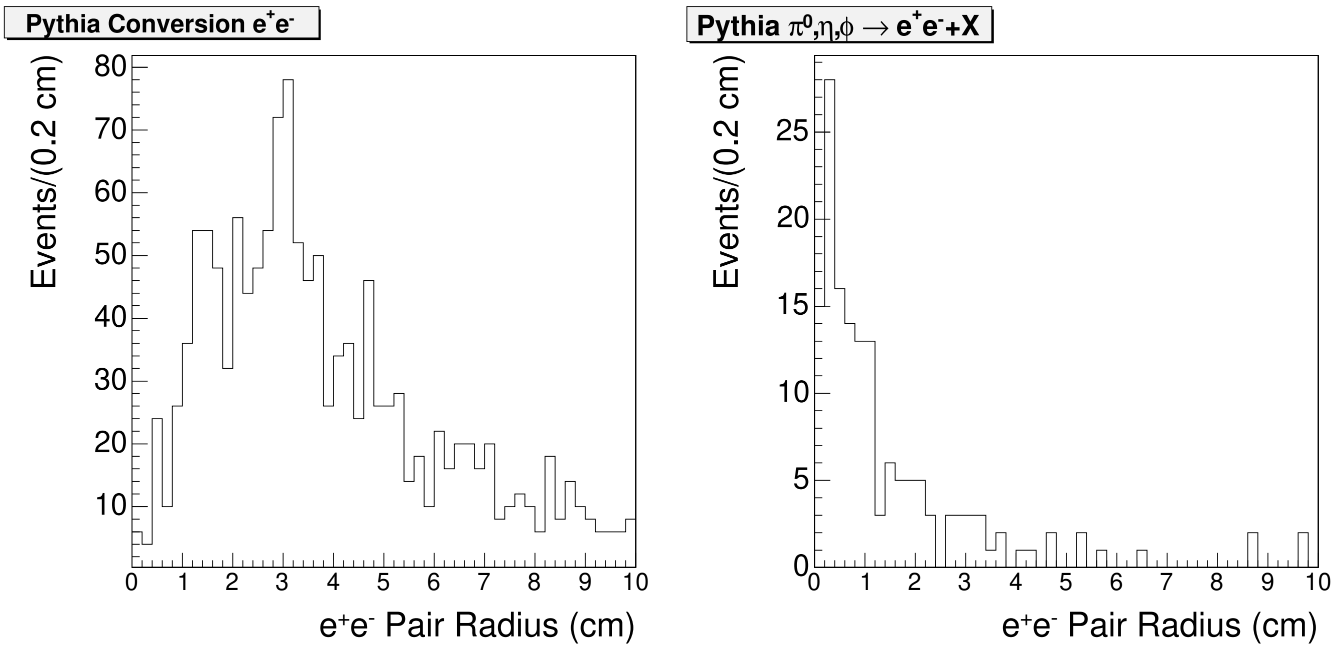

Figure 17: R_{ee} of e^+e^- pairs in Pythia. Left: e^+e^- from photon conversion. Right: e^+e^- from light neutral meson decays

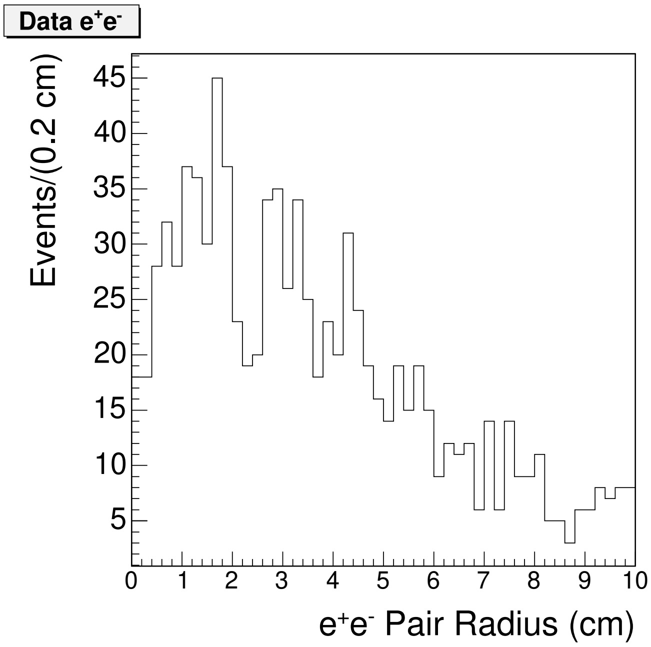

Figure 18: R_{ee} of e^+e^- pairs in data.

we can count the size of the asymmetry and use that as an estimate for a particular type of conversion electrons. We can then apply the conversion removal cuts and recount the asymmetry to find the efficiency for removing these conversion events. In practice we must first subtract out the contribution to the asymmetry from the other electron sources. Since we do not know the normalization of $J/\psi + e$ events from B_c decays, we only count the asymmetry in the $|d_0^{sign}| > 0.1cm$ regions, which excludes the B_c events. Figure 22 shows the efficiency for removing conversion events that are counted from the asymmetry and compares it to the expected efficiency in Pythia. All bins but the lowest p_T bin are within 1 sigma. In the lowest p_T bin we extract a correction of 0.86 for the conversion veto efficiency as determined by Pythia. We will discuss the systematic effect of this correction later.

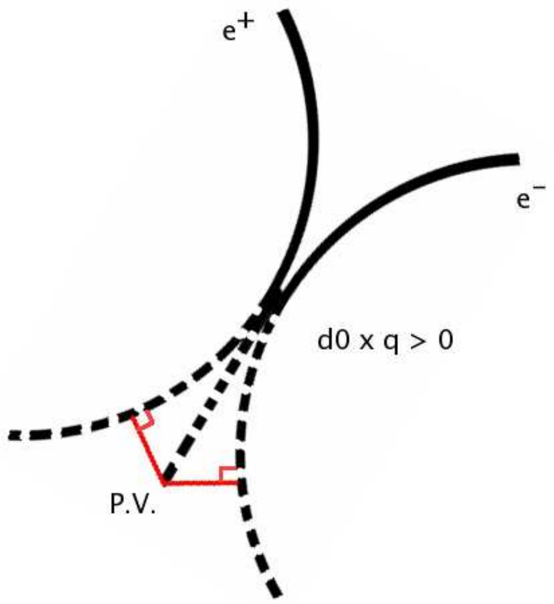

Figure 19: Illustration of a photon conversion. The small opening angle means the sign of the impact parameter will tend to be the same as the particles charge.

3.3.4 Residual Conversion Normalization

Now that we have the veto efficiencies for e^+e^- events, we can estimate the residual background using the following equation:

$$N_{res} = \sum_{p_T} F_{\pi^0} \frac{(1-\epsilon_{\pi^0})}{\epsilon_{\pi^0}} N_{veto} + (1 - F_{\pi^0}) \frac{(1-\epsilon_{conv})}{\epsilon_{conv}} N_{veto}$$

Here the efficiencies and number of vetoed events are evaluated for each p_T bin and the expression is summed over the p_T bins. We must also take care to avoid double

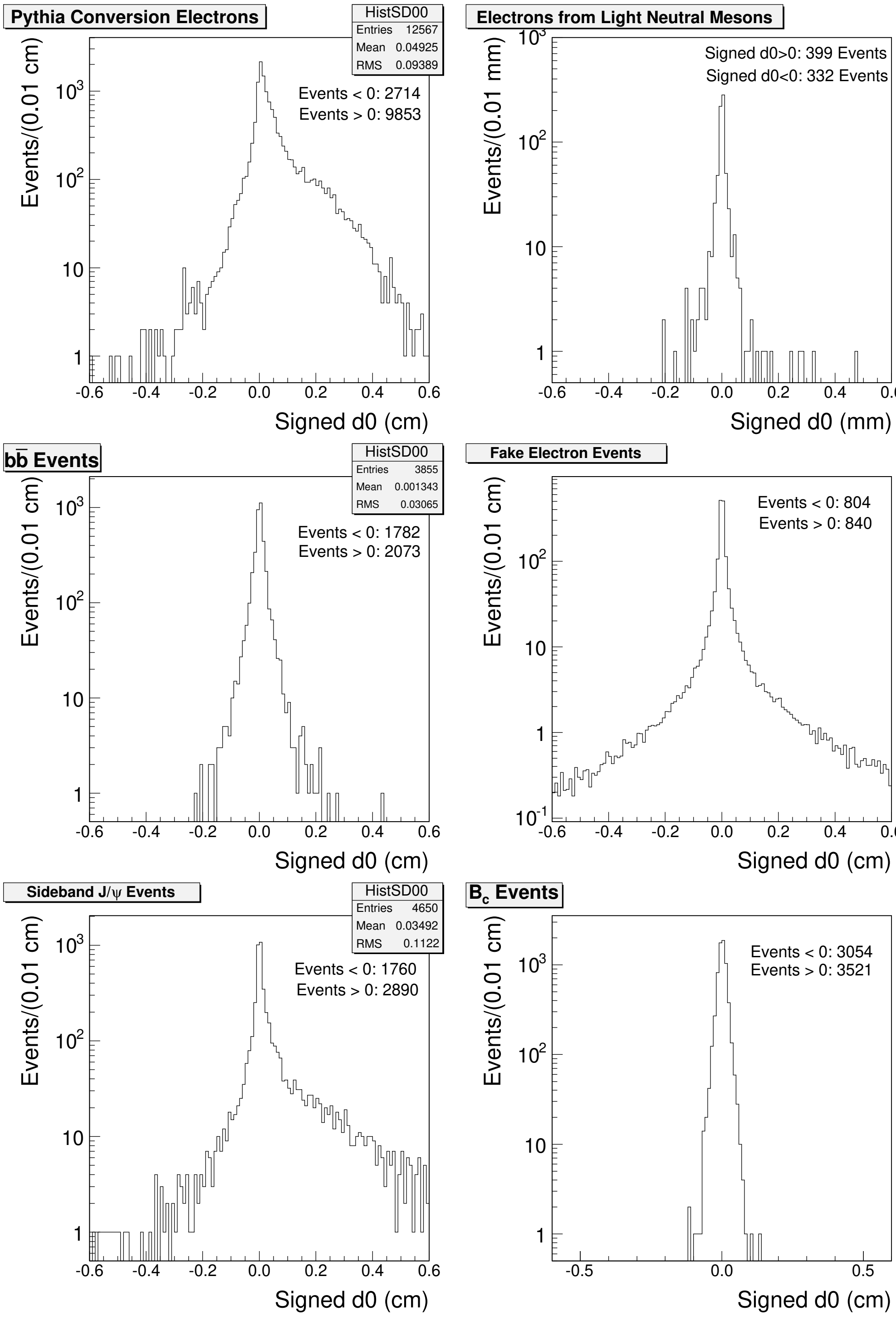

Figure 20: d_0^{sign} for electrons in $J/\psi + e$ events with various electron sources. Top left: conversion events in Pythia. Top Right: light neutral meson decays in Pythia. Middle Left: $b\bar{b}$ events in Pythia. Middle Right: fake electron events. Bottom Left: fake J/ψ events. Bottom Right: B_c decays from BGenerator.

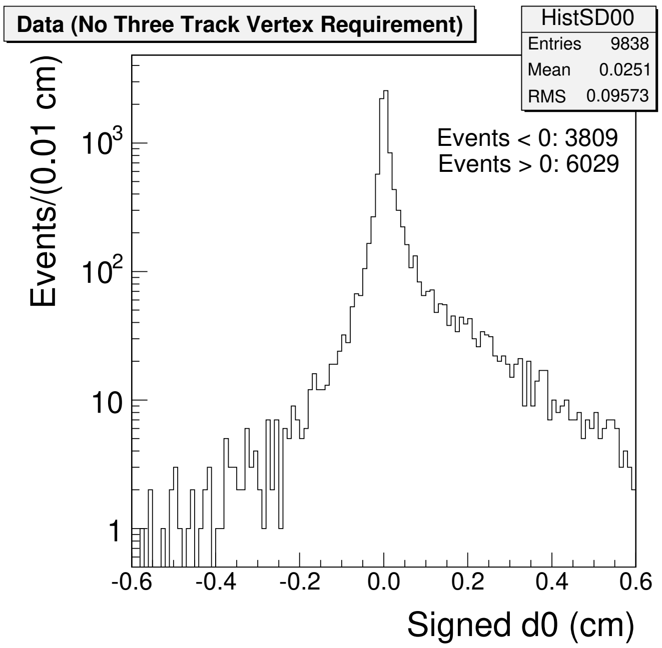

Figure 21: d_0^{sign} for electrons in $J/\psi + e$ events in data.

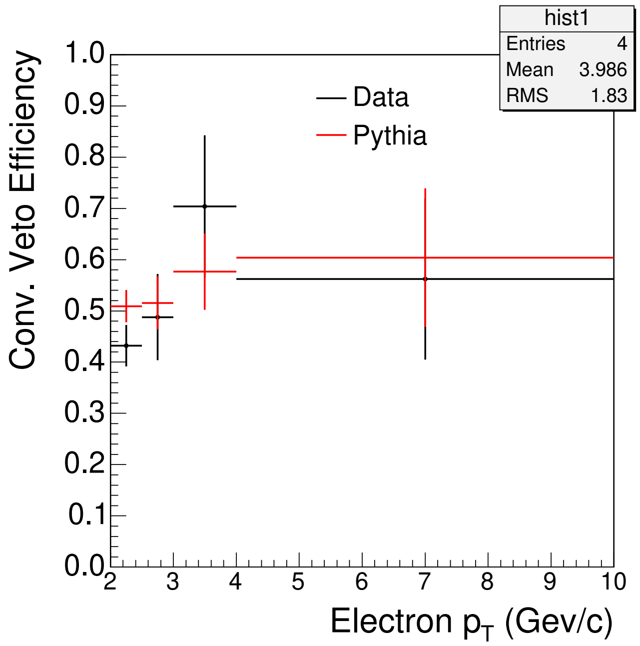

Figure 22: Efficiency of the conversion veto determined using d_0^{sign} asymmetries, compared to the efficiency from Pythia.

counting with the fake J/ψ background. To this end, we apply the above equation to the J/ψ sideband regions as well and subtract that component out of the residual conversion estimate. Following this procedure we find a residual conversion background estimate of 416.8 ± 41.5 events based on 368 vetoed events in the J/ψ signal region.

3.3.5 Residual Conversion ct^* Fit

We use the vetoed conversion events to model the ct^* of the residual conversion background, but it may be the case that our conversion veto efficiency has a ct^* or σ_{ct^*} dependence. Figure 23 shows profile histograms of the reweighting of vetoed events as a function of ct^* and σ_{ct^*}. Since there is a dependence, we must fit the reweighted distribution of events.

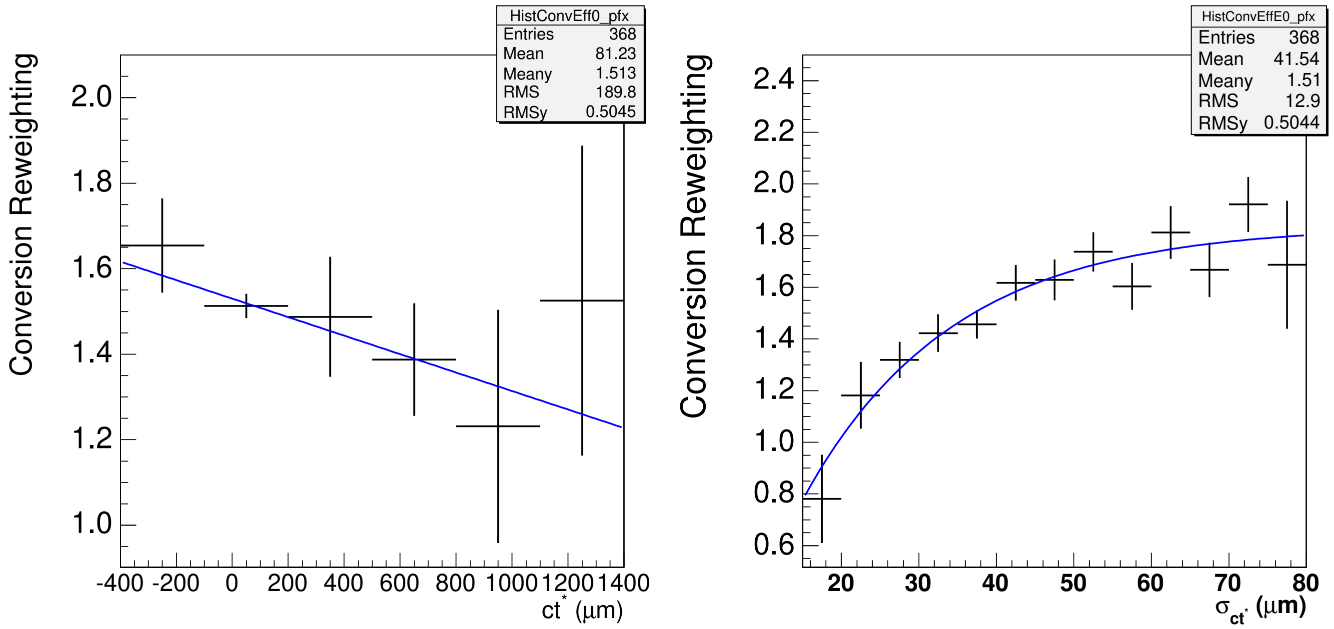

Figure 23: Conversion veto efficiency as a function of ct^* (left) and σ_{ct^*} (right).

As mentioned in the previous section, we want to avoid double counting with the fake J/ψ background, so we need to constrain the contribution from those events in the lifetime fit. Unfortunately, the vetoed conversion events in the J/ψ sidebands are not numerous enough to place a good constraint on their ct^* distribution. Therefore, we use the ct^* distribution of all $J/\psi+e$ events in the J/ψ sideband regions. Figure 24 shows the ct^* model for sideband $J/\psi + e$ events overlayed on those events where the electron is identified as a conversion. While the χ^2 probability is only 6%, we find that alternate attempts to fit this distribution do not return significantly better probabilities.

With a model for the fake J/ψ contribution to the residual background, we can proceed to fitting the events in the J/ψ signal region. As previously mentioned we must include the conversion reweighting ($W_{RC}(ct^*)$) in the fit:

$$L = \prod_i \frac{N_i}{W_{RC}} F_{RC}(ct_i^*, \sigma_i)$$

Where the normalization condition is required:

$$\int_{-\infty}^{\infty} \frac{N_i}{W_{RC}} F_{RC}(ct^*, \sigma_i) d(ct^*) = 1$$

We use a PDF of the form:

$$F_{RC}(ct^*, \sigma) =$$
$$F_{sig}[F_{prmt}\delta(ct^*) + \frac{F_+}{c\tau_+} e^{\frac{-ct^*}{c\tau_+}} \theta(ct^*)] \otimes \frac{1}{\sqrt{2\pi} s\sigma} e^{-\frac{1}{2}(\frac{ct^*}{s\sigma})^2} + (1 - F_{sig}) F_{FJ}(ct^*, \sigma)$$

The fit to data can be seen in Figure 25 and the parameter values are listed in Table 9.

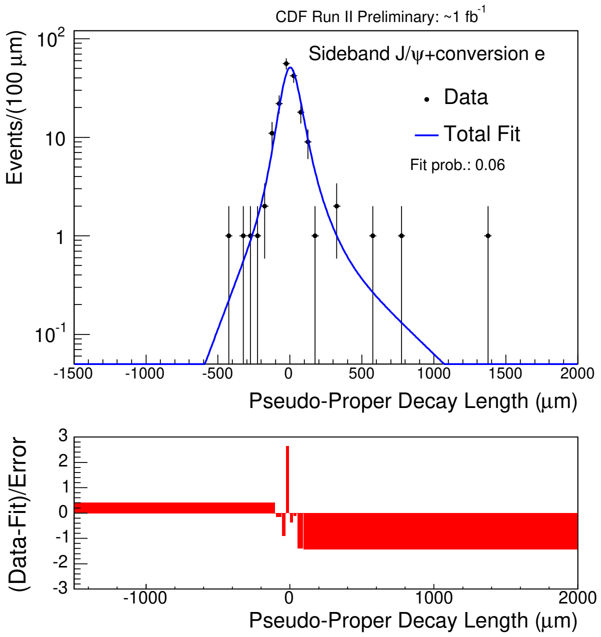

Figure 24: Fit of sideband $J/\psi + e$ events overlayed on sub-sample where the electrons are identified as conversion electrons.

3.3.6 Residual Conversion σ_{ct^*}

For the σ_{ct^*} we following the procedure for fitting reweighted events outlined in the previous section. We first fit the residual events in the J/ψ sideband regions. For this we use a PDF of the form:

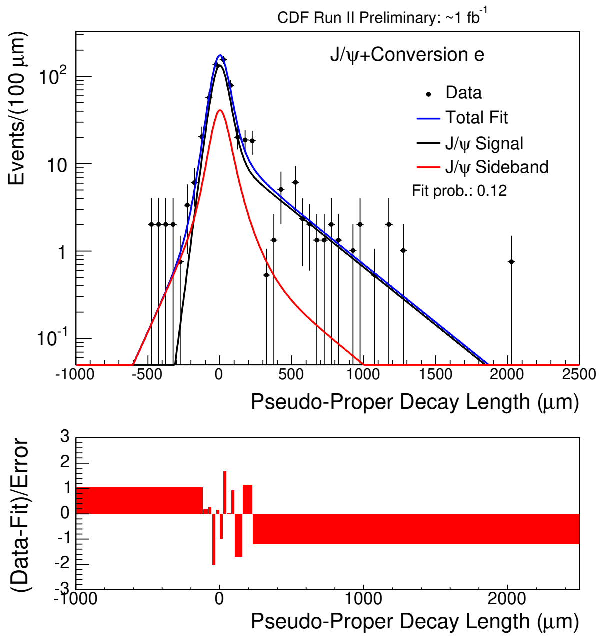

Figure 25: Fit of identified conversion events. Red is constrained fake J/ψ component.

Parameter	Fit Value	Error
s	1.31	0.02
F_{prmt}	0.790	0.067
F_{+}	0.221	0.040
$c\tau_{+}$	328	53
F_{sig}	0.776	0.027

Table 9: Parameters describing residual conversion ct^{*} fit. $c\tau$ are in μm

$$P_{FJ/RC}(\sigma) = \frac{1}{\sqrt{2\pi}P_0} e^{-\frac{1}{2}(\frac{\sigma}{P_0})^2} \otimes \frac{1}{P_1} e^{-\frac{(\sigma - P_2)}{P_1}}$$

The resulting fit can be seen in Figure 26 and the parameters are listen in Table 10. We then proceed to fit the events in the J/ψ signal regions, constraining the fake J/ψ events with the result of our fit from the sidebands. We use the PDF:

$$P_{RC}(\sigma) = F_{sig} \frac{1}{\sqrt{2\pi}P_0} e^{-\frac{1}{2}(\frac{\sigma}{P_0})^2} \otimes \frac{1}{P_1} e^{-\frac{(\sigma - P_2)}{P_1}} + (1 - F_{sig}) P_{FJ/RC}(\sigma)$$

The resulting fit can be seen in Figure 27 and the parameters are listed in Table 11.

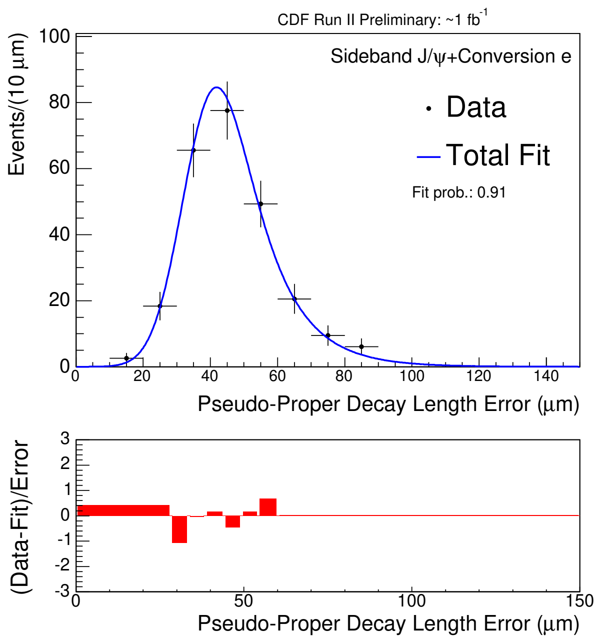

Figure 26: Fit of identified conversion events in the J/ψ sideband region.

Parameter	Fit Value	Error
P_0	8.17	1.04
P_1	11.6	1.9
P_2	34.9	1.7

Table 10: Parameters from σ_{ct^*} fit of conversion events in J/ψ sidebands.

3.4 $b\bar{b}$ Background

The events in our $b\bar{b}$ background consist of a J/ψ from one b jet and a electron from another, where the three tracks happen to pass our vertexing requirement. Since we

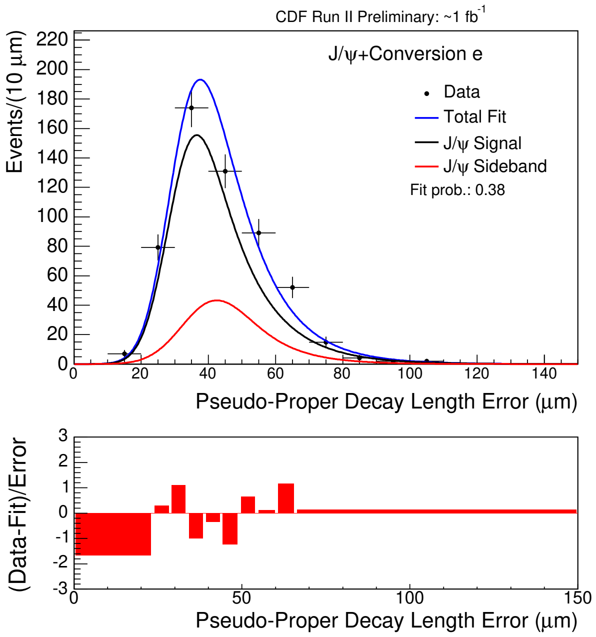

Figure 27: σ_{ct^*} fit of identified conversion events. Red is constrained fake J/ψ component.

Parameter	Fit Value	Error
P_0	6.60	0.77
P_1	12.9	1.5
P_2	29.9	1.3

Table 11: Parameters from residual conversion σ_{ct^*} fit.

have no method for constraining this background using data, we use a realistic Monte Carlo. We generate Pythia events with msel=1 (all tree level QCD) mode and select $b\bar{b}$. Events containing a $\bar{b}$ quark were forced to decay to a $J/\psi+X$, and the J/ψ was subsequently forced to decay to two muons. The mesons containing the b quark were allowed to decay according to the default decay table.

The Pythia $b\bar{b}$ background sample is normalized to give a prediction for data by fitting $B^{\pm} \to J/\psi K^{\pm}$in both data and Pythia, which provides an estimate of the relative $b\bar{b}$ production in the two samples. In CDF Note 7420 we describe a method for tuning the Pythia $b\bar{b}$ sample to data by adjusting the relative QCD production processes [5]. This tuning was using in the muon channel lifetime measurement and will be used here as well.

3.4.1 $b\bar{b}$ Normalization

The $b\bar{b}$ background events are normalized to data by measuring their rate relative to $B^{\pm} \to J/\psi K^{\pm}$ decays and comparing the reconstructed $B^{\pm}$ peaks in data and the Pythia sample. Figure 28 shows the $B^{\pm}$ mass fits for data and the Pythia sample broken into its QCD production processes. The number of $b\bar{b}$ $J/\psi+e$ events in the tuned Pythia sample is $N_{bb} = 410$. Normalizing to data we predict 222.5 ± 11.2 events

3.4.2 $b\bar{b}$ Normalization Check

As described in note 8155, we can remove the vertex probability cut between the J/ψ and electron to get a sample enhanced in $b\bar{b}$. We then look at the impact parameter of the electron with respect to the J/ψ vertex to verify that our Pythia model is a good description for data. The comparison of data and predicted distributions can be seen in Figure 29. We see good agreement for $d_0(e - J/\psi) > 0.02\ cm$, where the $b\bar{b}$ background dominates, indicating that the method for normalizing the $b\bar{b}$ contribution is correct. At small values, we see an excess in data which can be attributed to $B_c \to J/\psi + e + X$ events.

3.4.3 $b\bar{b}$ ct^* Fits

The ct^* of $b\bar{b}$ $J/\psi + e$ events is fitted with a template that contains two positive exponential decays:

$$F_{bb}(ct^*, \sigma) = [\frac{F_+}{c\tau_+} e^{-\frac{ct_i^*}{c\tau_+}} \theta(ct^*) + \frac{(1-F_+)}{c\tau_{++}} e^{-\frac{ct_i^*}{c\tau_{++}}} \theta(ct^*)] \otimes \frac{1}{\sqrt{2\pi} s\sigma} e^{-\frac{1}{2}(\frac{ct^*}{s\sigma})^2}$$

The fitted ct^* distributions can be seen in Figure 30 while the fitted parameters are listed in Table 12. While one might think that the $b\bar{b}$ ct^* distributions should exhibit a lifetime typical of B meson lifetimes, this is not the case. This is because the probability of vertexing the J/ψ with an electron from the other b jet falls off as the L_{xy} of the J/ψ increases.

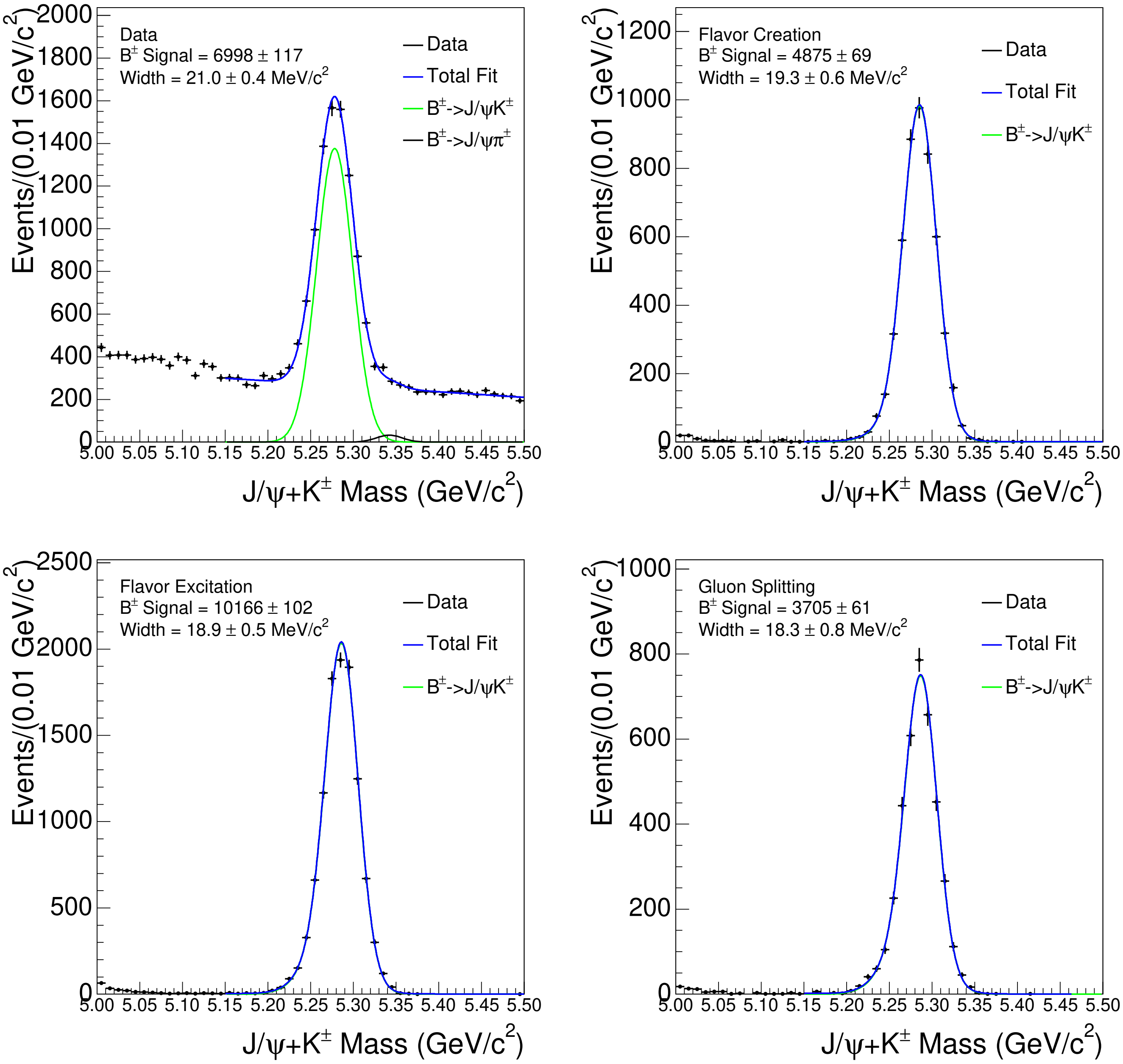

Figure 28: Fits of the $B^{\pm} \rightarrow J/\psi + K^{\pm}$ mass peak in: data with $B^{\pm} \rightarrow J/\psi + \pi^{\pm}$ component (top left), Pythia flavor creation (top right), Pythia flavor excitation (bottom left) and Pythia gluon splitting (bottom right).

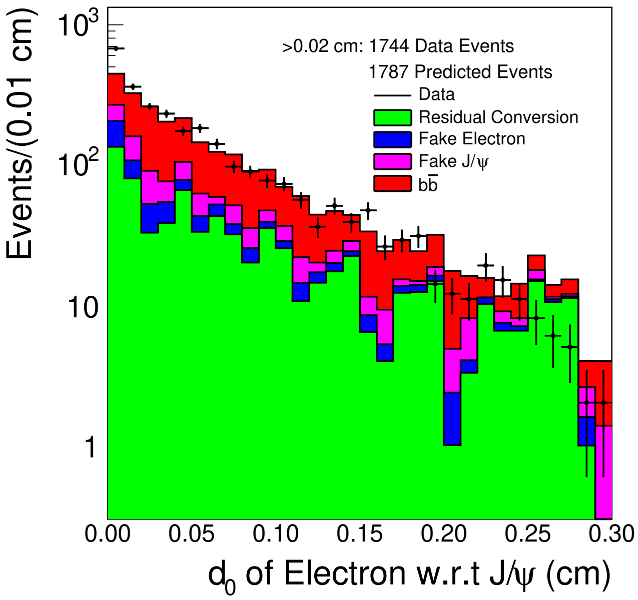

Figure 29: Impact parameter of the electron with respect to the J/ψ vertex in the non-vertexed sample. The histograms for the predicted background contributions are stacked.

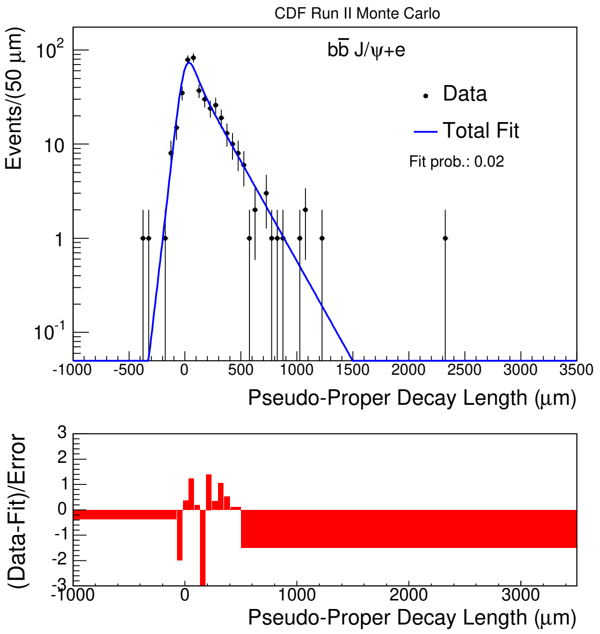

Figure 30: Fitted ct^* distributions for the $b\bar{b}$ $J/\psi + e$ events.

Parameter	Fit Value	Error
s	1.69	0.07
$c\tau_+$	20.8	11.4
F_+	0.29	0.07
$c\tau_{++}$	205	18

Table 12: Parameters from $b\bar{b}$ ct^* fit.

3.4.4 $b\bar{b}$ σ Fits

The σ_{ct^*} distributions of $b\bar{b}$ events is fitted with the template:

$$P_{bb}(\sigma) = \frac{1}{\sqrt{2\pi}P_0}e^{-\frac{1}{2}(\frac{\sigma}{P_0})^2} \otimes \frac{1}{P_1}e^{-\frac{(\sigma-P_2)}{P_1}}$$

The results of the fit can be seen in Figure 31 and the fitted parameters are listed in Table 13

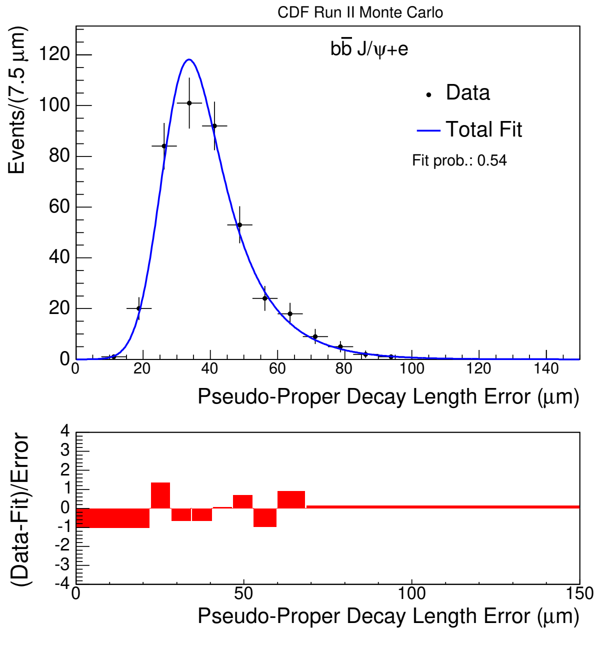

Figure 31: Fitted σ distribution for $b\bar{b}$ $J/\psi + e$ events.

3.5 Prompt Background

We do not directly constrain the prompt $J/\psi + e$ component of our background using data or Monte Carlo samples. To constrain the shape of the ct^* distribution we assume a Gaussian resolution function with per event scaled errors ($s\sigma$) of the form:

Parameter	Fit Value	Error
P_0	6.4	0.6
P_1	12.0	1.0
P_2	27.3	0.9

Table 13: Parameters from $b\bar{b}$ the σ_{ct^*} fit.

$$F_{PR}(ct^*, \sigma) = \frac{1}{\sqrt{2\pi} s\sigma} e^{-\frac{1}{2}(\frac{ct^*}{s\sigma})^2}$$

The single parameter, s, is extracted from a fit of ct^* in the J/ψ+track sample and is $s = 1.21 \pm 0.02$. As a systematic study, we will investigate the effect of a more complicated resolution function.

The normalization of the prompt background will be allowed to float in our fit of the $J/\psi + e$ events for the B_c lifetime.

3.5.1 Prompt σ_{ct^*} Fit

Determination of the σ_{ct^*} PDF for prompt events presents a problem, as we have no pure sample of prompt events. We do know that there is a large component of prompt J/ψ in the J/ψ+track sample. If we look in the negative ct^* region of the J/ψ+track sample and constrain the contribution from fake J/ψ using the J/ψ sideband regions, the remaining events will be predominantly prompt J/ψ+track. We use these events to model the σ_{ct^*} distribution for prompt $J/\psi + e$ events. The sideband J/ψ+track as well the signal component of the J/ψ+track sample are modeled with a PDF of the form:

$$P(\sigma) = \frac{1}{\sqrt{2\pi} P_0} e^{-\frac{1}{2}(\frac{\sigma}{P_0})^2} \otimes [\frac{P_5}{P_1} e^{-\frac{(\sigma - P_2)}{P_1}} + \frac{(1-P_5)}{P_3} e^{-\frac{(\sigma - P_4)}{P_3}}]$$

The constraints from the sideband fit are propagated to the fit of the signal region which is then fitted with J/ψ signal and constrained background components. The results of the sideband and signal region fits can be seen in Figure 32. The parameters of the signal component are listed in Table 14.

4 Sample Summary

We summarize the total number of predicted background events and candidates in Table 15. The excess is expected to consist of prompt and B_c events.

We look at the $J/\psi + e$ mass distribution for data events, where we have applied an $L_{xy}/\sigma_{xy} > 3.0$ to remove prompt events. We compare this to the background predictions and expect to see an excess of events in the $M(J/\psi + e) = 4 - 6\ GeV/^c$ region where we expect B_c events. We add a Monte Carlo of B_c events to the background

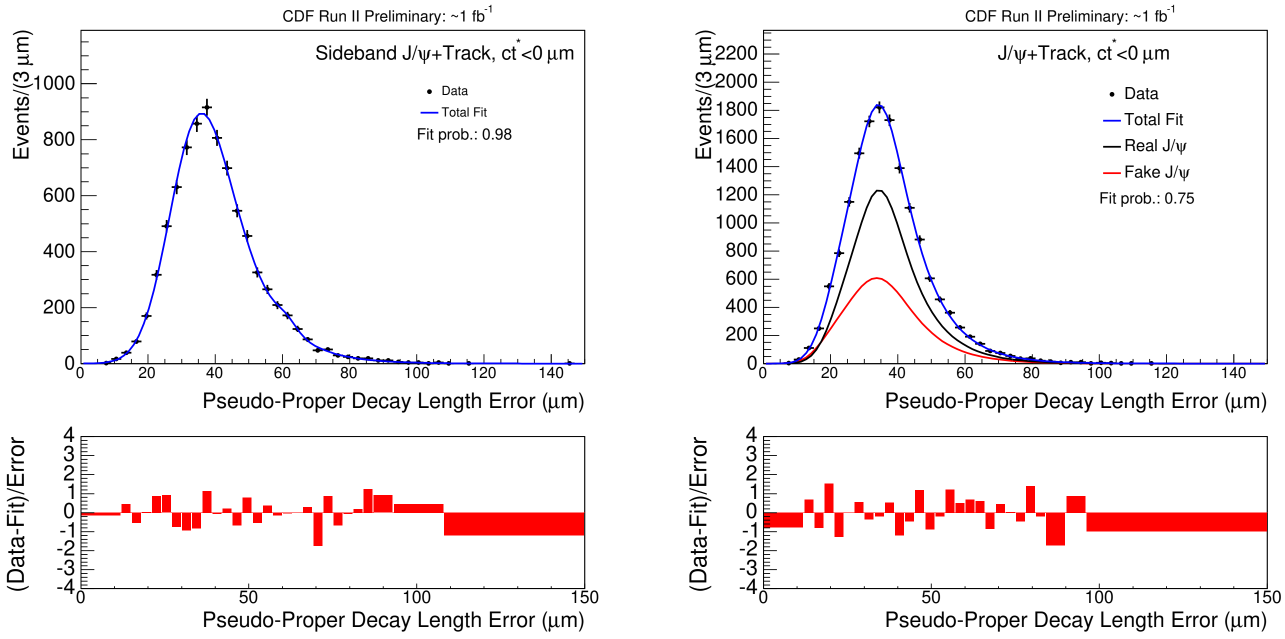

Figure 32: Fitted σ_{ct^*} distribution for sideband $J/\psi + track$ (left) and $J/\psi + track$ (right) data with $ct^* < 0$. Signal component from right fit is used to model σ_{ct^*} for the prompt $J/\psi + e$ background.

Parameter	Fit Value	Error
P_0	4.86	0.35
P_1	9.56	1.85
P_2	21.7	0.8
P_3	9.56	0.45
P_4	31.0	0.5
P_5	0.357	0.065

Table 14: J/ψ signal component parameters from fit of σ_{ct^*} for $J/\psi + track$ data with $ct^* < 0$.

Source	Number of Events
Fake Electron	312.0 ± 4.1
Fake J/ψ	325.2 ± 10.0
$b\bar{b}$	222.5 ± 11.2
Residual Conversion	416.8 ± 41.5
Candidates	1935

Table 15: Summary of background predictions and signal events

predictions, normalized to the excess in the $M(J/\psi + e) = 4 - 6\ GeV/^{c}$ region. The resulting distribution can be seen in Figure 33.

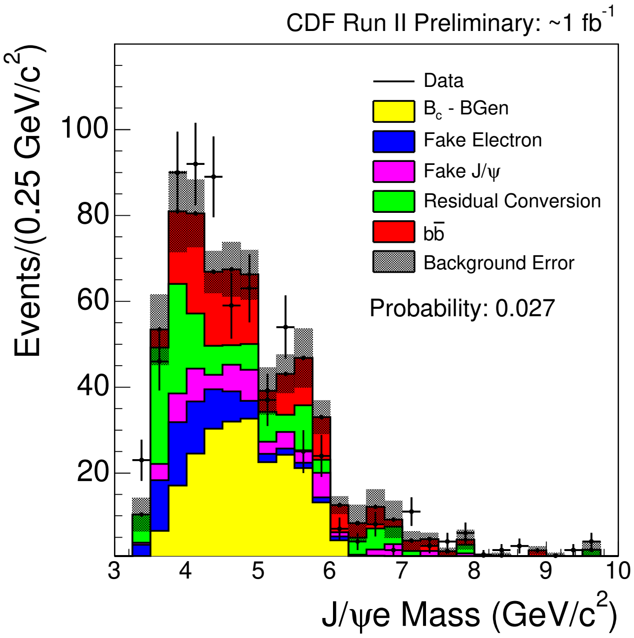

Figure 33: $J/\psi e$ mass for data and predicted.

5 Signal Model

To fit the ct^* of $J/\psi + e$ events and extract the B_c lifetime we will need to model effect of unmeasured particles in the B_c decay, which we do using a K factor. To do this we generate a sample of B_c decays with a J/ψ and electron in the final state using BGenerator. The input spectrum for the B_c events that we use is the same as that used in the $B_c \to J/\psi\pi$ analysis [6]. The branching fractions come from theoretical calculations [7] and are summarized in Table 5. The input lifetime for the BGenerator sample is 140 μm

5.1 B_c K Factor

Assuming the ct for signal events are distributed according to an exponential decay law, we can write the expected distribution of ct^* in terms of the average proper decay length, $c\tau$ and the distribution of K, H(K):

$$F_{BC}(ct^*, \sigma) = \int dK H(K) \frac{K}{c\tau}\theta(ct^*) exp(-\frac{Kct^*}{c\tau}) \otimes \frac{1}{\sqrt{2\pi}s\sigma} e^{-\frac{1}{2}(\frac{ct^*}{s\sigma})^2}$$

	$J/\psi + e + X$ Fraction	
Decay Mode	Generator Level	Candidate Level
$J/\psi + e + \nu_e$	0.8515	0.9629
$J/\psi + \tau + \nu_\tau$	0.0379	0.0114
$\psi(2S) + e + \nu_e$	0.0242	0.0187
$\psi(2S) + \tau + \nu_\tau$	0.0005	0.0002
$B_s + e + \nu_e$	0.0215	0.0002
$B_s^* + e + \nu_e$	0.0273	0
$B^0 + e + \nu_e$	0.0018	0
$B^{0*} + e + \nu_e$	0.0027	0
$D_s + J/\psi$	0.0061	0.0014
$D_s^* + J/\psi$	0.0246	0.0041
$D^+ + J/\psi$	0.0007	0.0002
$D^{+*} + J/\psi$	0.0013	0.0002

Here K is defined in the expression that relates ct to ct^*:

$$ct \times \frac{\vec{P}(B_c)\cdot\vec{p_T}(J/\psi e)/p_T(J/\psi e)}{p_T(J/\psi e)} = \frac{ct}{K}$$

We use the truth information from our Monte Carlo sample of B_c events to construct the distribution of K factors, H(K), which can be seen in Figure 34.

5.2 B_c σ_{ct^*}

To avoid uncertainties related to tracking resolution differences in detector simulation and data, we do not use our BGenerator sample to model the σ_{ct^*} distribution of B_c events. Instead, we use a template of the form used for many of our backgrounds, and allow the parameters to float in the B_c lifetime fit:

$$P_{BC}(\sigma) = \frac{1}{\sqrt{2\pi}P_0} e^{-\frac{1}{2}(\frac{\sigma}{P_0})^2} \otimes \frac{1}{P_1} e^{-\frac{(\sigma - P_2)}{P_1}}$$

5.3 Construction of Likelihood

Having defined our signal and background PDFs we are now ready to construct the likelihood function we will use to estimate $c\tau$ of $B_c^\pm$ from the ct^* distribution of $J/\psi+e$ events. Assuming our sample size of N_{sig} varies with Poisson statistics around the mean ν, we can begin by writing an extended likelihood of the form:

$$L = \frac{e^{-\nu}\nu^{N_{sig}}}{N_{sig}!} \times e^{(-\frac{1}{2}V_p^T C_p^{-1} V_p)} \times e^{(-\frac{1}{2}\frac{(N_{FE} - <N_{FE}>)^2}{E_{FE}^2})} \times$$

$$e^{(-\frac{1}{2}\frac{(N_{FJ} - <N_{FJ}>)^2}{E_{FJ}^2})} \times e^{(-\frac{1}{2}\frac{(N_{bb} - <N_{bb}>)^2}{E_{bb}^2})} \times e^{(-\frac{1}{2}\frac{(N_{RC} - <N_{RC}>)^2}{E_{RC}^2})} \times$$

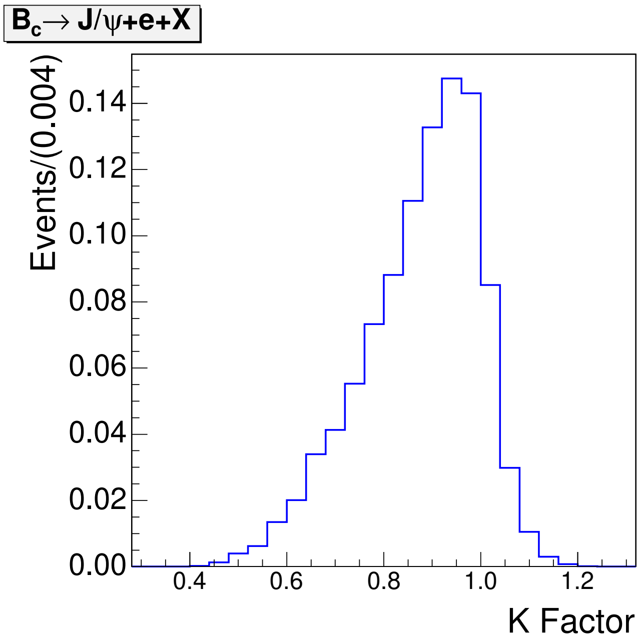

Figure 34: K factor distribution for $J/\psi + e$ events from the BGenerator sample of B_c events.

$$\Pi_i[f_{BC}P_{BC}(\sigma_i)F_{BC}(ct_i^*,\sigma_i) + f_{FE}P_{FE}(\sigma_i)F_{FE}(ct_i^*,\sigma_i)+$$
$$f_{RC}P_{RC}(\sigma_i)F_{RC}(ct_i^*,\sigma_i) + f_{FJ}P_{FJ}(\sigma_i)F_{FJ}(ct_i^*,\sigma_i)+$$
$$f_{bb}P_{bb}(\sigma_i)F_{bb}(ct_i^*,\sigma_i) + f_{PR}P_{PR}(\sigma_i)F_{PR}(ct_i^*,\sigma_i)]$$

Here f_{xx} are the fractions of each component and P_{xx} and F_{xx} are the PDFs for σ and ct^* respectively for each component. $< N_{xx} >$ and predicted numbers of the backgrounds respectively and E_{xx} are the errors associated with those predictions. V_P and C_P are a vector and covariance matrix that constrain the ct^* and σ fits that model the backgrounds.

We can write the likelihood in terms of number of events instead of fractions by moving our N_{sig} factors of ν inside of the product and distributing those factors amongst the fit components. We do this and take at $-2ln(L)$, to get the form that will be minimized:

$$-2ln(L) =$$
$$\Sigma_i[-2ln(N_{BC}P_{BC}F_{BC} + N_{FE}P_{FE}F_{FE} + N_{FJ}P_{FJ}F_{FJ} + N_{RC}P_{RC}F_{RC}+$$
$$N_{bb}P_{bb}F_{bb} + N_{PR}P_{PR}F_{PR})] + 2\nu + 2ln(N_{sig}!) + V_p^TC_p^{-1}V_p+$$
$$\frac{(N_{FE}-<N_{FE}>)^2}{E_{FE}^2} + \frac{(N_{FJ}-<N_{FJ}>)^2}{E_{FJ}^2} + \frac{(N_{bb}-<N_{bb}>)^2}{E_{bb}^2} + \frac{(N_{RC}-<N_{RC}>)^2}{E_{RC}^2}$$

6 Fitter Check

We check that the fitter returns an unbiased measurement of the B_c lifetime by run toy Monte Carlo experiments with B_c $c\tau$ of 80, 140 and 200 μm. We apply the fitter to 1000 trials at each input lifetime. The pulls of the measured lifetimes can be seen in Figure 35. The distribution of measured values for the lifetime can be seen in Figure 36. We see no significant bias, although there are a number of trials that fail to converge in the $c\tau = 80$ μm scenario. This is because the fitter has difficulty differentiating B_c and prompt events when the B_c lifetime is very short.

7 Systematic Studies and Uncertainties

We carry out a number of systematic checks to ensure that our methods for estimating backgrounds and signal properties do not propagate any large systematic uncertainties to the final B_c average lifetime measurement. The general procedure followed is to vary the signal or background models used to generate toys, while fitting with the models that will be used in the lifetime fit to data. We list the shift in the average lifetime as an estimate of the systematic uncertainty.

7.1 B_c Branching Fractions

The BGenerator sample used to model B_c signal events requires an input of B_c branching fractions that give $J/\psi + e + X$ in the final state, as discussed in Section 5. Since these branching fractions come from theoretical calculations, we would like to assign a systematic uncertainty related to the choice of branching fractions. The variation in the fraction of $J/\psi + e + \nu_e$ relative to other fractions among theoretical models, leads us to believe that a doubling or halving of the branching fractions (other than $J/\psi+e+\nu_e$) is a reasonable estimate of the uncertainty [7]. Figure 37 shows the effect of adjusting the branching fractions on the K factors. We see no significant change in the σ_{ct^*} fitted functions. We use models with the doubled and halved fractions as inputs to toy Monte Carlos, and the resulting systematic shifts in the measured B_c lifetime are listed in Table 16.

	Systematic Shift (μm)		
Systematic	$c\tau = 80$ μm	$c\tau = 140$ μm	$c\tau = 200$ μm
Halved Fractions	-0.2	-0.3	-0.5
Doubled Fractions	+0.5	+0.4	+0.3

Table 16: Shifts from systematic study of B_c branching fractions.

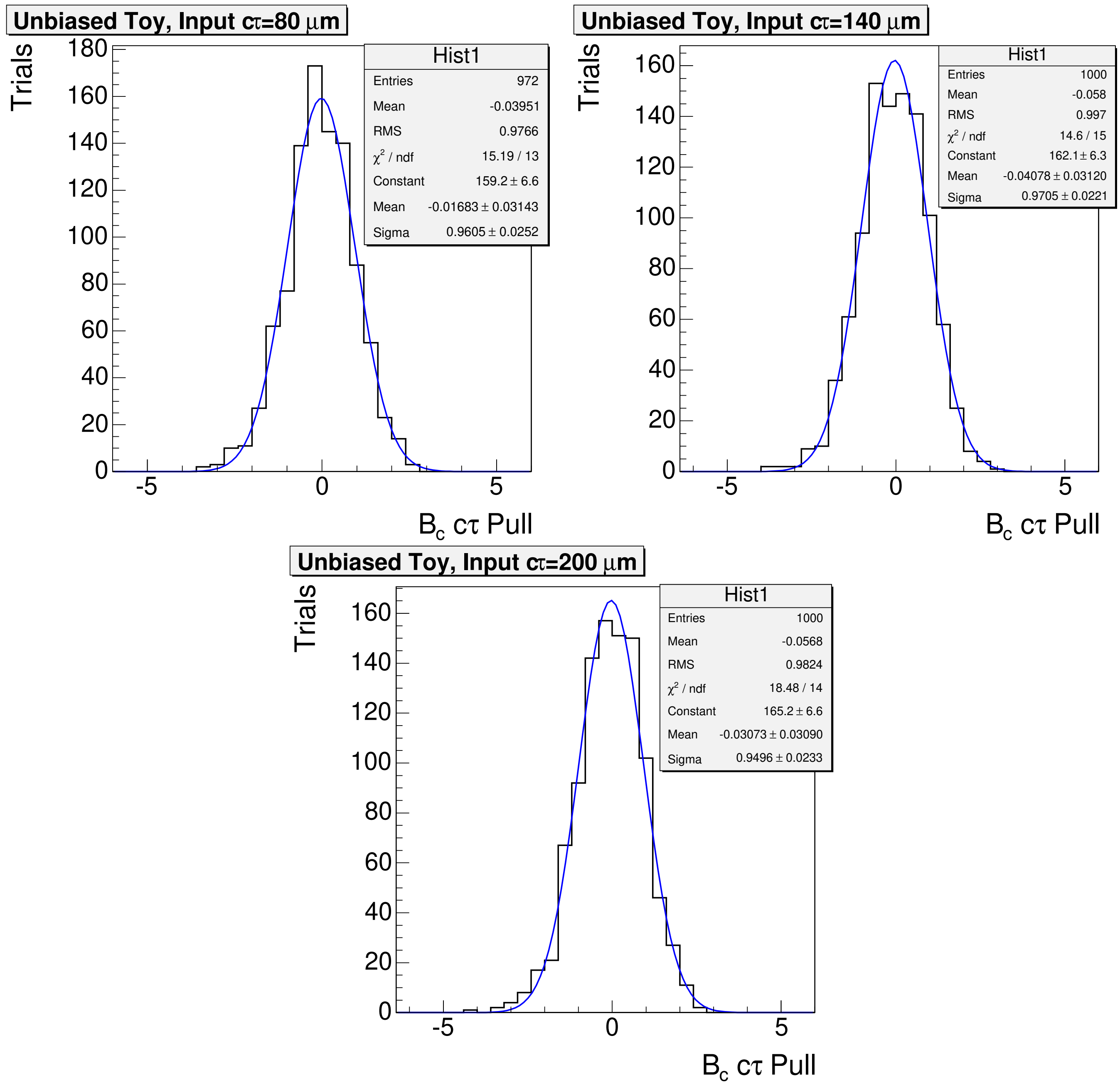

Figure 35: Pull distributions of $c\tau$ for unbiased toy Monte Carlos with input lifetimes of: 80 μm (top left), 140 μm (top right), and 200 μm (bottom).

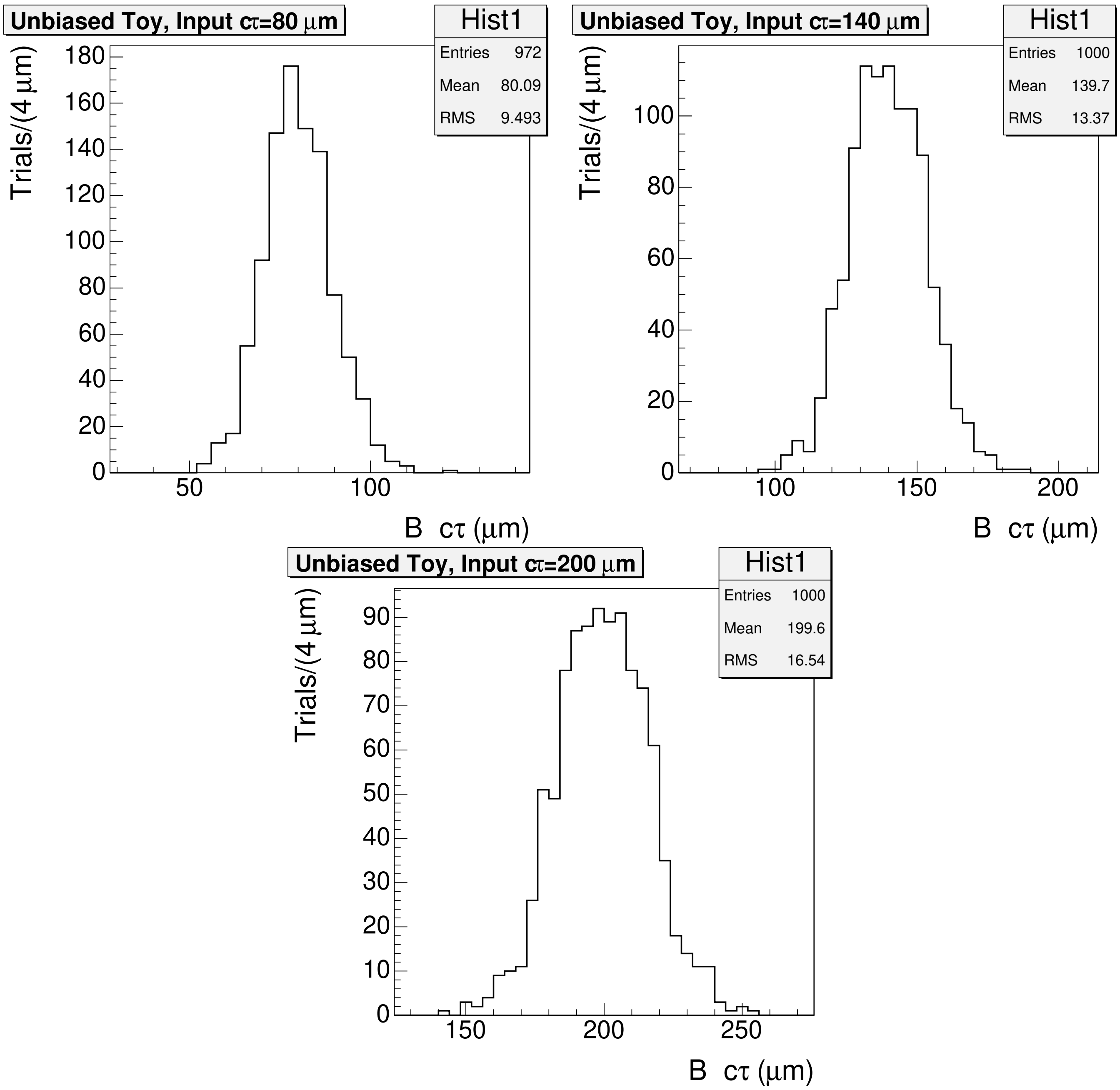

Figure 36: Distributions of $c\tau$ for unbiased toy Monte Carlos with input lifetimes of: 80 μm (top left), 140 μm (top right), and 200 μm (bottom).

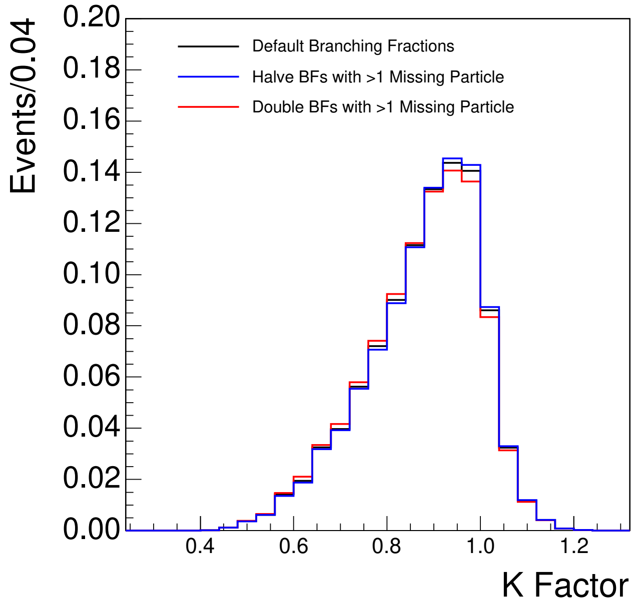

Figure 37: Comparison of K factor distributions for different B_c branching fractions.

7.2 B_c Spectrum

As discussed in Section 4, the Monte Carlo events that are used to model the K factor for B_c signal, are generated using BGenerator, where the input spectrum is calculated from theory. We want to test our sensitivity to the choice of B_c spectrum by using signal models with harder or softer spectra. For a harder spectrum, we assume that the B_c spectrum should be no harder than the spectrum of the lighter B mesons, and we use the lighter B meson spectrum to generate B_c events. For a softer spectrum, we assume an uncertainty in the B_c spectrum that is equal to its deviation from the B spectrum. We take the weighting distribution that will convert the B spectrum to a B_c spectrum and then apply it to the B_c spectrum. Figure 38 shows a comparison of the B_c and B spectra, as well as the weighting used for the softer spectrum.

The spectra after analysis cuts for the hard, soft and default scenarios, as well as the K factor distributions can be seen in Figure 39. We use the distributions for the hard and soft spectra as inputs to toys, with the shifts in the measured $c\tau$ summarized in Table 17.

	Systematic Shift (μm)		
Systematic	$c\tau = 80\ \mu m$	$c\tau = 140\ \mu m$	$c\tau = 200\ \mu m$
Harder Spectrum	-0.6	-0.2	-0.5
Softer Spectrum	+0.7	+0.3	+0.6

Table 17: Shifts from systematic study of the B_c spectrum.

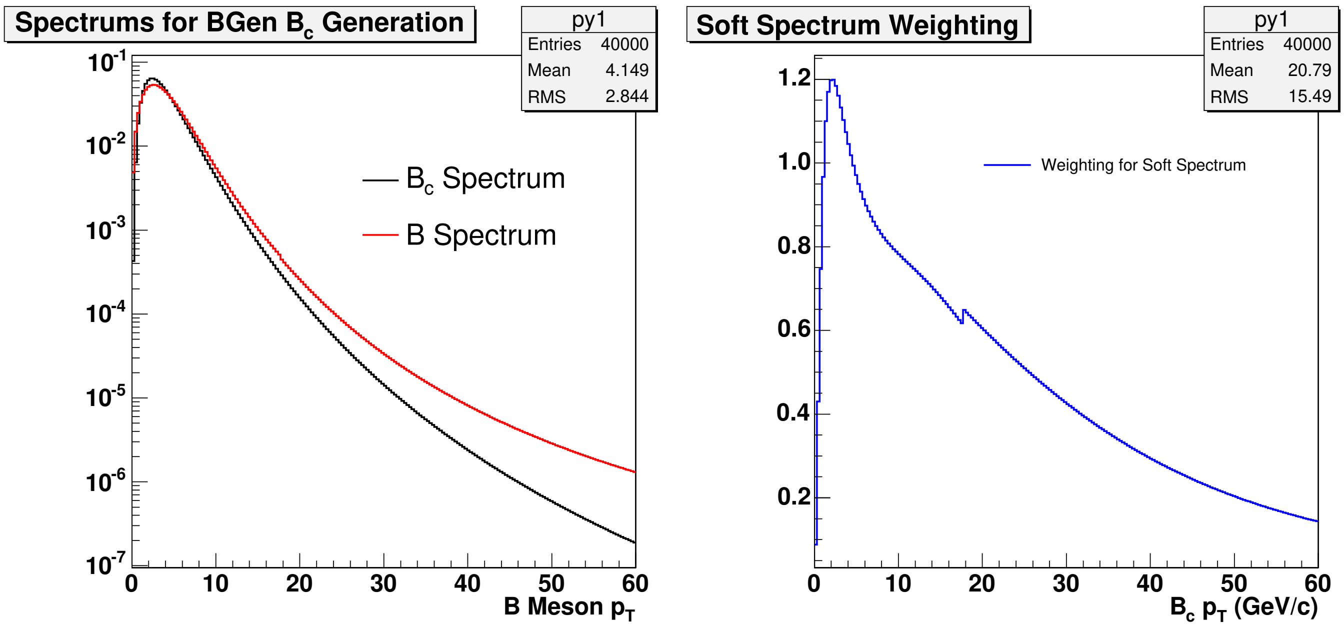

Figure 38: Left: Comparison of B_c and B input spectra for BGenerator. Right: Weighting applied to B_c spectrum to get softer spectrum

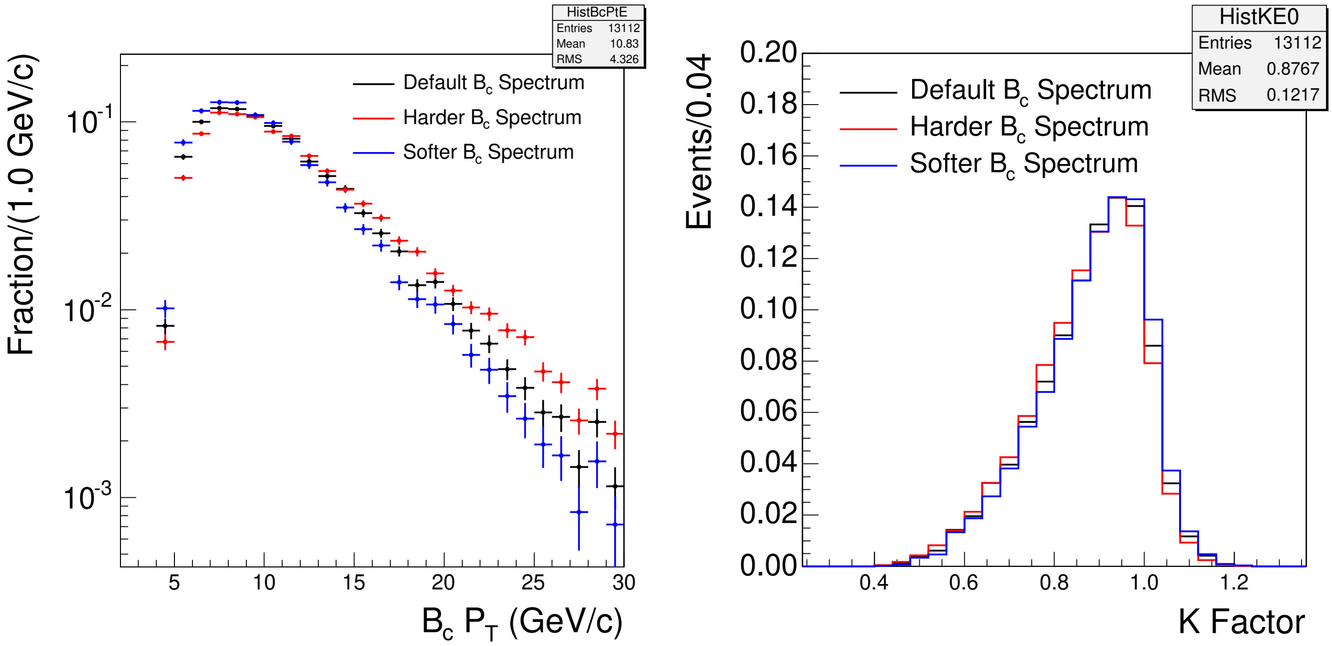

Figure 39: Left: Comparison of spectra after B_c analysis cuts have benn applied Right: Comparison of K factor distributions for different spectra.

7.3 Conversion Veto Efficiency

As discussed in Section 3.3.3, the study of conversion veto efficiencies using the signed impact parameter of electrons leads us to make a correction of 0.86 to the conversion veto efficiency in the $p_T = 2.0 - 2.5\ GeV/c$ bin. Since this correction is based on a discrepancy of only $\sim 1.5\sigma$, we study the effect of leaving out the correction. Without the correction, we estimate 370.4 ± 40.9 residual conversion events, compared to 416.8 ± 41.5 with the correction. We use the estimate without the correction as an input to generating toys. The resulting shifts in the measured B_c lifetime are listed in Table 18.

	Systematic Shift (μm)		
Systematic	$c\tau = 80\ \mu m$	$c\tau = 140\ \mu m$	$c\tau = 200\ \mu m$
No adjustment	-1.2	-1.9	-1.8

Table 18: Shifts from systematic study of conversion veto efficiency in the $p_T = 2.0 = 2.5\ GeV/c$ region.

7.4 Fake Electron Estimate Method

In Section 3.2 we estimate the size of the fake electron background using the $J/\psi + track$ sample. We use dE/dx and TOF information to estimate the particle composition of the third tracks before apply our cut on Z_e/σ_Z. We then recalculate the particle composition for a $J/\psi + track$ sample with the Z_e/σ_Z by applying efficiencies for the various particle types. The recalculated particle composition is then used with a $J/\psi + track$ sample that has the Z_e/σ_Z cut applied.

One can imagine a different method of estimating the fake electron background. Suppose we do not apply the Z_e/σ_Z cut to the $J/\psi + track$ sample, and instead include the efficiency for the cut in our fake electron rates. In this case we would not need to recalculate the particle composition and we would be less sensitive to the electron fraction in the $J/\psi + track$ sample. The disadvantage is that we are more sensitive to the estimation of the Z_e/σ_Z cut efficiencies. As a systematic check we compare the two methods and see 295.86 ± 3.31 events compared to 311.95 ± 4.05 events for the original method. We use the new estimate as an input to toys, with the resulting B_c lifetime shifts listed in Table 19.

	Systematic Shift (μm)		
Systematic	$c\tau = 80\ \mu m$	$c\tau = 140\ \mu m$	$c\tau = 200\ \mu m$
Efficiencies in fake rates	-0.1	0.0	-0.1

Table 19: Systematic uncertainties from study of Z_e and fake electron background.

7.5 J/ψ+track Proton Fraction

For the fake electron background estimate we use TOF information while determining the particle composition of third tracks with $p = 2 - 3\ GeV/c$ in the J/ψ+track sample. This allows for a direct measurement of the proton fraction. For third tracks with $p > 3\ GeV/c$ we only use dE/dx information, which cannot differentiate protons and kaons very well. For this reason, we use a Pythia model of the proton fraction to constrain the fraction in data. The Pythia model shows a proton fraction that falls off with third track p. As a systematic check, we assume the proton fraction is flat and constrain it to the average measured fraction in the $p = 2 - 3\ GeV/c$ region. Using the flat proton fraction we see a change of less than 1 event in the fake electron estimate, and assign a systematic of 0 μm.

7.6 Fake J/ψ ct^* Template

We fit the sideband $J/\psi + e$ events to get our Fake J/ψ background template using a function that contains a prompt component, two positive decay components and one negative decay component. The statistics in the long lived positive and negative tails are limited, so the uncertainty on those parameters are large. As a check, we fit the sideband J/ψ+track sample which has much more statistics, as can be seen in Figure 40. Here we fit three positive and negative decay components. We then take the fitted template from the J/ψ+track and adjust the relative fraction of prompt vs. decay components to get good agreement with the sideband $J/\psi + e$ sample. This adjusted template can be seen compared to the default fake $J/\psi + e$ template in Figure 41. We use this template as an input to toys, with the resulting shifts in $c\tau$ listed in Table 20.

	Systematic Shift (μm)		
Systematic	$c\tau = 80\ \mu m$	$c\tau = 140\ \mu m$	$c\tau = 200\ \mu m$
Template from fake J/ψ+track	+0.7	+0.5	+1.2

Table 20: Shifts from systematic study of ct^* template used for fake J/ψ background.

7.7 Resolution Function Systematic

For our models of the B_c signal component and the prompt background component we have assumed a per event smearing due to experimental resolution that is represented by a Gaussian function. The per event width of the Gaussian is the the measured σ_{ct^*} times a scale factor that is measured using the J/ψ+track sample and fixed at 1.21. As a systematic check, we refit the ct^* distribution of the J/ψ+track sample with a resolution function consisting of two Gaussians:

$$F(ct^*, \sigma_{ct^*}) = \frac{(1-F_1)}{\sqrt{2\pi} s_0 \sigma_{ct^*}} e^{-(\frac{ct^*}{s_0 \sigma_{ct^*}})^2} + \frac{F_1}{\sqrt{2\pi} s_1 \sigma_{ct^*}} e^{-(\frac{ct^*}{s_1 \sigma_{ct^*}})^2}$$

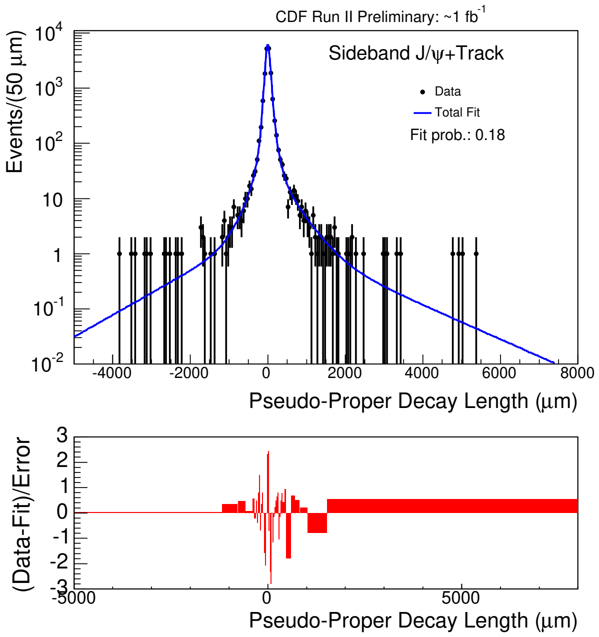

Figure 40: Fit of ct^* for sideband $J/\psi + track$ events.

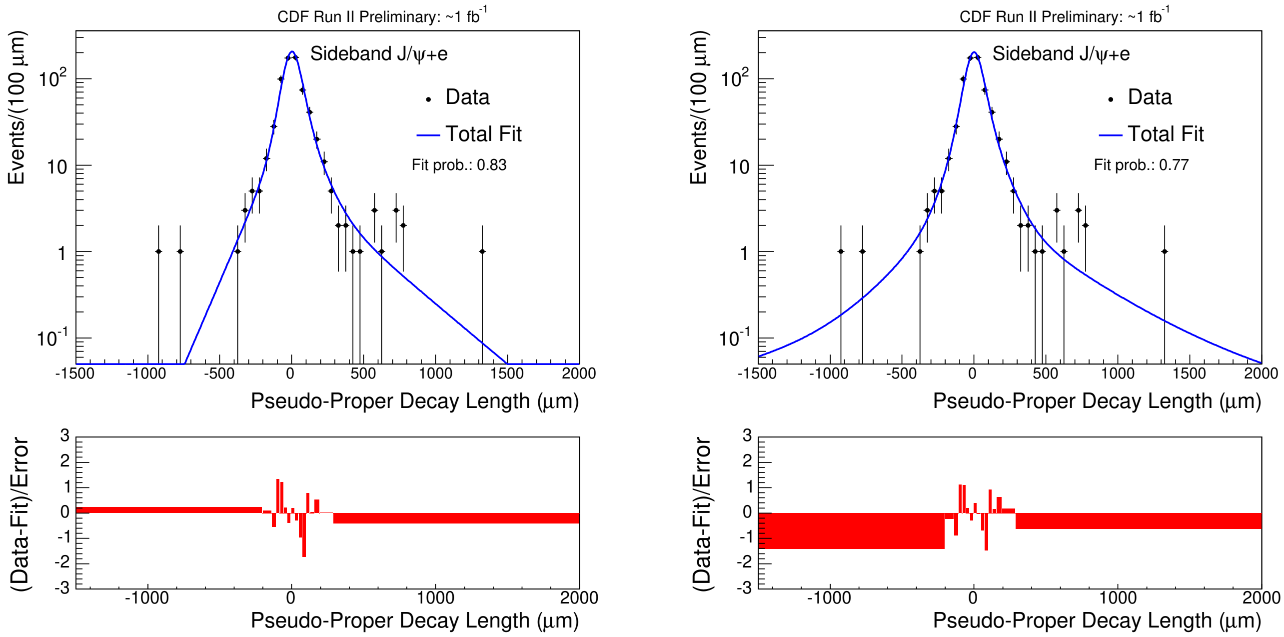

Figure 41: Left: Default ct^* template for the fake J/ψ background. Right: Fake J/ψ ct^* template based off of sideband $J/\psi + track$ sample.

The fitted parameters are listed in Table 21 and Figure 42 shows a comparison of the single and double Gaussian resolution functions. Figure 43 shows the ct^* fit of the J/ψ+track sample using the two Gaussian resolution function hypotheses. We use the double Gaussian function as an input to a toy, with the resulting shifts in B_c lifetime listed in Table 22.

Parameter	Single Gaussian	Double Gaussian
s_0	1.21 ± 0.02	1.12 ± 0.01
s_1	-	2.41 ± 0.11
F_1	-	0.16 ± 0.02

Table 21: Parameters for single gauss and double gauss resolution functions

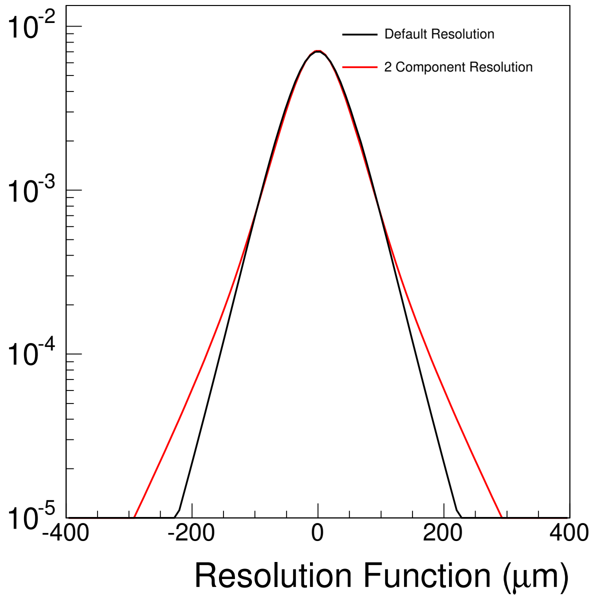

Figure 42: Plot of single and double Gaussian resolution functions.

7.8 $b\bar{b}$ QCD Process Scaling

As discussed previously, we adjust the relative fractions of QCD processes in Pythia by tuning the Pythia to data. As a systematic check we look at two different scenarios for the QCD process scaling. First we look at the default Pythia sample which gives a $b\bar{b}$ estimate of 160.8 events compared to our estimate of 222.5 events when the tuning is applied. Next we adjust the scale factor for the gluon splitting component of the $b\bar{b}$ up by 1σ which gives a estimate of 245.4 events. We use these two models as inputs to toys, with the resulting shifts listed in Table 23.

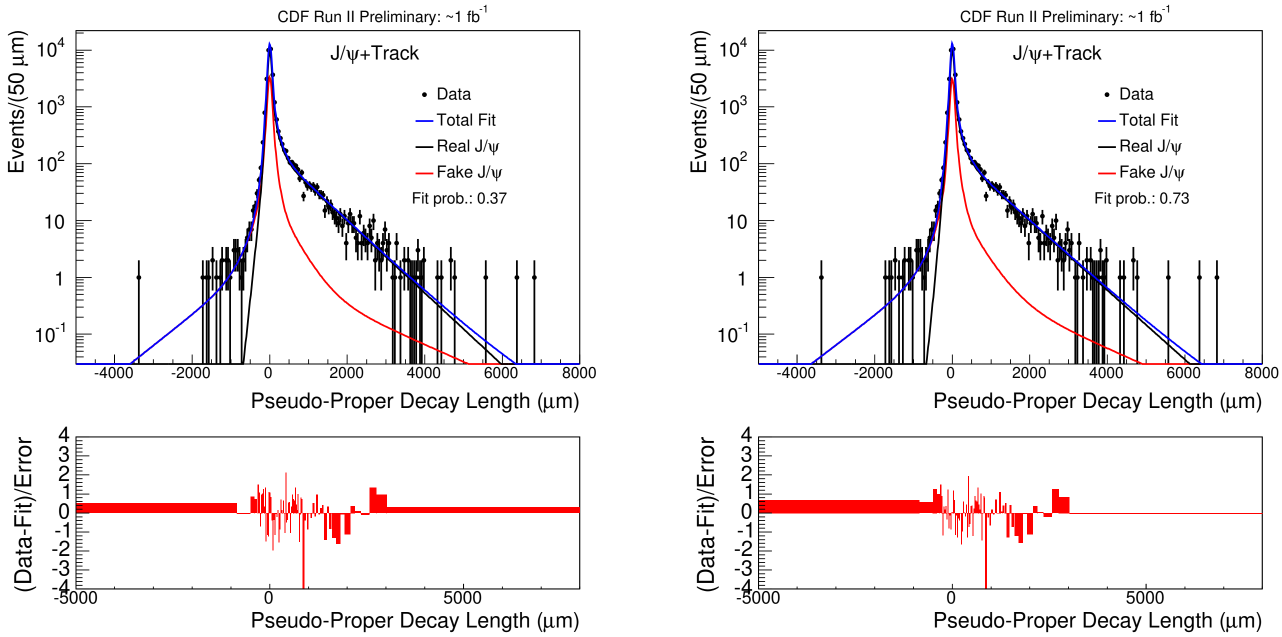

Figure 43: J/ψ+*track* ct^* fits with single Gaussian (left) and double Gaussian (right) resolution functions.

	Systematic Shift (μm)		
Systematic	$c\tau = 80\ \mu m$	$c\tau = 140\ \mu m$	$c\tau = 200\ \mu m$
Double Gaussian resolution	-2.1	+1.7	+3.1

Table 22: Shifts from systematic study of difference between single and double Gaussian resolution functions

	Systematic Shift (μm)		
Systematic	$c\tau = 80\ \mu m$	$c\tau = 140\ \mu m$	$c\tau = 200\ \mu m$
Default Pythia	-4.5	-2.5	+3.0
GS $+1\sigma$	+1.7	-1.5	-4.1

Table 23: Shifts from systematic study adjusting the relative amounts of QCD processes in the Pythia sample used to model the $b\bar{b}$

7.9 Pythia Track Parameter Errors

As discussed in the muon channel note, we do a comparison of track parameters errors for data and Pythia samples to determine reweighting based on the track parameter errors [2]. We apply the reweighting in the electron channel as well, and find 240.3 events, compared to 222.5 events without the reweighting. We use the reweighted data as an input to a toy with the resulting shifts listed in Table 24.

	Systematic Shift (μm)		
Systematic	$c\tau = 80\ \mu m$	$c\tau = 140\ \mu m$	$c\tau = 200\ \mu m$
Reweighted Errors	+1.1	+1.8	+1.2

Table 24: Shifts from systematic study of the Pythia track parameter errors.

7.9.1 Summary of Systematic Errors

We summarize the systematic errors in Table 25. For each input lifetime we add the values of the independent systematic errors in quadrature, independent of sign.

	Systematic Shift (μm)		
Systematic	$c\tau = 80\ \mu m$	$c\tau = 140\ \mu m$	$c\tau = 200\ \mu m$
Halved B_c Fractions	-0.2	-0.3	-0.5
Doubled B_c Fractions	+0.5	+0.4	+0.3
Harder B_c Spectrum	-0.6	-0.2	-0.5
Softer B_c Spectrum	+0.7	+0.3	+0.6
No Conv. Eff. Adjustment	-1.2	-1.9	-1.8
Fake Electron Calculation	-0.1	0.0	-0.1
Fake J/ψ Template	+0.7	+0.5	+1.2
Resolution Function	-2.1	+1.7	+3.1
Default Pythia QCD	-4.5	-2.5	+3.0
GS $+1\sigma$	+1.7	-1.5	-4.1
Reweighted Pythia Errors	+1.1	+1.8	+1.2
Total in quadrature	5.6	4.1	5.8
Approximate Statistical Error	14	16	18

Table 25: Summary of systematic errors. The approximate statistical errors come from our toys.

8 B_c Average Lifetime Measurement

Having verified the fitter and tested for a number of systematic uncertainties, we are ready to fit the data and extract a value for the B_c average lifetime. The measured

Parameter	Value	Parabolic Error
B_c $c\tau$ (μm)	121.743	17.2747
B_c Normalization	342.674	43.9571
Prompt Normalization	280.97	54.3681
B_c σ_{ct^*} Parameters		
bce0	5.95854	0.810196
bce1	11.1268	1.99261
bce2	23.5526	1.40462

Table 26: Free parameters for lifetime fit.

value of the average B_c lifetime is $121.7^{+18.0}_{-16.3}$ μm where the errors are calculated using the MINOS algorithm. The fitted ct^* and σ_{ct^*} distributions can be seen in Figure 44 and Figure 45. The likelihood value as a function of B_c average lifetime can be seen in Figure 46. In addition to the B_c lifetime, the normalization of the B_c and prompt components, as well as the parameters that describe the B_c σ_{ct^*} are free parameters in the fit. These parameters are summarized in Table 26. Figure 47 shows that the fitted σ_{ct^*} for B_c events is in good agreement with the distribution of σ_{ct^*} for B_c events in the BGenerator sample. There are also a number of constrained parameters in the fit, which are summarized in Tables 27, 28.

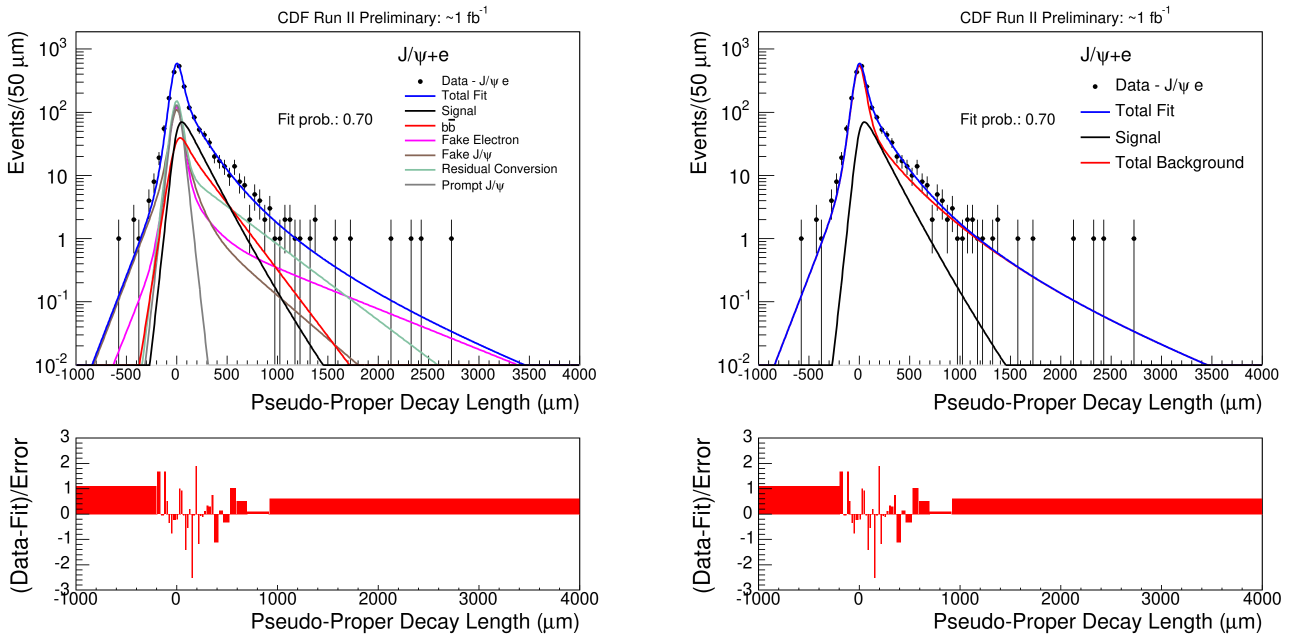

Figure 44: Fitted ct^* distribution for $J/\psi e$ candidates.

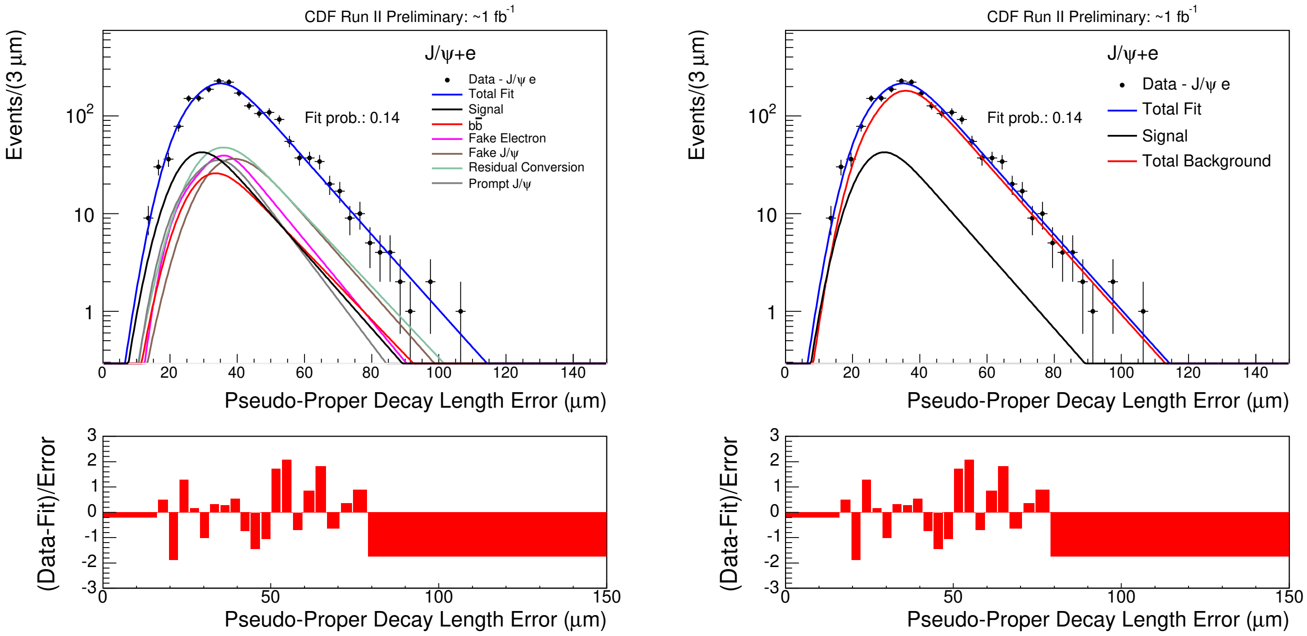

Figure 45: Fitted $\sigma(ct^*)$ distribution for $J/\psi e$ candidates.

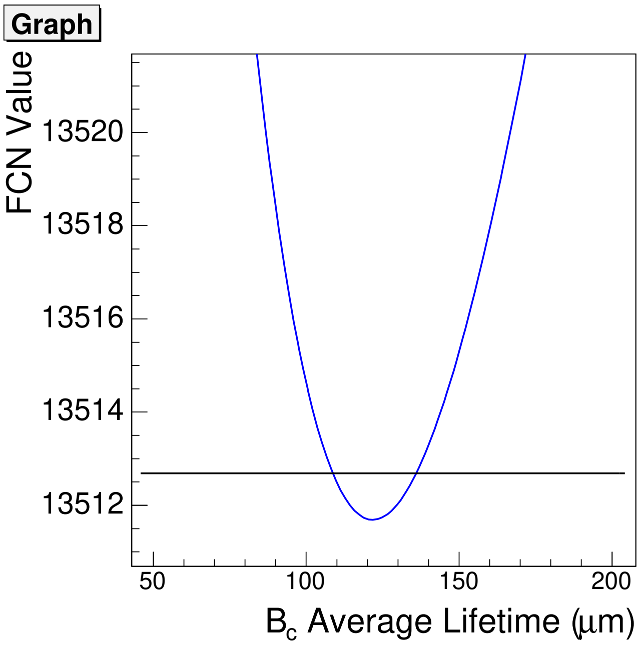

Figure 46: Scan of FCN for variation of $c\tau$ for B_c in the fit.

Parameter	Value	Parabolic Error
s - Error scale factor	1.21232	0.0199595
Fake Electron Normalizaton	313.049	4.55742
Fake Electron ct^* Template		
f_{prompt}	0.829578	0.0110106
$c\tau_{++}$	678.046	29.1995
f_{++}	0.0636087	0.00401307
$c\tau_{+}$	137.506	17.1151
f_{+}	0.0836909	0.00566558
$c\tau_{-}$	108.754	26.3149
f_{-}	0.0201761	0.00473879
s_{fe}	1.27368	0.0122113
Fake Electron σ_{ct^*} Template		
fee0	4.36559	0.116831
fee1	10.4726	1.59476
fee2	22.5224	0.310663
fee3	10.4307	0.38512
fee4	32.1855	0.254597
fee5	0.352813	0.0419908
Fake J/ψ Normalization	329.61	15.9266
Fake J/ψ ct^* Template		
s_{fj}	1.30235	0.0188621
f_{prompt}	0.631676	0.0473716
$c\tau_{++}$	316.496	84.5661
f_{++}	0.0561393	0.0232725
$c\tau_{-}$	104.916	14.027
f_{-}	0.143708	0.0227023
$c\tau_{+}$	83.8496	18.9201
f_{+}	0.163288	0.0446012
Fake J/ψ σ_{ct^*} Template		
fje0	7.29641	0.440185
fje1	11.1461	0.683604
fje2	32.619	0.625891

Table 27: Constrained parameters for lifetime fit.

Parameter	Value	Parabolic Error
Residual Conversion Normalization	428.857	50.2244
Residual Conversion ct^* Template		
s_{rc}	1.3111	0.0193482
$c\tau_+$	361.574	44.4194
f_{prompt}	0.785218	0.0647383
f_+	0.215454	0.0359438
Residual Conversion σ_{ct^*} Template		
rce0	6.91415	0.765458
rce1	11.883	1.05426
rce2	29.2899	1.06932
$b\bar{b}$ Normalization	224.036	11.0936
$b\bar{b}$ ct^* Template		
s_{bb}	1.71743	0.0669948
$c\tau_+$	19.0437	11.3998
$c\tau_{++}$	206.134	16.8702
f_+	0.287989	0.0643129
$b\bar{b}$ σ_{ct^*} Template		
bbe0	6.29392	0.617188
bbe1	12.1127	0.900916
bbe2	27.2739	0.808979
Prompt σ_{ct^*} Template		
pre0	4.8401	0.222053
pre1	9.54614	1.6976
pre2	21.8095	0.739581
pre3	9.54361	0.418998
pre4	31.1019	0.492129
pre5	0.366967	0.0617412

Table 28: Constrained parameters for lifetime fit.

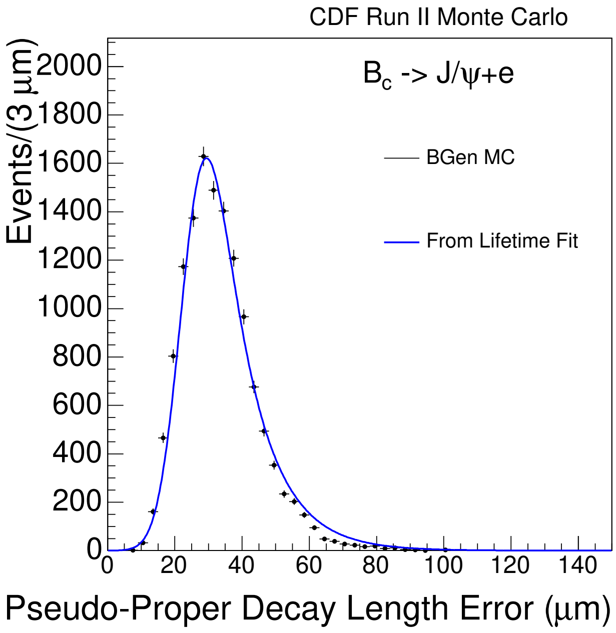

Figure 47: Fitted $\sigma(ct^*)$ for B_c events in lifetime fit compared to B_c event in the BGenerator sample.

8.1 $J/\psi e$ Mass

Having fitted the lifetime, we update the comparison of the predicted $J/\psi e$ mass distribution to data. We limit ourselves to events with $ct^* > 120\ \mu m$ to remove prompt events and we used the fitted normalizations for the background and signal from the lifetime fit. The resulting distribution can be seen in Figure 48 and we see good agreement between the predicted distribution and data.

9 Final Systematic Uncertainties

We finalize our systematic uncertainties, by running the systematic toys at the measured value of the B_c lifetime, $121.7^{+18.0}_{-16.3}$ and $\pm 1\sigma$. We take the total systematic uncertainty for the largest input B_c $c\tau$ as our total systematic uncertainty. We have also added an additional systematic uncertainty which we describe here.

9.1 B_c σ_{ct^*} Functional Form

The σ_{ct^*} of B_c events in the lifetime fit is modeled with the functional form:

$$P_{BC}(\sigma) = \frac{1}{\sqrt{2\pi}P_0} e^{-\frac{1}{2}(\frac{\sigma}{P_0})^2} \otimes \frac{1}{P_1} e^{-\frac{(\sigma - P_2)}{P_1}} \theta(\sigma - P_2)$$

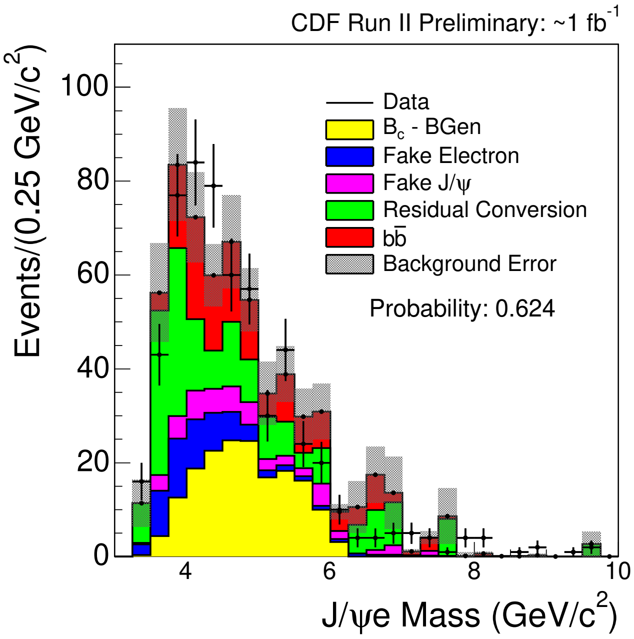

Figure 48: $J/\psi e$ mass for data and predicted from lifetime fit.

We have seen that the fitted function is in good agreement with the σ_{ct^*} distribution for B_c events from BGenerator (Figure 47). Fits to σ_{ct^*} distribution from BGenerator show that one needs a PDF from σ_{ct^*} with more degrees of freedom to get a fit with a good probablility. The PDF used for fitting the BGenerator sample is:

$$P_{BC}(\sigma) =$$
$$\frac{1}{\sqrt{2\pi}P_0}e^{-\frac{1}{2}(\frac{\sigma}{P_0})^2} \otimes \frac{P_6}{P_1}e^{-\frac{(\sigma-P_2)}{P_1}}\theta(\sigma-P_2) + \frac{1}{\sqrt{2\pi}P_3}e^{-\frac{1}{2}(\frac{\sigma}{P_3})^2} \otimes \frac{(1-P_6)}{P_4}e^{-\frac{(\sigma-P_5)}{P_4}}\theta(\sigma-P_5)$$

The fitted σ_{ct^*} distribution from BGenerator can be seen in Figure 49 and the parameters are listed in Table 29. For our systematic study, we use the fitted σ_{ct^*} from BGenerator while generating B_c events in our toy, and fit with the standard fitter. We see a shift of 0.5 μm in the measured lifetime.

9.2 Summary of Systematics

Table 30 summarizes the systematic uncertainties evaluated at the measured B_c lifetime and $\pm 1\sigma$. For each systematic where the variation is done in two directions, we take the larger error. We add the systematics in quadrature for a total systematic uncertainty of 8.0 μm, seen with an input $c\tau$ of 105 μm.

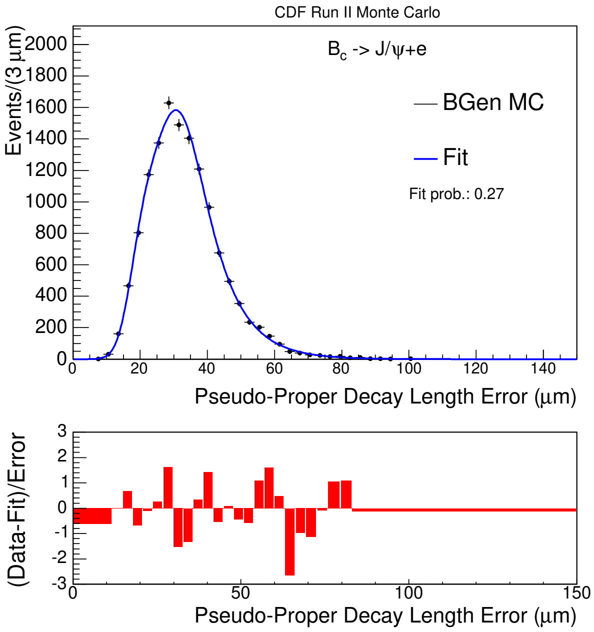

Figure 49: Fit of $J/\psi + e$ σ distribution for B_c events from BGenerator

Parameter	Fit Value	Error
P_0	3.48	0.29
P_1	17.14	1.74
P_2	5.71	0.58
P_3	8.61	0.27
P_4	7.99	0.37
P_5	26.2	0.59
P_6	0.265	0.068

Table 29: Parameters from σ_{ct^*} fit of B_c events from BGenerator.

	Systematic Shift ($\pm 0.5 \mu m$)		
Description	$c\tau = 105\mu m$	$c\tau = 122\mu m$	$c\tau = 140\mu m$
$b\bar{b}$ QCD Processes			
Default Pythia Settings	-6.3	-4.4	-3.4
Fitted $+1\sigma$	2.3	2.6	1.1
Pythia Track Errors	1.4	1.5	1.0
B_c Spectrum			
Hard	0.6	1.2	1.4
Soft	-0.9	-1.0	-1.0
B_c Branching Fractions			
x2 for >1 Unmeasured Particle	0.4	0.5	0.8
x1/2 for >1 Unmeasured Particle	-0.3	-0.2	0.1
B_c σ_{ct^*}	0.5	0.5	0.6
Fake J/ψ ct^*	0.5	0.6	1.0
Resolution Function	3.6	2.5	-3.0
Silicon Alignment	2.0	2.0	2.0
Fake Electron Normalization	-0.3	-0.2	-0.2
Residual Conversion Eff. Correction	-2.1	-2.2	-2.0
Total in Quadrature	8.0	6.3	5.8

Table 30: Summary of systematic errors evaluated at the nominal B_c $c\tau$ and $\pm 1\sigma$

10 Combined Result with Muon Channel

In CDF note 8155 we describe a measurement of the B_c lifetime using $B_c \to J/\psi + \mu + X$ decays. We measure a lifetime of $179.1^{+32.6}_{-27.2}(stat.) \pm 9.2(syst.)$ μm. To combine the muon channel result with the result from the electron channel, we multiply the likelihood functions (or add $-2Log(L)$) from the fits in each channels. To evaluate the $-2Log(L)$ as a function of $c\tau$, we fix $c\tau$ for a large range of values and minimize the remaining parameters for each value of $c\tau$. We take the minimum of the subsequent curve to be the measured value, and the $c\tau$ values corresponding to a 1 unit increase in $-2Log(L)$ correspond to the 68% confidence limits. Figure 50 shows $-2Log(L)$ minimized for varying values of B_c $c\tau$ for both channels. For the combined result we add the $-2Log(L)$ of both channels. This can be seen in Figure 51. The resulting B_c $c\tau$ from the combined channels is:

$$c\tau = 142.5^{+15.8}_{-14.8}(stat.)$$

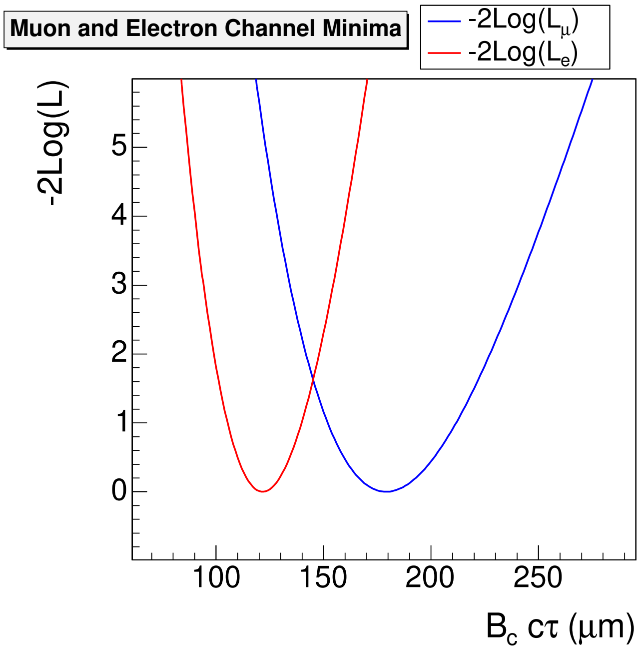

Figure 50: $-2Log(L)$ minimized for varying values of B_c $c\tau$ for muon and electron channel measurements.

10.1 Combined Systematic Uncertainty

For the average result we combine the systematic uncertainties for the two channels. We begin by defining the weighted sum of our B_c lifetimes as:

$$c\tau_{total} = (\frac{c\tau_e}{E_e^2} + \frac{c\tau_\mu}{E_\mu^2})/(\frac{1}{E_e^2} + \frac{1}{E_\mu^2})$$

In this equation, $c\tau_e$ and $c\tau_\mu$ are the measured lifetimes and E_e and E_μ are the statistical errors. We can take the derivative with respect to $c\tau_e$:

$$\frac{d(c\tau_{total})}{d(c\tau_e)} = \frac{E_\mu^2}{E_e^2+E_\mu^2}$$

We can write a general equation for adding systematic errors (S_e and S_μ) for the two channels:

$$S_{total} = \sqrt{\frac{d(c\tau_{total})}{d(c\tau_e)}^2 S_e^2 + \frac{d(c\tau_{total})}{d(c\tau_\mu)}^2 S_\mu^2 + 2\frac{d(c\tau_{total})}{d(c\tau_e)}\frac{d(c\tau_{total})}{d(c\tau_\mu)} S_e S_\mu}$$

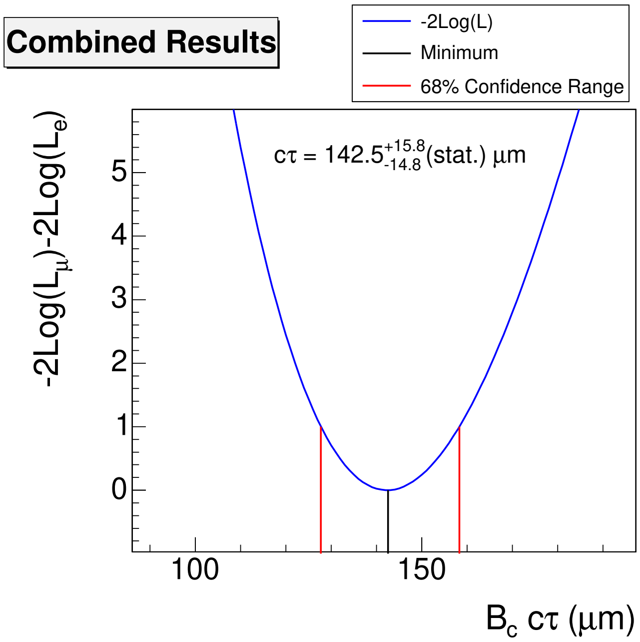

Figure 51: $-2Log(L_e) - 2Log(L_\mu)$. Minimum gives B_c $c\tau$ for combined result.

Here the last term is only present for errors that are correlated between the two channels.

We evaluate the systematic uncertainties for each channel individually for input lifetimes at the nominal value of the combined result and $\pm 1\sigma$. After combining the systematics for the two channels, we chose the largest total systematic uncertainty among the three input lifetimes. Table 31 lists the systematic errors for both channels and their weighted combinations. The weighted combinations of systematic uncertainties added in quadrature give a total systematic uncertainty of 5.5 μm.

11 Conclusion

We have carried out a measurement of the B_c lifetime using $B_c \to J/\psi + e + X$ decays from ~ 1 fb^{-1} of data. Our measured lifetime is:

$$121.7^{+18.0}_{-16.3}(stat.) \pm 8.0(syst.)\ \mu m$$

We combine the electron channel result with the muon channel result outlined in CDF Note 8155 to obtain an average result for $B_c \to J/\psi + l + X$ of:

$$142.5^{+15.8}_{-14.8}(stat.)5.5(syst.)\ \mu m$$

	Systematic Shift (μm)								
	$c\tau = 127.7\ \mu m$			$c\tau = 142.5\ \mu m$			$c\tau = 158.3\ \mu m$		
Description	e	μ	Total	e	μ	Total	e	μ	Total
$b\bar{b}$ QCD Processes									
Default Pythia	-3.9	0.2	2.8	-3.4	1.9	2.9	-1.8	3.9	2.4
Fitted $+1\sigma$	1.5	1.2	1.4	1.1	0.6	1.0	0.8	0.2	0.6
Pythia Track Errors	1.2	1.8	1.4	1.0	1.4	1.1	0.5	1.2	0.7
B_c Spectrum									
Hard	1.1	0.8	1.0	1.4	0.9	1.3	1.4	1.1	1.3
Soft	-1.1	-0.8	1.0	-1.0	-1.0	1.0	-1.2	-1.0	1.1
B_c Branching Fractions									
x2 Rates	0.6	0.3	0.5	0.8	0.2	0.6	0.6	0.3	0.5
x1/2 Rates	-0.2	-0.6	0.3	0.1	-0.7	0.3	-0.3	-0.7	0.3
$B_c\ \sigma_{ct^*}$	0.5	0.1	0.4	0.6	0.0	0.4	0.6	0.0	0.4
Fake $J/\psi\ ct^*$	0.7	-1.0	0.6	1.0	-0.9	0.7	1.1	-0.4	0.8
Resolution Function	-0.6	-5.5	2.1	-3.0	3.5	3.2	-4.7	1.8	3.8
Silicon Alignment	2.0	2.0	2.0	2.0	2.0	2.0	2.0	2.0	2.0
Fake J/ψ Normalization	-	-1.6	0.5	-	-1.4	0.4	-	-1.4	0.4
$J/\psi + track$ p Fraction	-	1.3	0.4	-	1.3	0.4	-	1.4	0.4
Decay-in-flight Correction	-	1.3	0.4	-	1.3	0.4	-	1.4	0.4
Residual Conversion Eff.	-2.1	-	1.5	-2.0	-	1.4	-2.2	-	1.5
Fake Electron Method	-0.3	-	0.2	-0.2	-	0.1	-0.3	-	0.2
Total in Quadrature			4.9			5.4			5.5

Table 31: Summary of combined systematic uncertainties for the two channels evaluated at the nominal B_c $c\tau$ and $\pm 1\sigma$.

Our results are in good agreement with previous measurements of the B_c lifetime at both CDF and D0 and represent a 30% improvement in precision over the previous CDF measurement.

Appendix

A Hadron Faking Electron Probabilities

To estimate the probability of a hadron faking an electron we use hadrons identified as decay products in a fully reconstructed system of particles with a narrow mass peak. We measure the probablility that these hadrons pass our electron likelihood cut which is our fake electron probability. We carry out these measurements in p_T bins since we expect the fake probabilities to be dependent on p_T.

Pions and kaons are identified by reconstructing the decay chain $D^{*+} \to D^0\pi^+ \to \pi^+K^-\pi^+ + c.c.$. The positively identified particles are the D^0 decay products, and are identified by the charge of the soft pion from the D^{*+} decay. We skim the two track hadronic trigger datasets, xbhd0d-i, selecting D^{*+} tagged D^0 decays using the cuts listed in Table 32.

For protons we use the decay $\Lambda \to p+\pi$ where the track with the higher momentum is identified as the proton. Once again, we skim the two track hadronic trigger datasets, xbhd0d-i, selecting events using the cuts listed in Table 33.

Selection Requirement	Value
D^0 legs p_T	π or K $p_T > 2.0\ GeV/c$
Third track requirement	One of D^0 legs meets third track requirements
D^0 p_T	$> 3.0\ GeV/c$
K/π $\Delta\phi$	> 0.035 and < 2.36
K/π Δz	$< 8\ cm$
D^0 Vertex Prob.	> 0.001
D^0 L_{xy}	$> 0.01\ cm$
$\|M(D^0) - 1.865\|$	$< 0.1\ GeV/c^2$
D^* Vertex Prob.	> 0.001
$D^0/soft\ \pi$ $\Delta\phi$	< 0.7854
$\|[M(D^*) - M(D^0)] - 0.1457\|$	$< 0.002\ GeV/c^2$
$Q(\pi) * Q(soft\ \pi)$	$= 1$

Table 32: Cuts applied to two track hadronic trigger datasets to skim D^{*+} tagged D^0 decays.

A.0.1 Mass Fits and Fake Probabilities

Having skimmed the tagged D^0 events, we look at D^0 mass plots for the case where the pion or kaon leg meets the third track requirements from the J/ψ+track sample. The mass fits are shown in Figure 52, Figure 53, Figure 54 and Figure 55 for π^+, π^-, K^+ and K^- respectively. The number of events in the D^0 mass peak are the

Selection Requirement	Value
Proton Leg p_T	$p_T > 2.0\ GeV/c$
Pion Leg p_T	$p_T > 2.0\ GeV/c$
Third track requirement	Proton leg meets third track requirements
Proton d_0	$> 0.012\ cm$
$p\pi\ \Delta z$	$< 8\ cm$
Λ Vertex Prob.	> 0.01
$\Lambda\ L_{xy}$	$> 0.85\ cm$
$\lvert M(\Lambda) - 1.116\rvert$	$< 0.04\ GeV/c^2$

Table 33: Cuts applied to two track hadronic trigger datasets to skim Λ decays.

candidates where the relevant leg has the possibility of faking an electron. We call these the "parent" mass distributions.

Next we require the pion and kaon legs to pass the electron likelihood requirement from the $J/\psi + e$ sample. The resulting mass fits can be seen in Figure 56, Figure 57, Figure 58 and Figure 59 for π^+, π^-, K^+ and K^- respectively. We call these the "daughter" mass distributions. The statistics in these mass plots set the size of the p_T bins. By taking the ratio of events in the D^0 mass peak for the daughter and parent distributions, we can estimate the probability that a pion or kaon with a given p_T can fake a electron.

For protons we carry out the same procedure, using fits to the Λ mass peak. The parent distributions can be seen in Figure 60 and Figure 61 and the daughter distributions in Figure 62 and Figure 63.

A.1 Isolation Reweighting

Before we take the ratio of events in the parent and daughter distributions we want to correct for the difference in isolation between tracks in our D^0 and Λ samples and third tracks in the J/ψ+track sample. Here isolation is defined using tracks in a $\Delta R = \sqrt{(\Delta\phi)^2 + (\Delta\eta)^2} < 0.7$ cone around the track of interest and is the sum of p_T^i of tracks in that cone divided by the p_T^0 of the track of interest: $I = \sum_i p_T^i / p_T^0$. Figure 64 shows a comparison of the isolation for our samples, an we apply a reweighting of events in the parent and daughter mass fits, based on the ratio of these isolation distributions.

With the events reweighted by isolation we can derive the fake rates from the ratio of fitted signal events in the parent and daughter distributions. The fake rates are summarized in Figure 11 in Section 3.2.1.

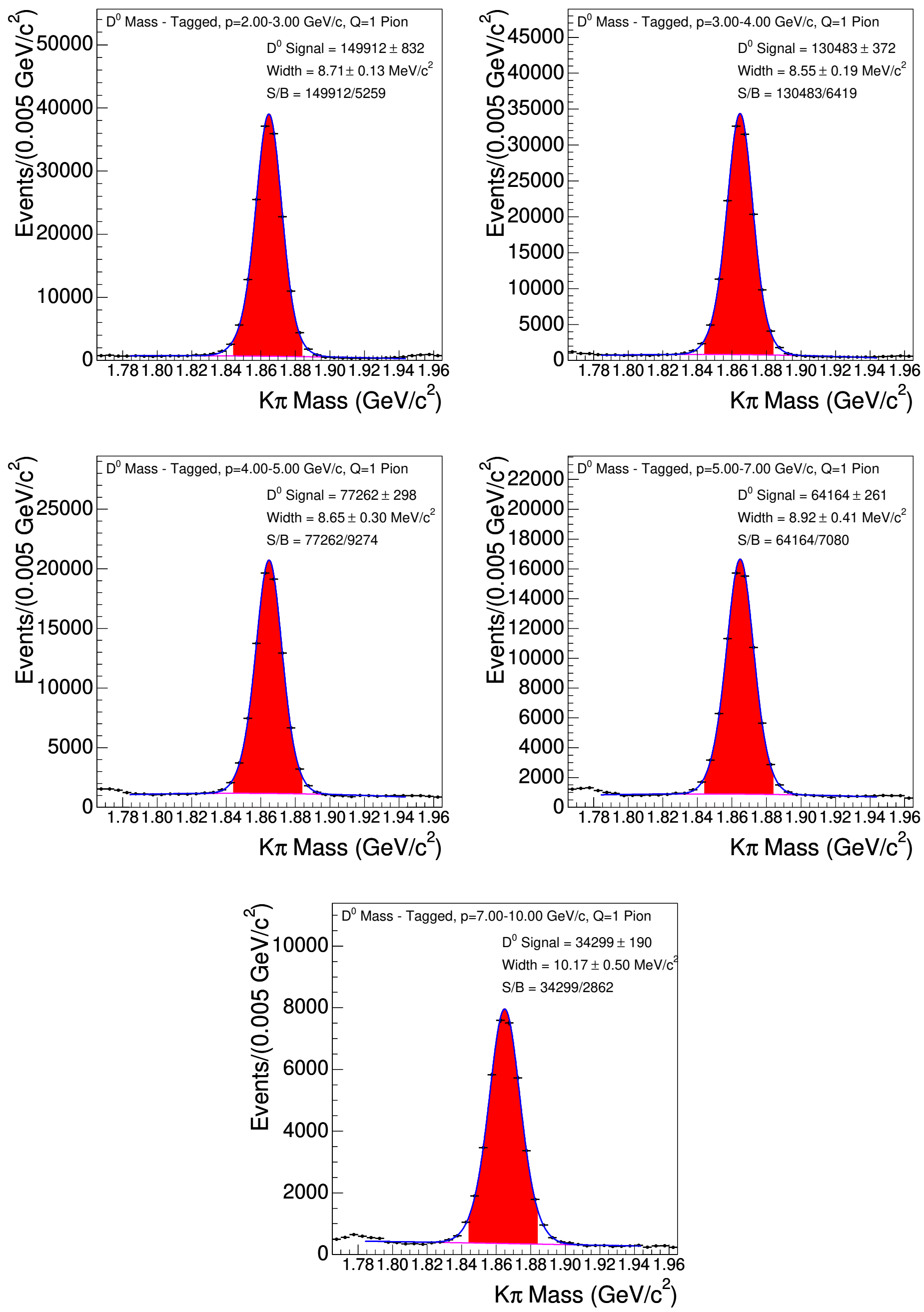

Figure 52: Fitted D^0 mass peaks where π^+ leg meets third track requirements. Broken into p_T bins of: 2-3 GeV/c (top left), 3-4 GeV/c (top right), 4-5 GeV/c (middle left), 5-7 GeV/c (middle right), >7 GeV/c (bottom).

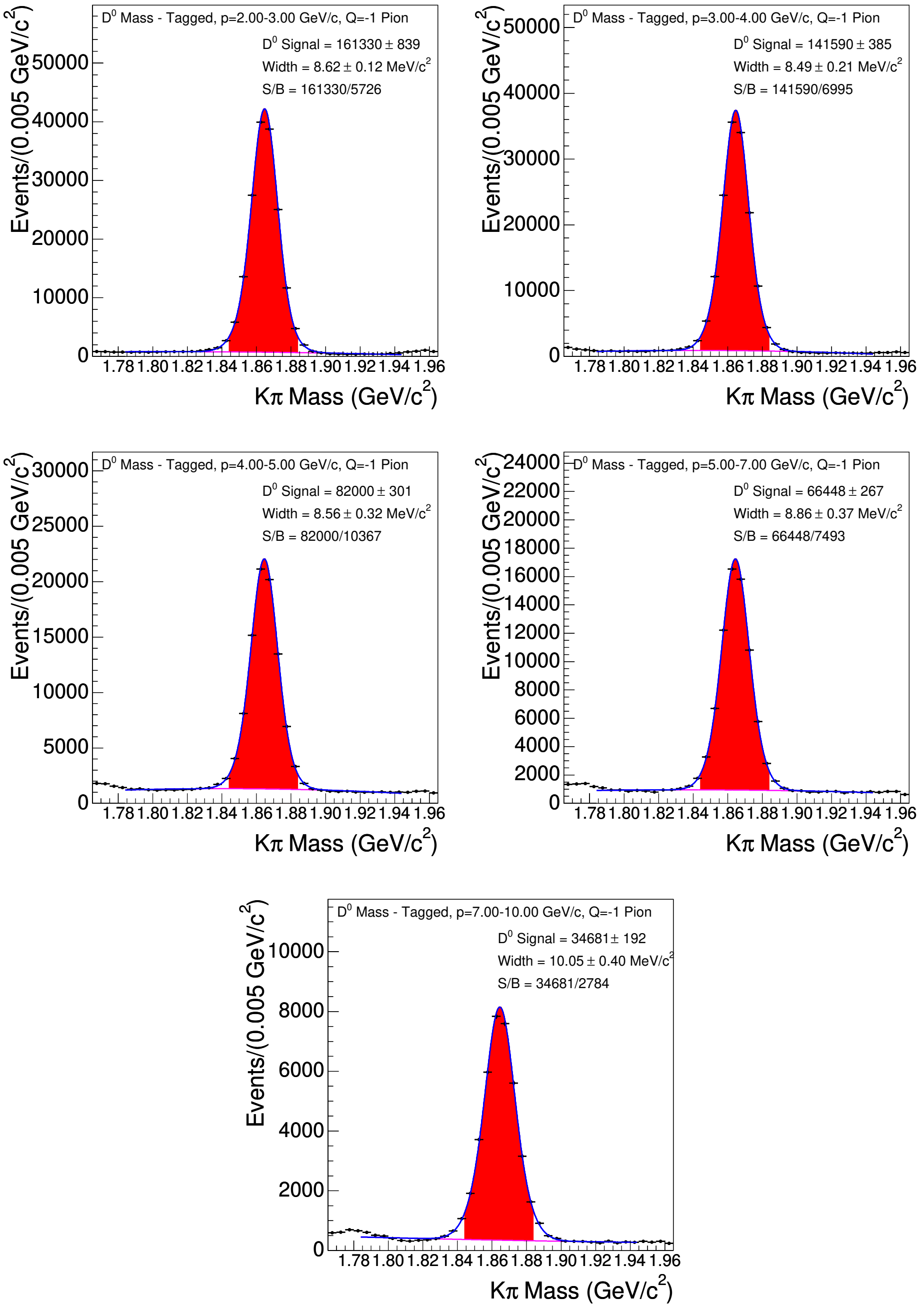

Figure 53: Fitted D^0 mass peaks where π^- leg meets third track requirements. Broken into p_T bins of: 2-3 GeV/c (top left), 3-4 GeV/c (top right), 4-5 GeV/c (middle left), 5-7 GeV/c (middle right), >7 GeV/c (bottom).

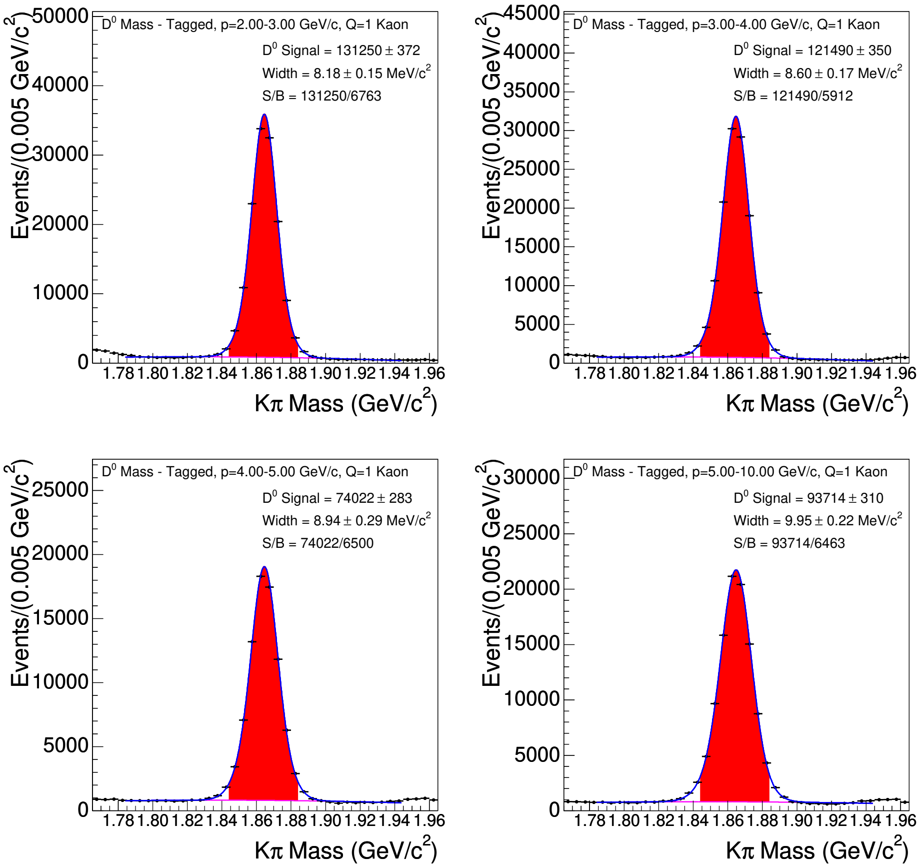

Figure 54: Fitted D^0 mass peaks where K^+ leg meets third track requirements. Broken into p_T bins of: 2-3 GeV/c (top left), 3-4 GeV/c (top right), 4-5 GeV/c (bottom left), >5 GeV/c (bottom right).

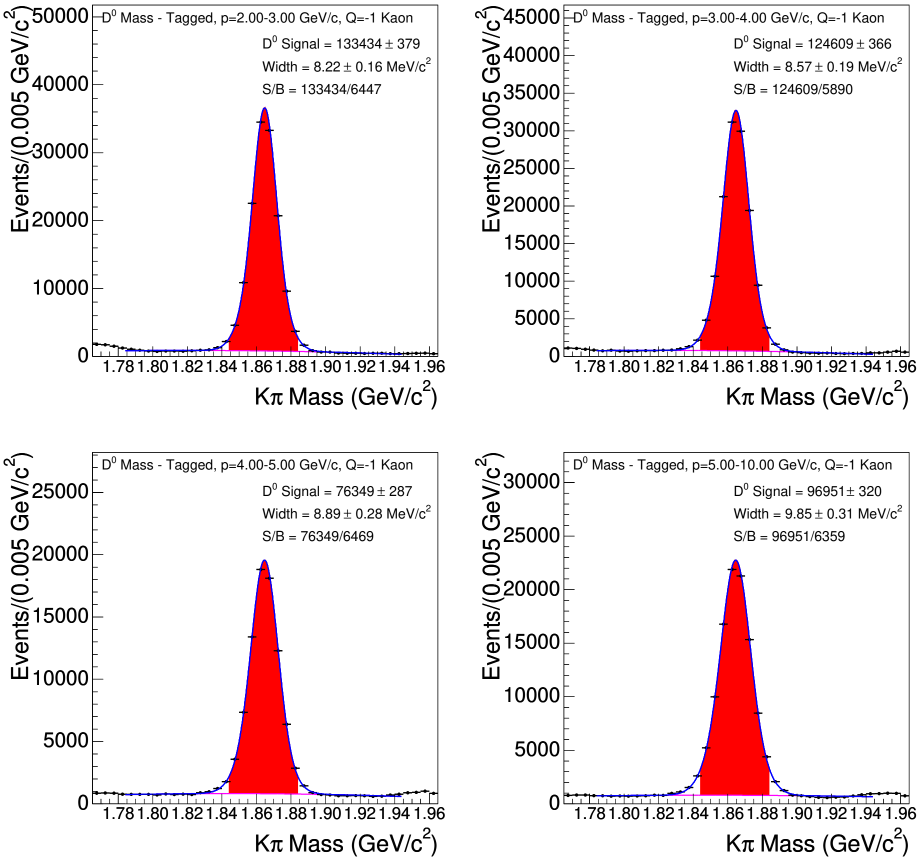

Figure 55: Fitted D^0 mass peaks where K^- leg meets third track requirements. Broken into p_T bins of: 2-3 GeV/c (top left), 3-4 GeV/c (top right), 4-5 GeV/c (bottom left), >5 GeV/c (bottom right)

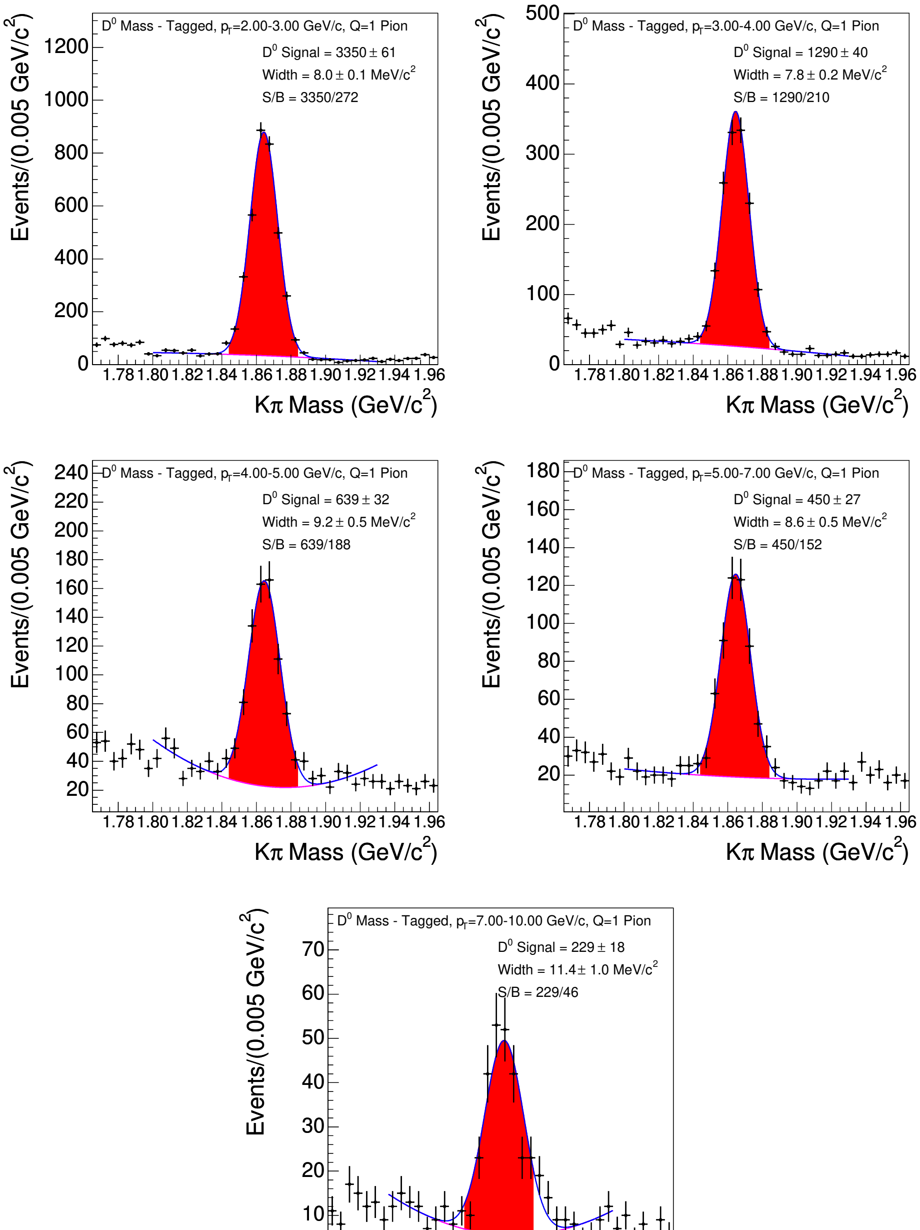

Figure 56: Fitted D^0 mass peaks where π^+ leg passes electron selection. Broken into p_T bins of: 2-3 GeV/c (top left), 3-4 GeV/c (top right), 4-5 GeV/c (middle left), 5-7 GeV/c (middle right), >7 GeV/c (bottom).

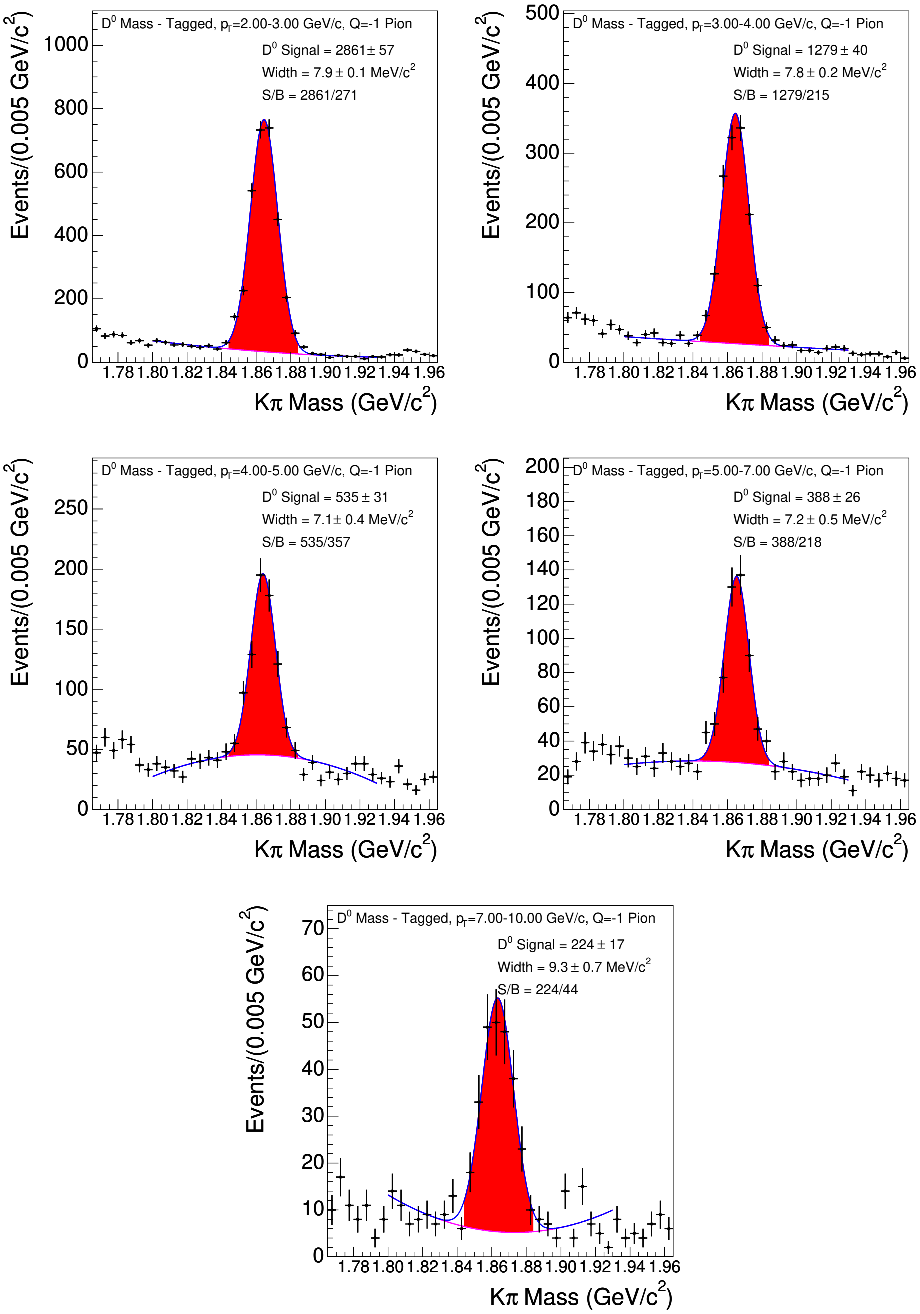

Figure 57: Fitted D^0 mass peaks where π^- leg passes electron selection. Broken into p_T bins of: 2-3 GeV/c (top left), 3-4 GeV/c (top right), 4-5 GeV/c (middle left), 5-7 GeV/c (middle right), >7 GeV/c (bottom).

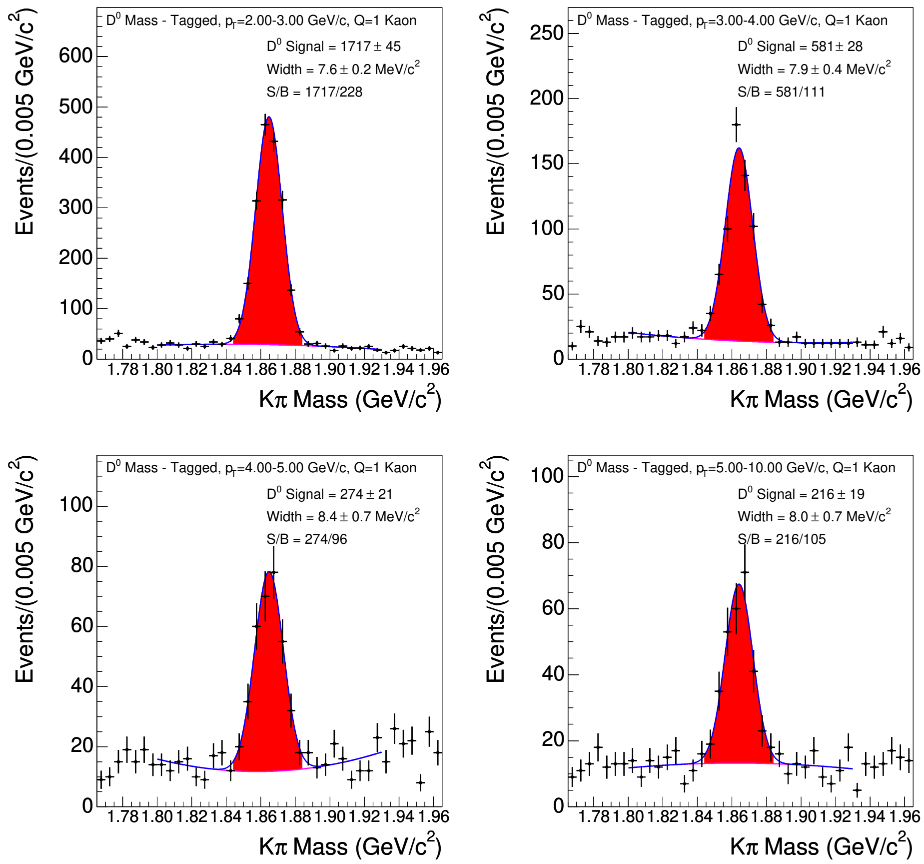

Figure 58: Fitted D^0 mass peaks where K^+ leg passes electron selection. Broken into p_T bins of: 2-3 GeV/c (top left), 3-4 GeV/c (top right), 4-5 GeV/c (bottom left), >5 GeV/c (bottom right).

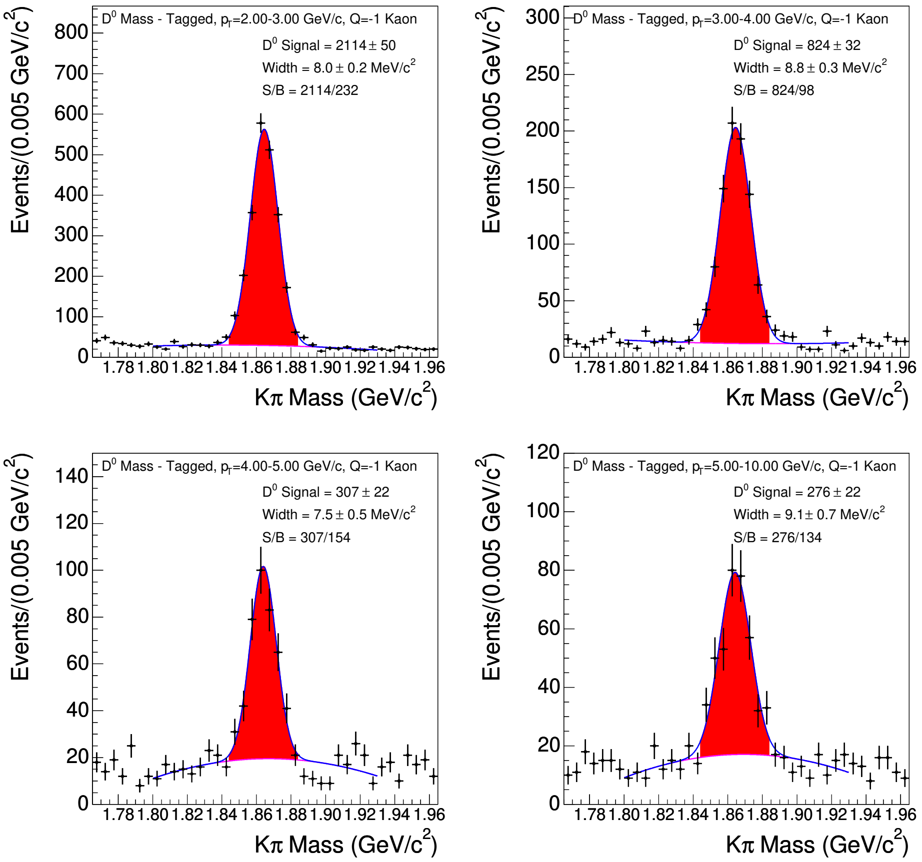

Figure 59: Fitted D^0 mass peaks where K^- leg passes electron selection. Broken into p_T bins of: 2-3 GeV/c (top left), 3-4 GeV/c (top right), 4-5 GeV/c (bottom left), >5 GeV/c (bottom right)

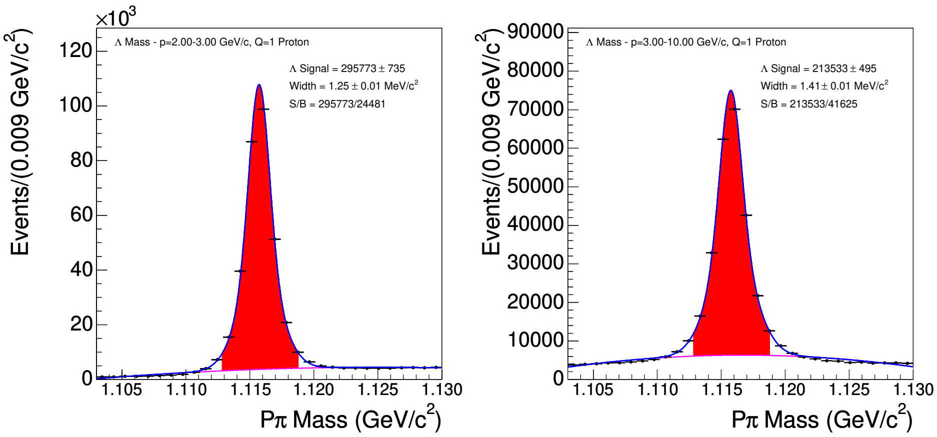

Figure 60: Fitted Λ mass peaks where p^+ meets third track requirements. Broken into p_T bins of: 2-3 GeV/c (left), >3 GeV/c (right).

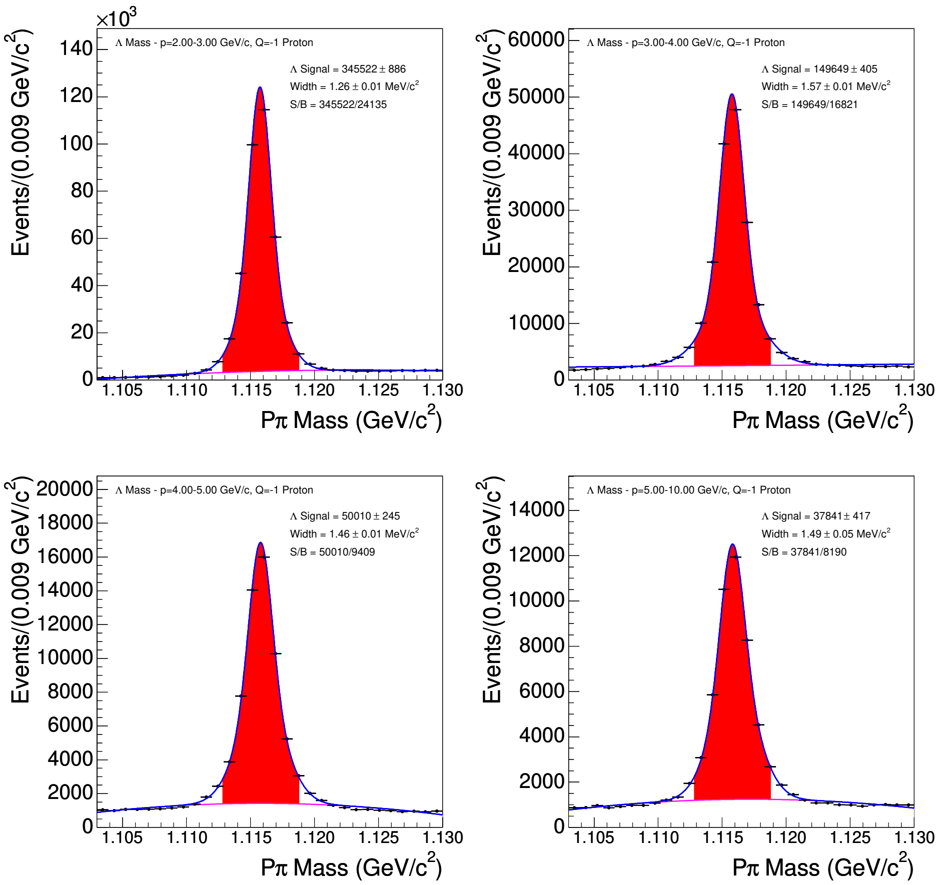

Figure 61: Fitted Λ mass peaks where p^- meets third track requirements. Broken into p_T bins of: 2-3 GeV/c (top left), 3-4 GeV/c (top right), 4-5 GeV/c (bottom left), >5 GeV/c (bottom right)

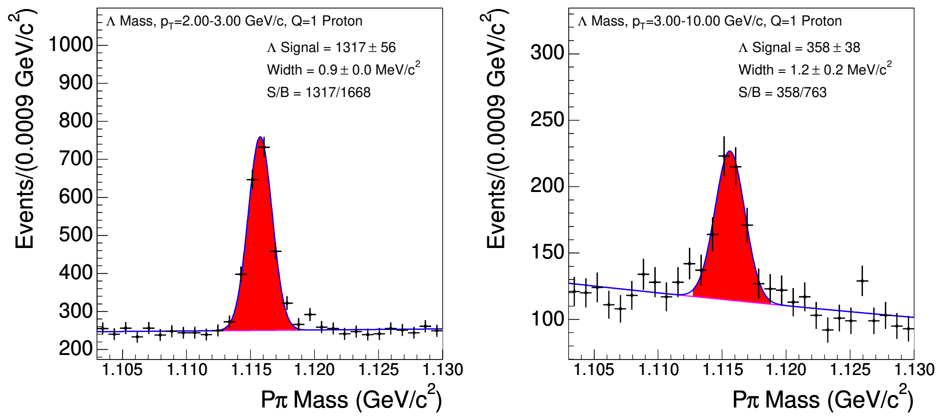

Figure 62: Fitted Λ mass peaks where p^+ leg passes electron selection. Broken into p_T bins of: 2-3 GeV/c (left), >3 GeV/c (right).

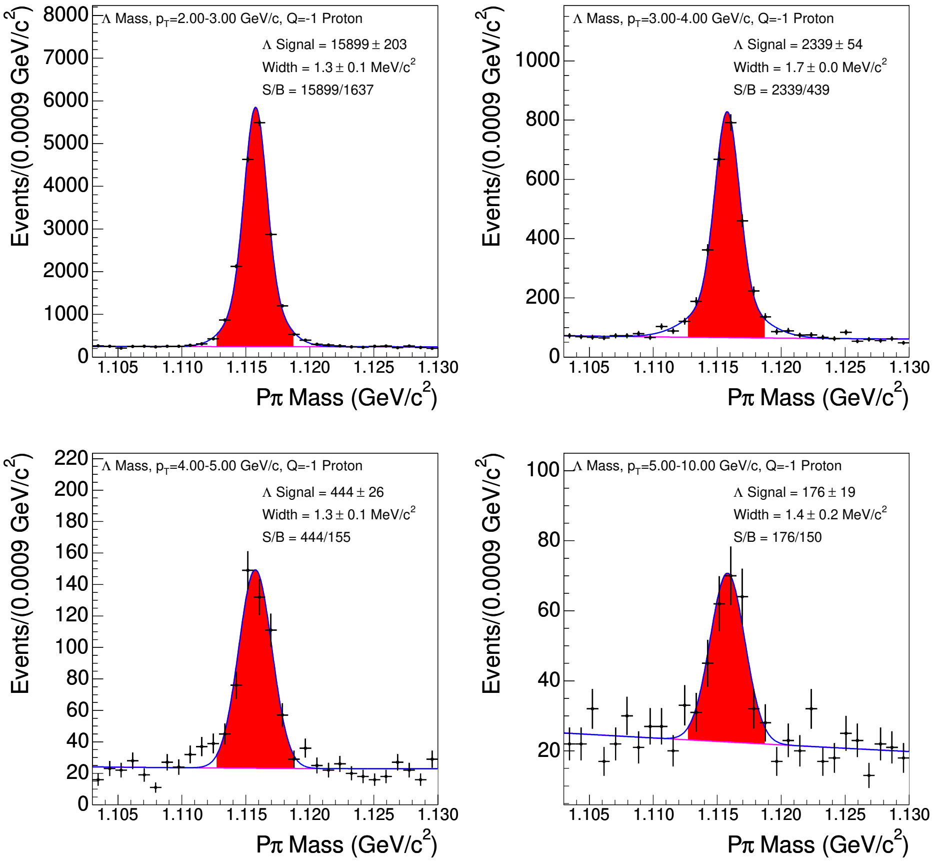

Figure 63: Fitted Λ mass peaks where p^- leg passes electron selection. Broken into p_T bins of: 2-3 GeV/c (top left), 3-4 GeV/c (top right), 4-5 GeV/c (bottom left), >5 GeV/c (bottom right)

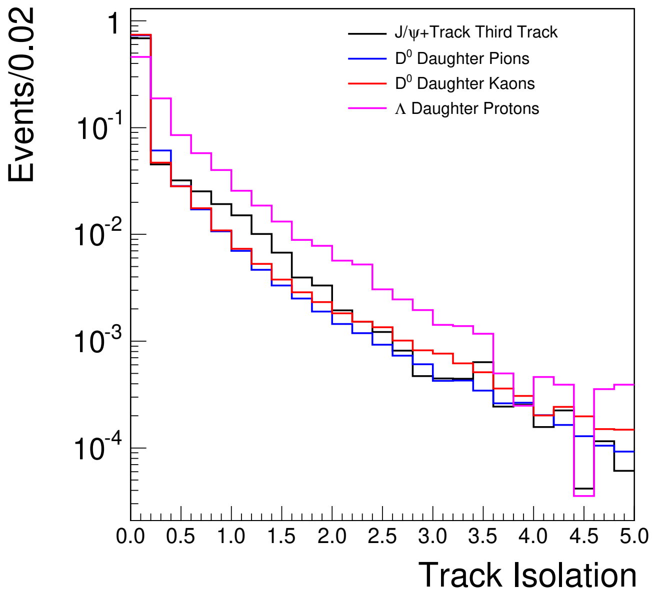

Figure 64: Isolation distributions for the samples used for estimating fake rate and the J/ψ+track sample.

B Third Track Particle ID

To study the types of particles that make up the third tracks in our J/ψ+track sample, we use two methods of particle identification: time of flight of the particle through the tracking volume (TOF) and energy loss in the tracking volume (dE/dx). While we are unable to positively identify any single event, using these two methods we are able to estimate the fractional composition of the sample for a given value of the third track momentum. For tracks with $p < 3.0\ GeV/c$ we find it is useful to used both TOF and dE/dx information since the TOF is able to separate protons and kaons in that region. For tracks with $p > 3.0\ GeV/c$ we lose our ability to separate protons and kaons, so we use a Pythia model of p_T dependent proton fractions which is normalized based on the measured fractions in the $p < 3.0\ GeV/c$ region and only use dE/dx information. We have broken the J/ψ+track sample up into three regions, $ct^* > 150\ \mu m$ which is dominated by B decays, $0 < ct^* < 150\ \mu m$ which contains prompt J/ψ, B decays and $b\bar{b}$, and $ct^* < 0\ \mu m$ which is dominated by prompt J/ψ. All dE/dx and TOF fits are carried out before the $Z_e/\sigma > -1.3$ cut is applied, and afterward the fitted particle fractions are recalculated given the efficiencies for the $Z_e/\sigma > -1.3$ cut.

B.1 TOF+dE/dx Fits in $p = 2.0 - 3.0$ GeV/c Region

In the third track $p = 2.0 - 3.0$ GeV/c region we measure the particle fractions of the third tracks using TOF and dE/dx information. We begin by defining pull variables for both dE/dx and TOF:

$$Z_\pi = \frac{ln(dE/dx)}{ln(<dE/dx>_\pi)}$$

$$Z_{pull} = \frac{Z_\pi}{\sigma(Z)_\pi}$$

$$TOF_{pull} = \frac{TOF-<TOF>_\pi}{\sigma(TOF)_\pi}$$

$< dE/dx >_\pi$ and $< TOF >_\pi$ are the predicted values of dE/dx and TOF respectively for a particle of given momentum with a pion hypothesis, while $\sigma(Z)_\pi$ and $\sigma(TOF)_\pi$ are the predicted errors on the Z_{pi} and TOF measurements. We then fit the two dimensional distributions of dE/dx_{pull} and TOF_{pull} for the $ct^* < 0$ region (Figure 65, Figure 66), the $0 < ct^* < 150$ μm region (Figure 67, Figure 68) and the $ct^* > 150$ μm region (Figure 69, Figure 70). For each ct^* region we have broken the sample up into two third track momentum bins: 2.0-2.5 GeV/c and 2.5-3.0 GeV/c and fitted positive and negative charge tracks separately.

B.2 Proton Fraction for $p > 3.0$ GeV/c

For the proton fraction in the $p > 3.0$ GeV/c region we use the same method that is described in the muon channel note [2]. We used a Pythia sample to constrain the p dependence of the proton fraction, which is shown in Figure 71. We find that the final answer for the fake electron estimate does not depend on our choice of p dependence for the proton fraction.

B.3 dE/dx Fits in $p > 3.0$ GeV/c Region

For tracks with $p > 3.0$ GeV/c we use dE/dx only to fit the particle fractions. As in the previous section, we fit the Z_π pull distribution. The fits are broken up by charge, into the previously described ct^* regions, and by momentum of the third track. Proton fractions are constrained using the p dependence described in the previous section. Figures 72, 73, 74, 75, 76, 77 show the fits that give the particle fractions for third tracks in the J/ψ+track sample.

B.4 The Muon Fraction

We expect the J/ψ+track sample to contain some fraction of third tracks that are muons. In our dE/dx fits we cannot extract a muon fraction since the muon and pion

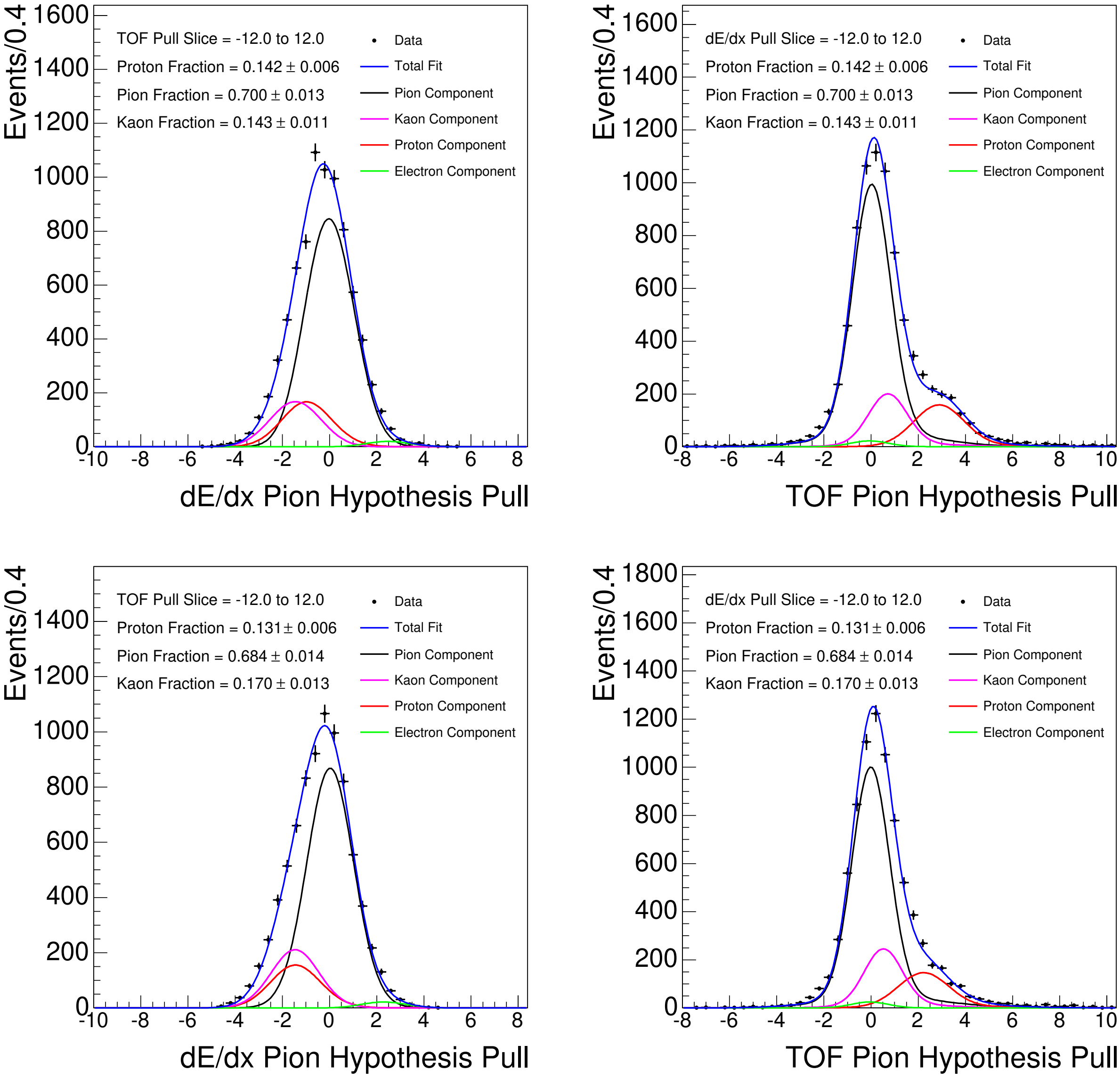

Figure 65: dE/dx (left) and TOF (right) projections of fits for particle fractions in the $p = 2.0 - 2.5\ GeV/c$ (top) and $p = 2.0 - 2.5\ GeV/c$ (bottom) momentum bins for positively charged third tracks in the J/ψ+track sample. Events with $ct^* < 0\ \mu m$

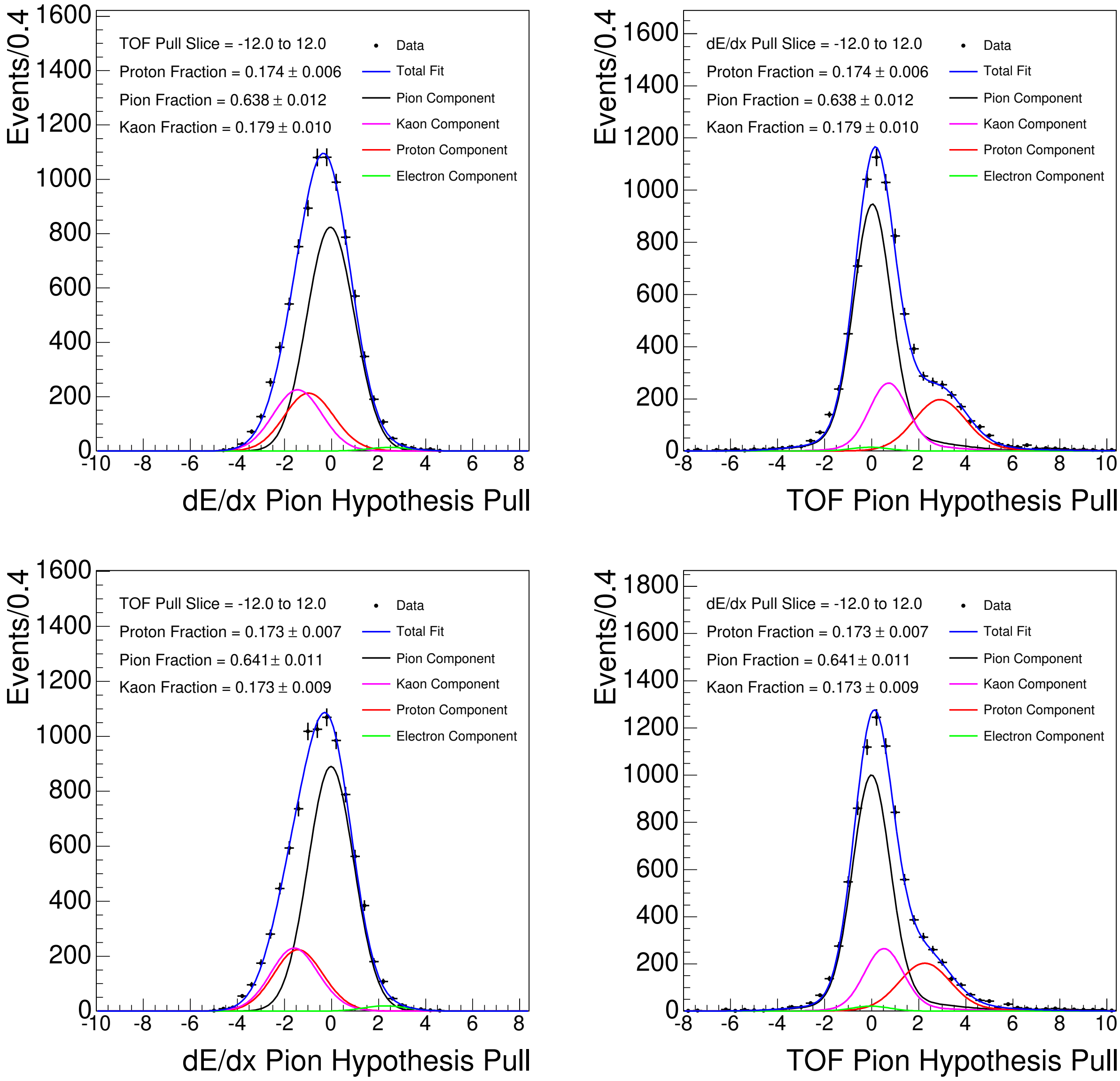

Figure 66: dE/dx (left) and TOF (right) projections of fits for particle fractions in the $p = 2.0 - 2.5\ GeV/c$ (top) and $p = 2.0 - 2.5\ GeV/c$ (bottom) momentum bins for negatively charged third tracks in the J/ψ+track sample. Events with $ct^* < 0\ \mu m$

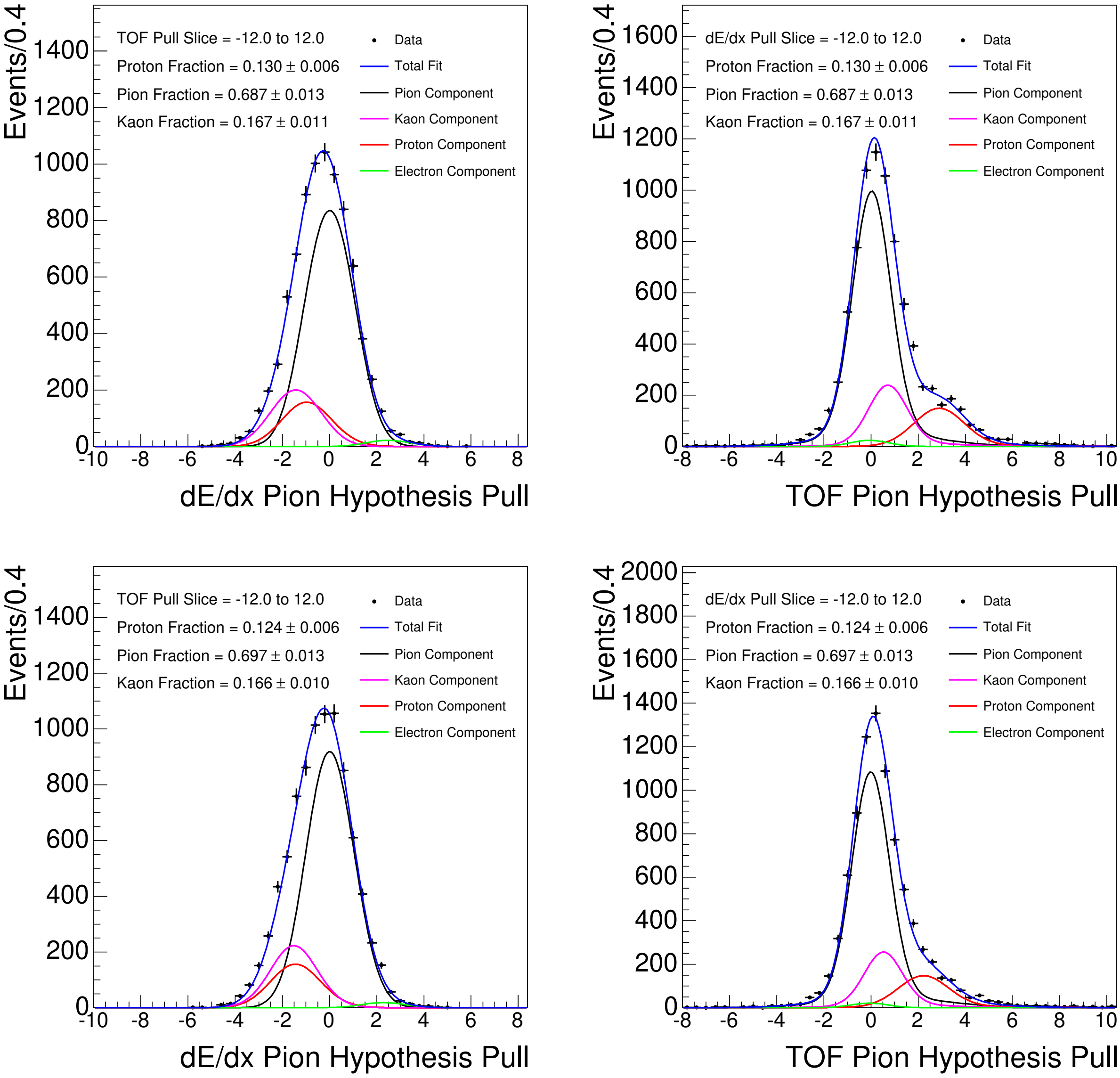

Figure 67: dE/dx (left) and TOF (right) projections of fits for particle fractions in the $p = 2.0 - 2.5\ GeV/c$ (top) and $p = 2.0 - 2.5\ GeV/c$ (bottom) momentum bins for positively charged third tracks in the J/ψ+track sample. Events with $0 < ct^* < 150$ μm

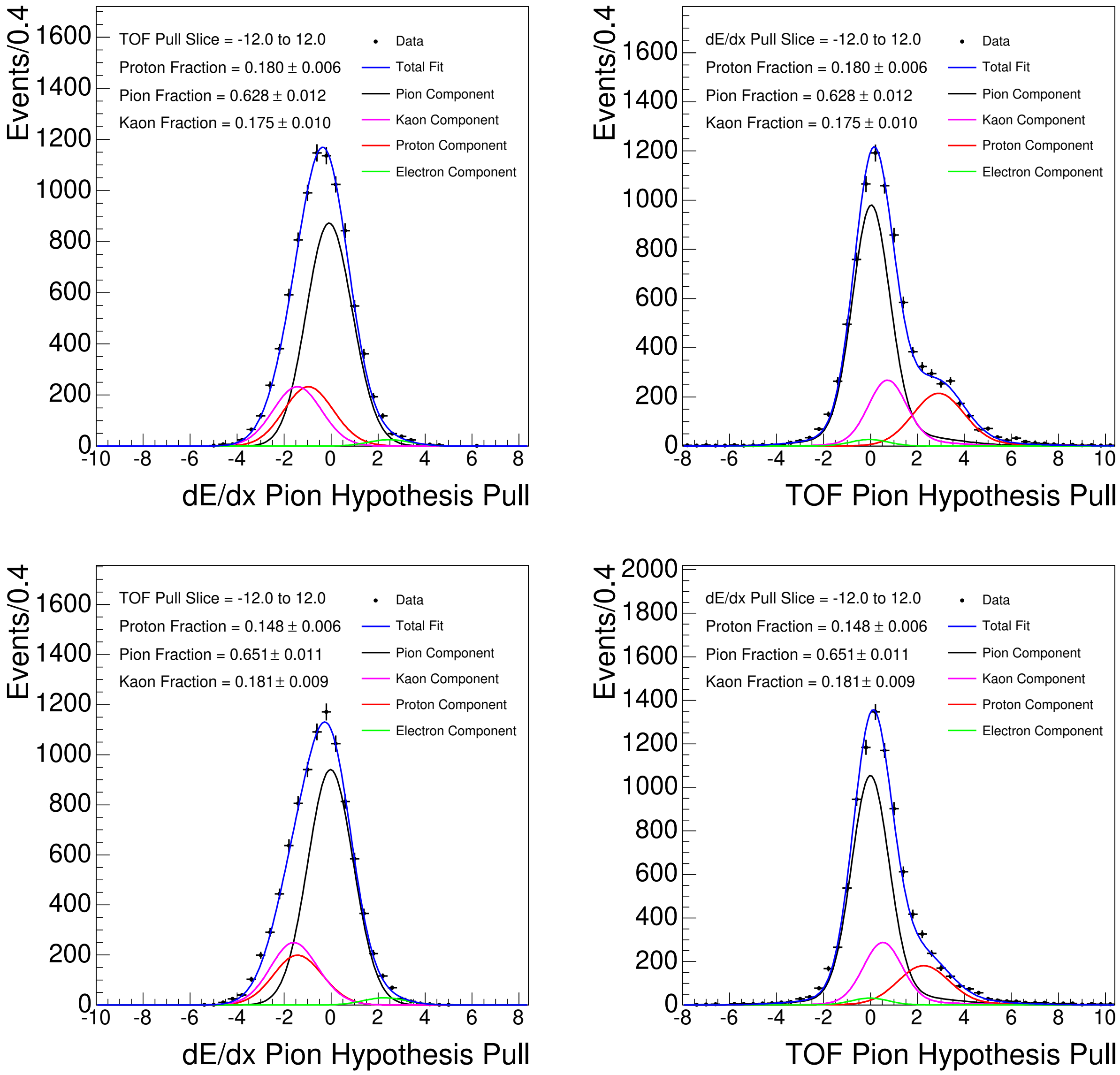

Figure 68: dE/dx (left) and TOF (right) projections of fits for particle fractions in the $p = 2.0 - 2.5\ GeV/c$ (top) and $p = 2.0 - 2.5\ GeV/c$ (bottom) momentum bins for negatively charged third tracks in the J/ψ+track sample. Events with $0 < ct^* < 150$ μm

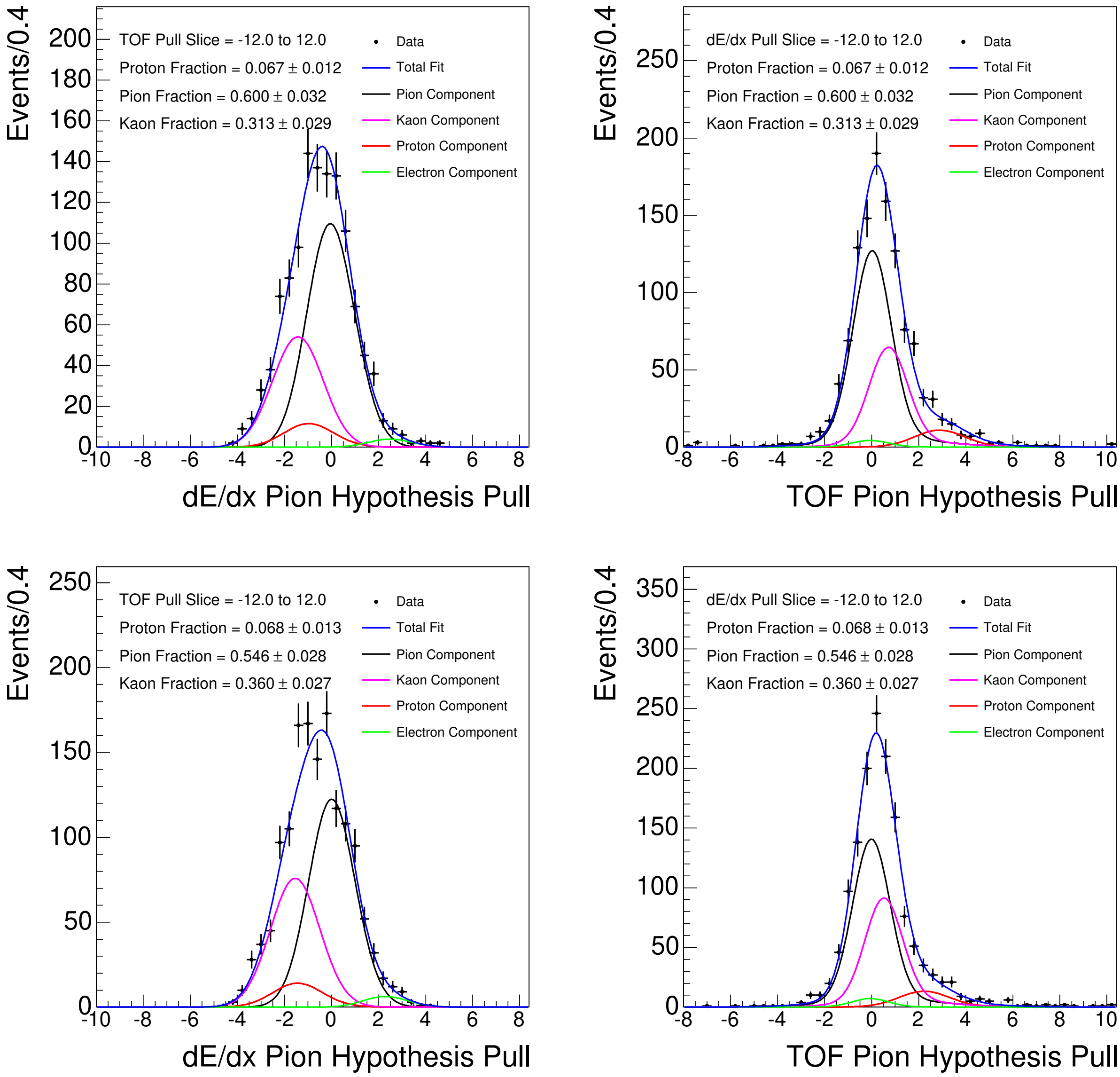

Figure 69: dE/dx (left) and TOF (right) projections of fits for particle fractions in the $p = 2.0 - 2.5\ GeV/c$ (top) and $p = 2.0 - 2.5\ GeV/c$ (bottom) momentum bins for positively charged third tracks in the J/ψ+track sample. Events with $ct^* > 150\ \mu m$

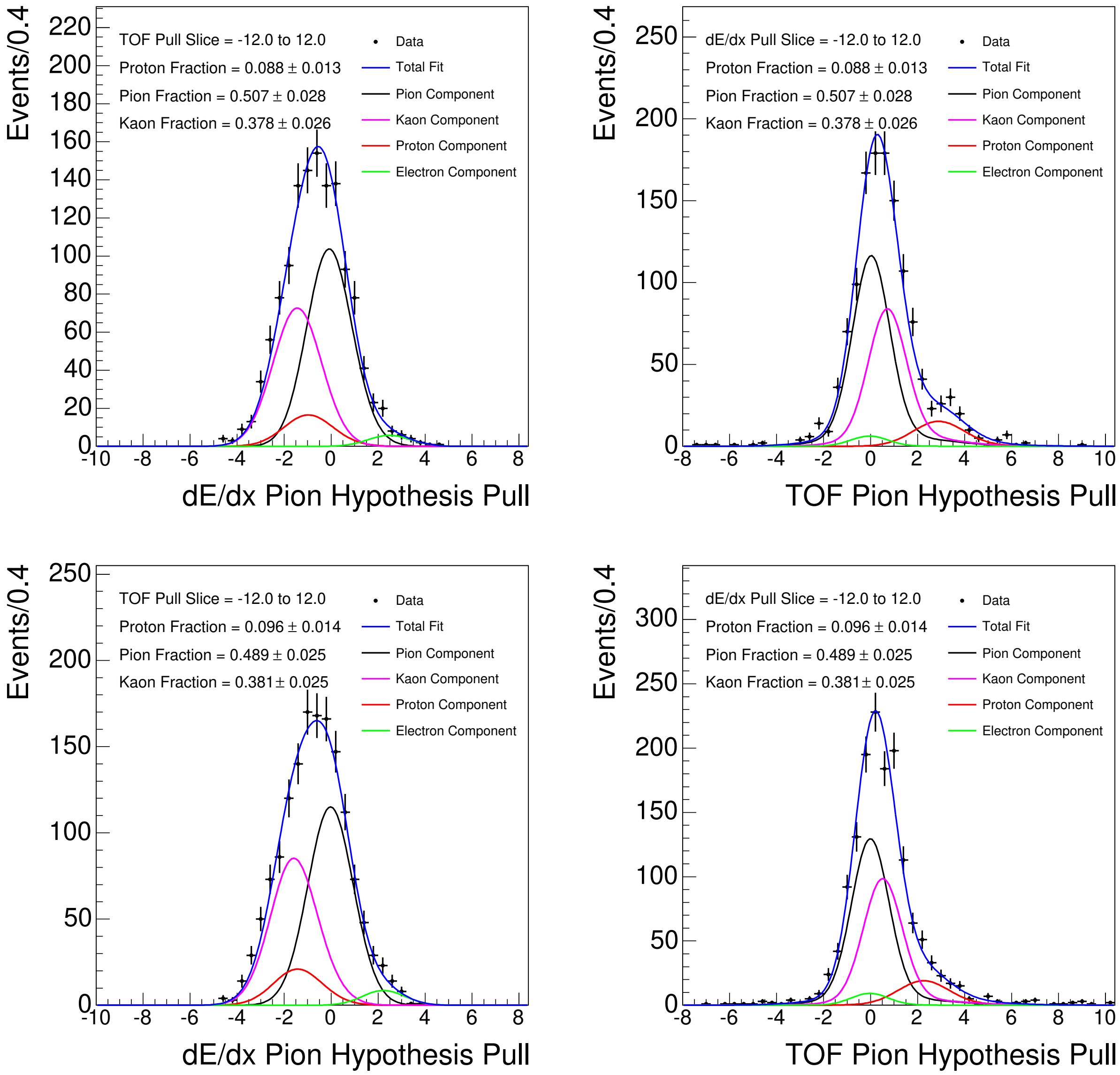

Figure 70: dE/dx (left) and TOF (right) projections of fits for particle fractions in the $p = 2.0 - 2.5\ GeV/c$ (top) and $p = 2.0 - 2.5\ GeV/c$ (bottom) momentum bins for negatively charged third tracks in the J/ψ+track sample. Events with $ct^* > 150\ \mu m$

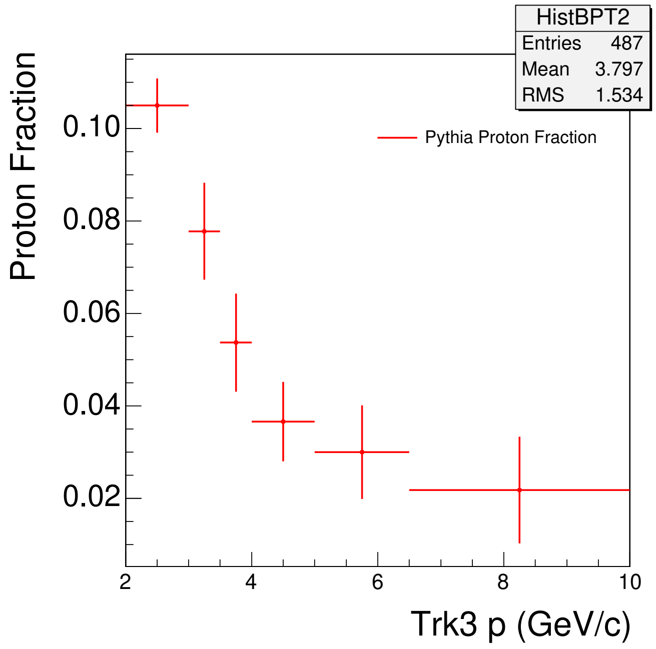

Figure 71: Proton fraction of J/ψ+track events in Pythia sample as a function of momentum of the third track.

dE/dx are so similar due to their similar masses. Instead, we use the CMU and CMX detectors to identify the number of muons in the J/ψ+track sample. Obviously those numbers will be missing muons that are not in the fiducials or are not identified by the muon detectors and they will include hadrons that fake muons. We can write an equation for the number of identified muons, N_μ^{id}, based on the true number of muons, N_μ, the fraction of events in the fiducial, f_{fid}, the muon ID efficiency, ϵ_{id}, the pion and kaon fractions in the sample, f_π and f_K, the pion and kaon muon fake rates, r_π and r_k, and the total number of events in the sample N_T:

$$N_\mu^{id} = N_\mu \epsilon_{id} f_{fid} + N_T(f_\pi r_\pi f_{fid} + f_K r_K f_{fid})$$

ϵ_{id} and r_π and r_K have been measured previously and we use the numbers from CDF Note 8042 [8]. N_T, N_μ^{id} and f_{fid} all come directly from the J/ψ+track sample, and we have just measured f_π and f_K with our dE/dx fits. Before we proceed, we assume that the f_π that we measured is actually the true f_π plus the muon fraction. Taking that into account, we solve the equation for N_μ:

$$N_\mu = \frac{N_\mu^{id}/f_{fid} - N_T(f_\pi r_\pi + f_K r_K)}{\epsilon_{id} - r_\pi}$$

We use this equation for each momentum/Q/ct^* bin in which do the Z_π fits. We break the data up into $|\eta| < 0.6$,for which we use the CMU, and $|\eta| > 0.6$, for which

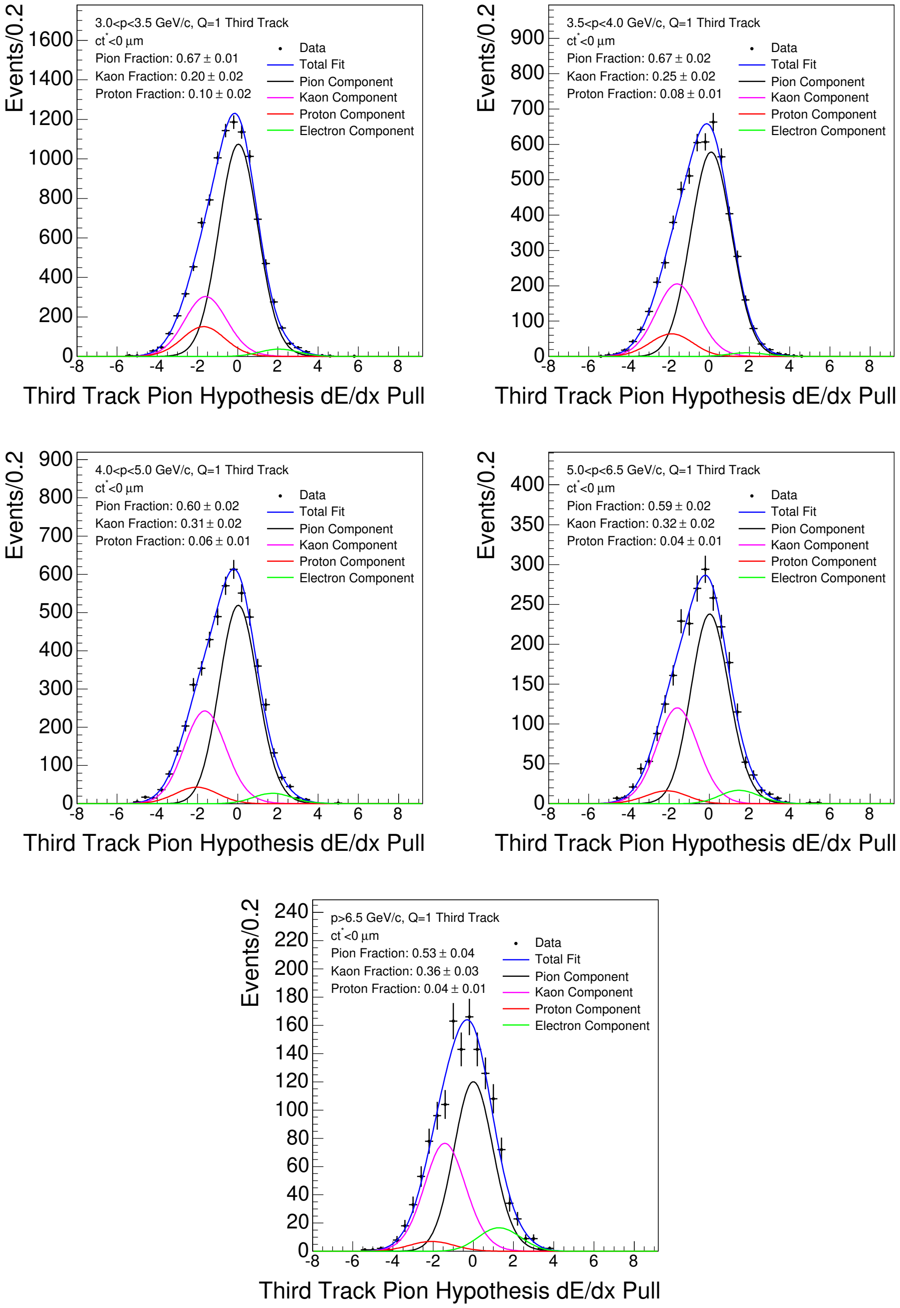

Figure 72: Fitted dE/dx distributions for $Q = 1$ and $ct^* < 0\ \mu m$. Broken into bins for the momentum of the third track: $3.0 - 3.5\ GeV/c$ (top left), $3.5 - 4.0\ GeV/c$ (top right), $4.0 - 5.0\ GeV/c$ (middle left), $5.0 - 6.5\ GeV/c$ (middle right) and > 6.5 (bottom).

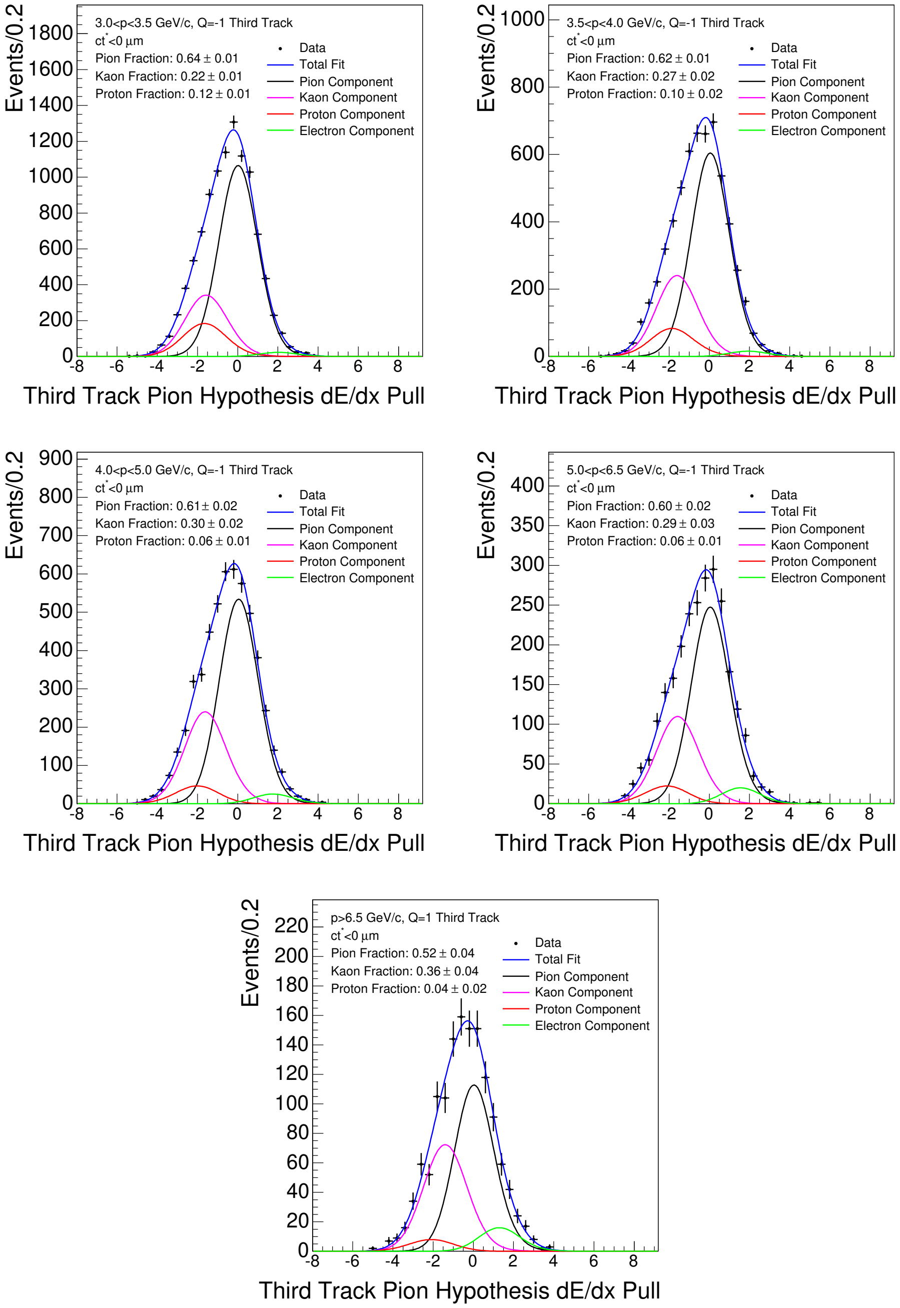

Figure 73: Fitted dE/dx distributions for $Q = -1$ and $ct^* < 0\ \mu m$. Broken into bins for the momentum of the third track: $3.0 - 3.5\ GeV/c$ (top left), $3.5 - 4.0\ GeV/c$ (top right), $4.0 - 5.0\ GeV/c$ (middle left), $5.0 - 6.5\ GeV/c$ (middle right) and > 6.5 (bottom).

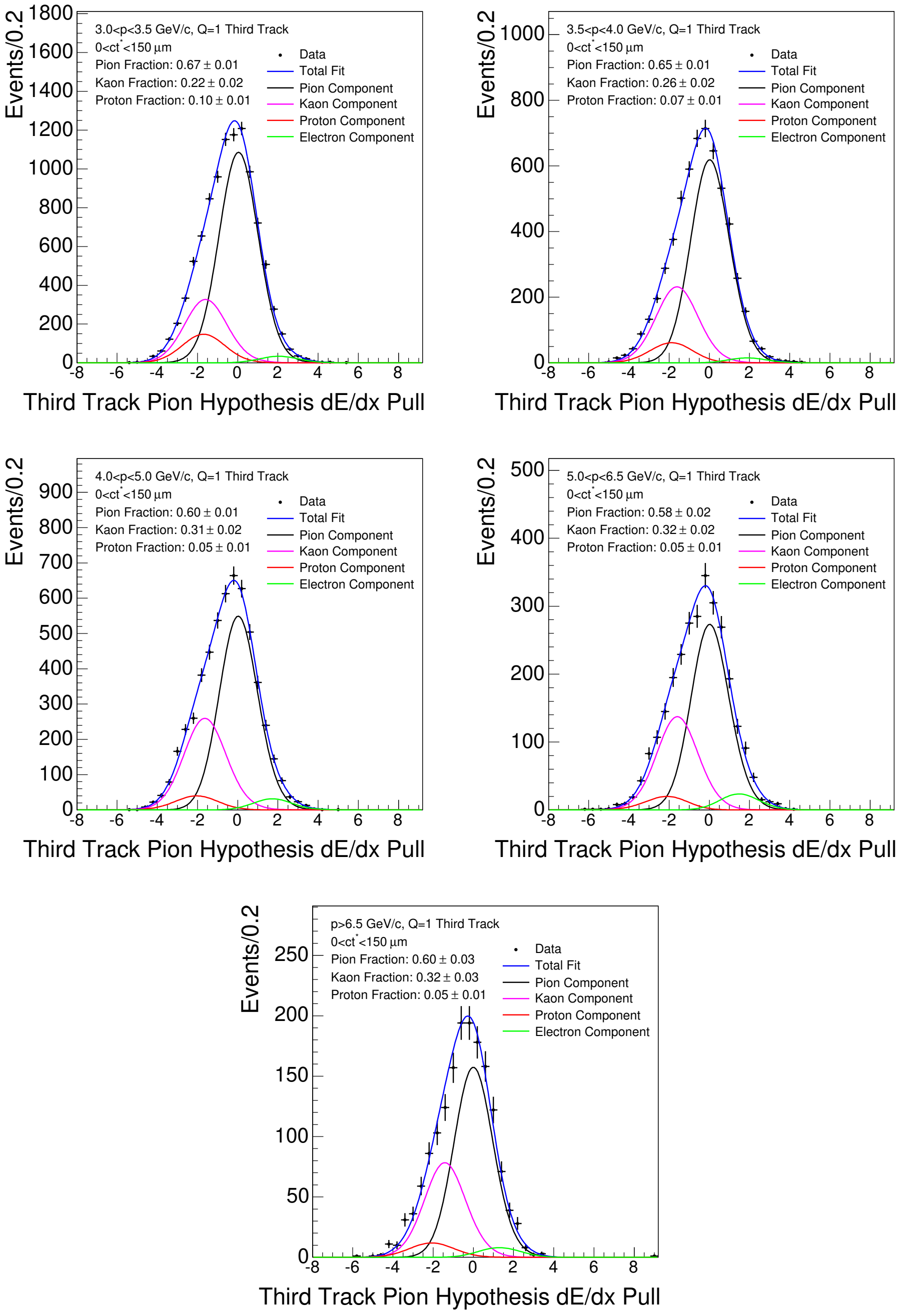

Figure 74: Fitted dE/dx distributions for $Q = 1$ and $0 < ct^* < 150\ \mu m$. Broken into bins for the momentum of the third track: $3.0 - 3.5\ GeV/c$ (top left), $3.5 - 4.0\ GeV/c$ (top right), $4.0 - 5.0\ GeV/c$ (middle left), $5.0 - 6.5\ GeV/c$ (middle right) and > 6.5 (bottom).

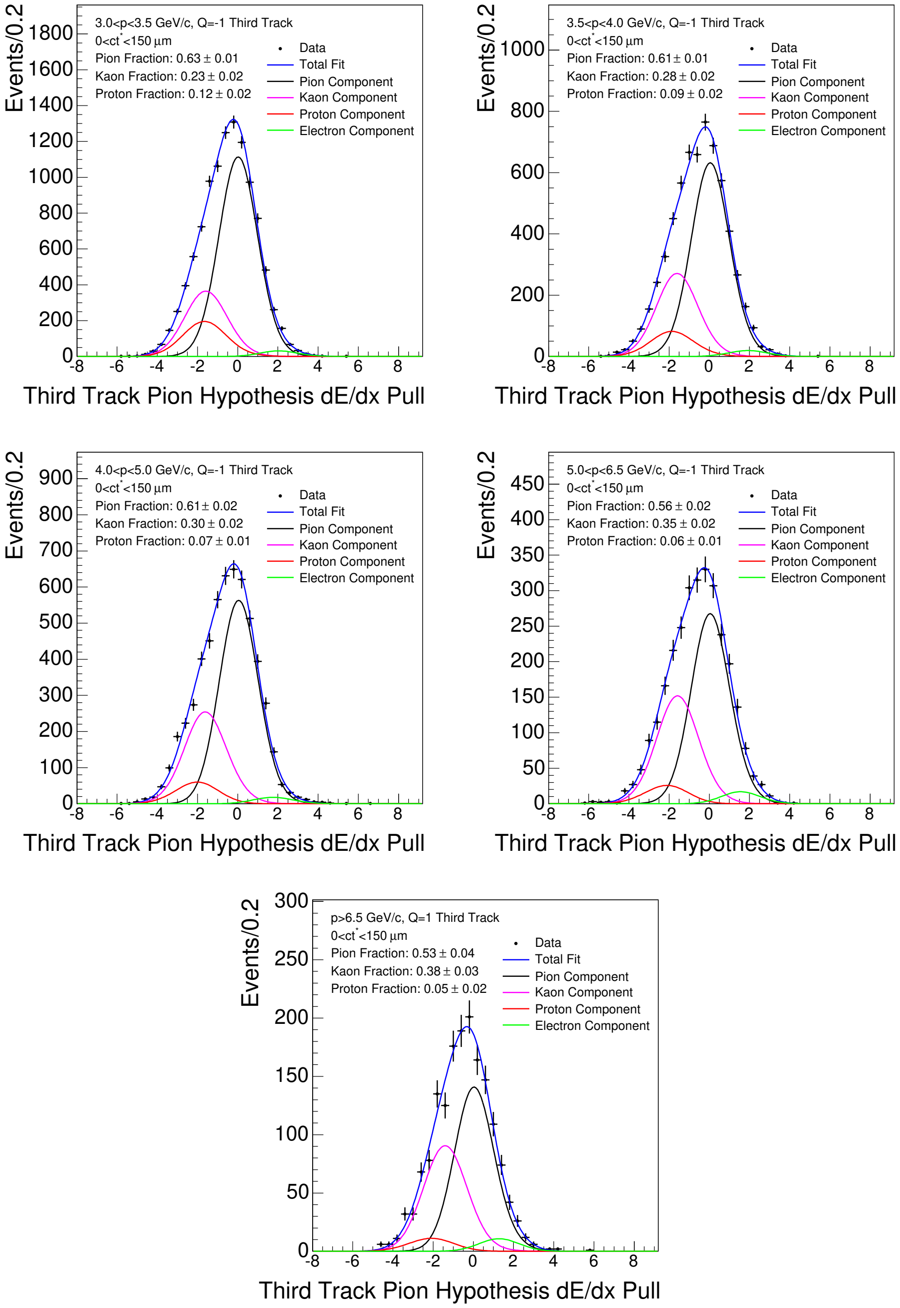

Figure 75: Fitted dE/dx distributions for $Q = -1$ and $0 < ct^* < 150$ μm. Broken into bins for the momentum of the third track: $3.0 - 3.5$ GeV/c (top left), $3.5 - 4.0$ GeV/c (top right), $4.0 - 5.0$ GeV/c (middle left), $5.0 - 6.5$ GeV/c (middle right) and > 6.5 (bottom).

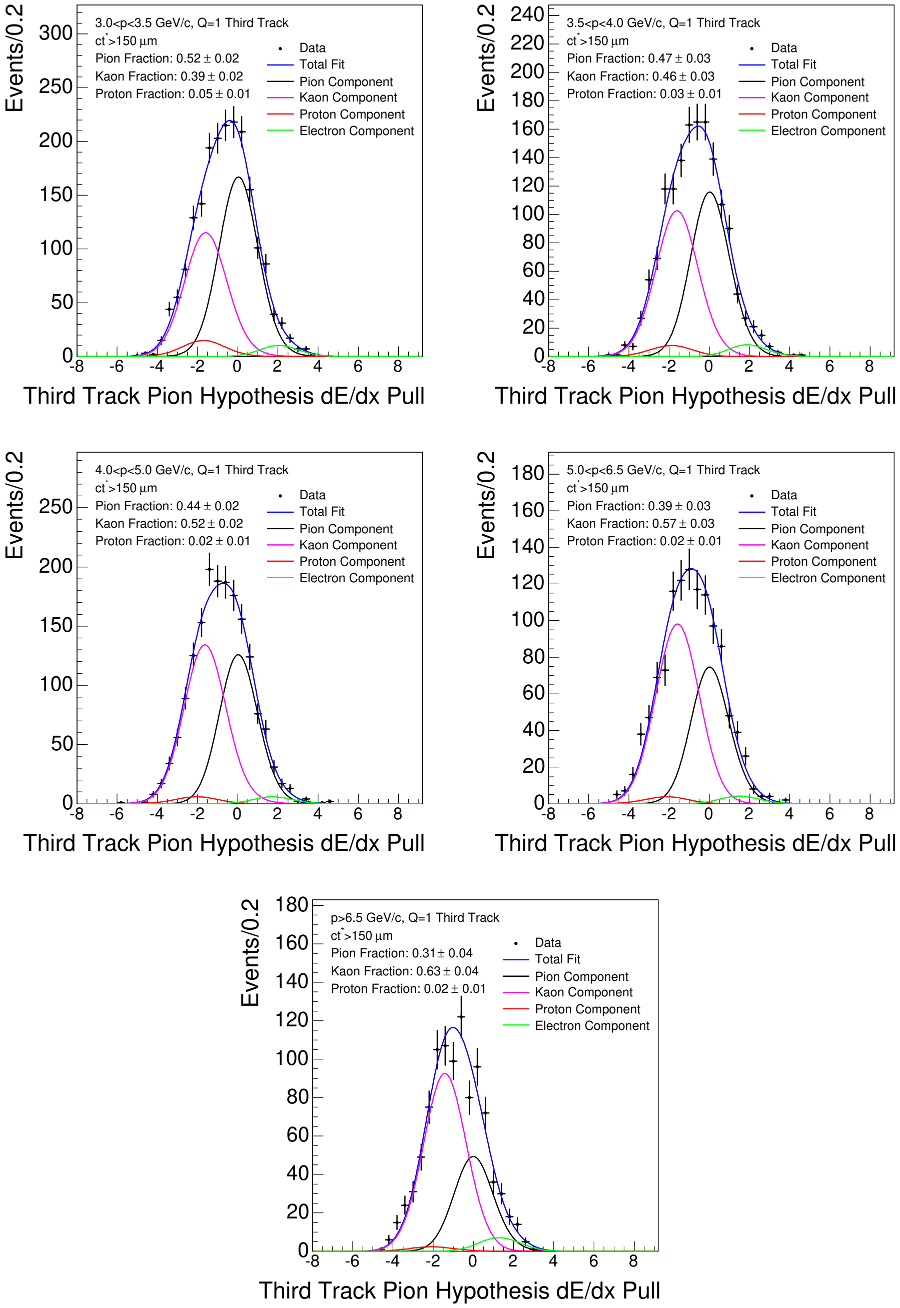

Figure 76: Fitted dE/dx distributions for $Q = 1$ and $ct^* > 150\ \mu m$. Broken into bins for the momentum of the third track: $3.0 - 3.5\ GeV/c$ (top left), $3.5 - 4.0\ GeV/c$ (top right), $4.0 - 5.0\ GeV/c$ (middle left), $5.0 - 6.5\ GeV/c$ (middle right) and > 6.5 (bottom).

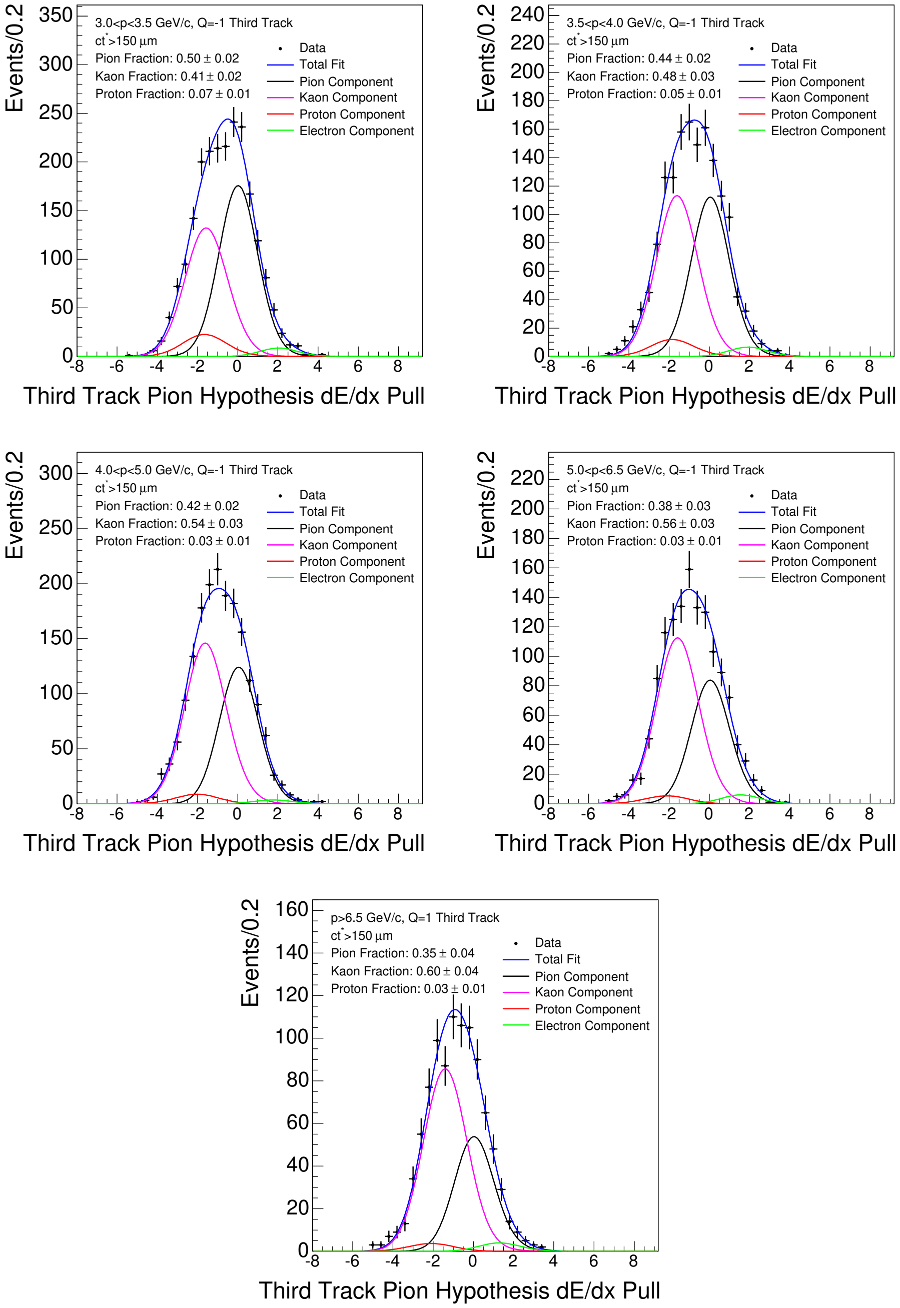

Figure 77: Fitted dE/dx distributions for $Q = -1$ and $ct^* > 150\ \mu m$. Broken into bins for the momentum of the third track: $3.0 - 3.5\ GeV/c$ (top left), $3.5 - 4.0\ GeV/c$ (top right), $4.0 - 5.0\ GeV/c$ (middle left), $5.0 - 6.5\ GeV/c$ (middle right) and > 6.5 (bottom).

we use the CMX. The derived muon fraction is subtracted from the pion fraction. The particle fractions after estimation of the muon fraction can be seen in Figure 78.

B.5 Z_e/σ Cut Efficiencies

As mentioned previously, the J/ψ+track sample used for the particle ID fits does not have the Z_e/σ cut applied. We measure the efficiencies for the Z_e/σ cut using hadrons from our D^0 and Λ samples and muons from J/ψ decays. The momentum dependent efficiencies are summarized in Figure 79.

Applying the measured efficiencies to the measured particle fractions, we get the final particle fractions for third tracks in the J/ψ+track sample, which are shown in Figure 12 in Section 3.2.2.

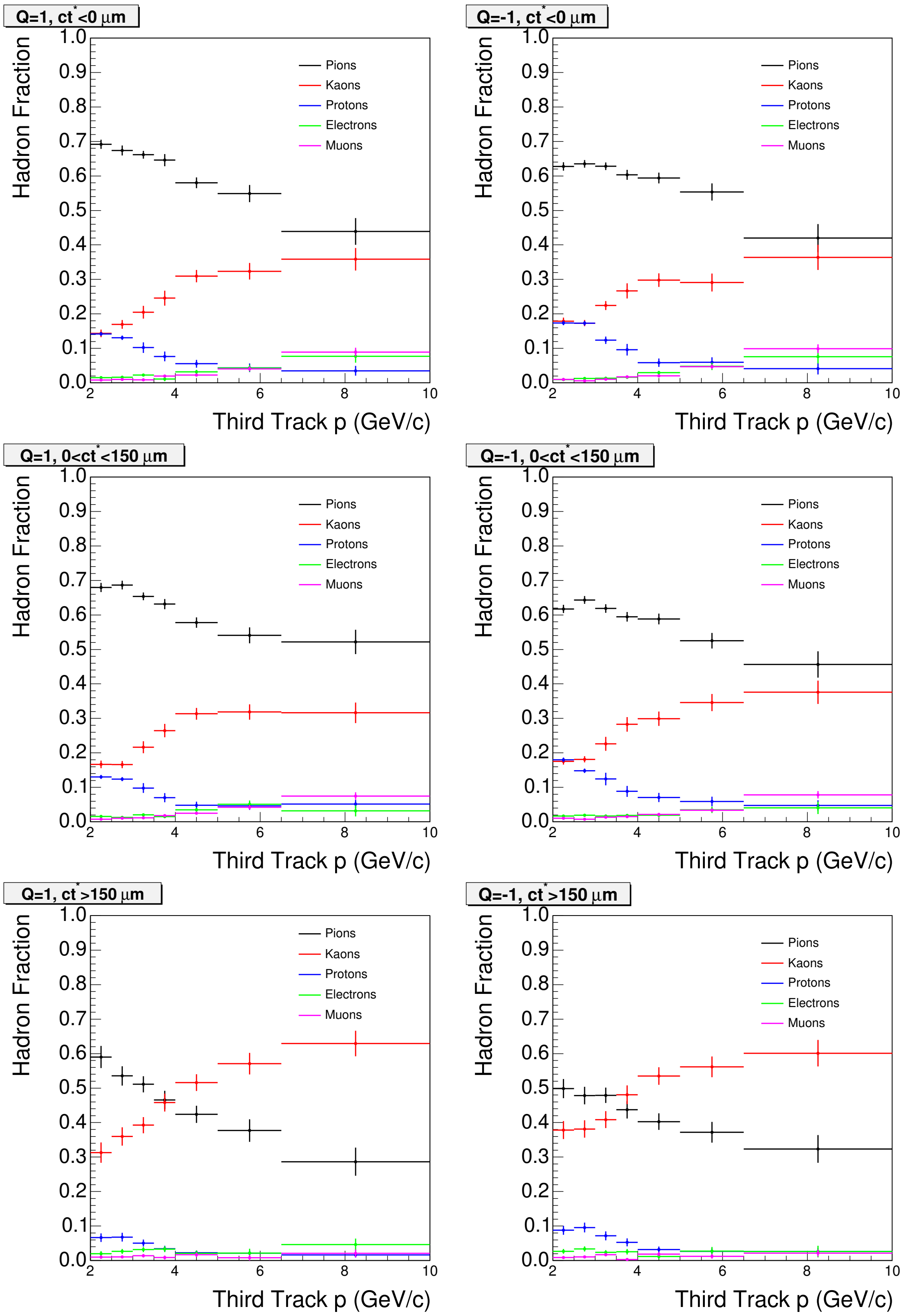

Figure 78: Particle composition fractions for third tracks in the J/ψ+track sample as a function of the third track momentum. Left are positive charge, right are negative charge. Top row is $ct^* < 0$ μm, middle row is $0 < ct^* < 150$ μm and bottom row is $ct^* > 150$ μm.

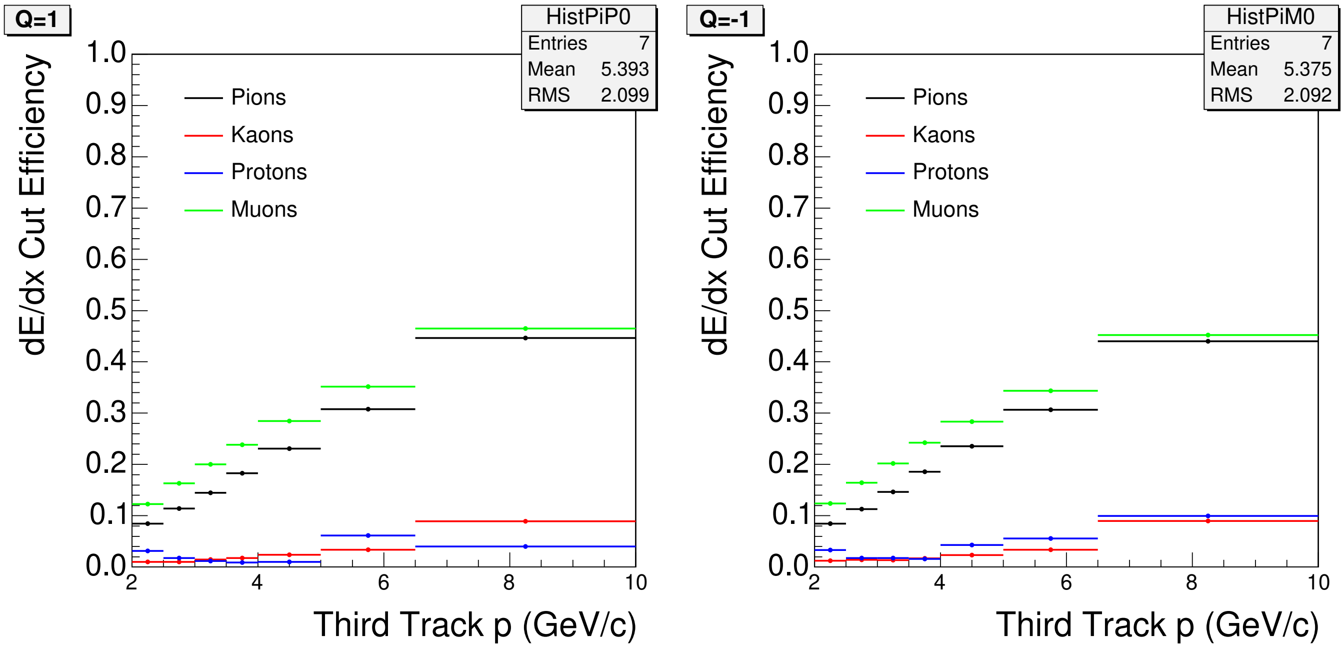

Figure 79: Measured Z_e/σ cut efficiencies for various particle types.

References

[1] Masato Aoiki et al., "Measurement of the B_c Lifetime using Semileptonic Decays" CDF Note 7758 (2005).

[2] M. Hartz, P. Shepard, T. Nigmanov and K. Gibson, "Measurement of the $B_c^{\pm}$ Lifetime in $B_c^{\pm} \to \mathrm{J}/\psi + \mu^{\pm} + \mathrm{X}$ with Run II Data" CDF Note 8155 (2008).

[3] T. Tiwari et al. "Likelihood Based Electron Tagging" CDF Note 7121 (2004).

[4] A. Affolder, "A Measurement of Bottom Quark-Antiquark Azimuthal Production Correlations" CDF Note 6263 (2003).

[5] M. Hartz, P. Shepard and T. Nigmanov, "Study of $b\bar{b}$ Background in $B_c^{\pm} \to \mathrm{J}/\psi + \mu^{\pm} + \mathrm{X}$ with Run II Data" CDF Note 7420 (2005).

[6] P. Bussey, it et al., "Search of a $B_c \to \mathrm{J}/\psi\pi$ signal: Monte Carlo validation" CDF Note 7018 (2004).

[7] V.V. Kiselev, "Decays of the B_c Meson", arXiv:hep-ph/0308214v1, 21 Aug 2003.

[8] E. Berry, it et al., "Study of Muon Matching Efficiencies and Mistag Rates" CDF Note 8042 (2006).